Assessing glucose metabolism in tumor and normal tissues for patients with lung cancer following fractionated radiotherapy

Azadeh Abravan

Faculty of Mathematics and Natural Sciences

Department of Physics

Biophysics and Medical Physics

UNIVERSITY OF OSLO

September 2014

II

Assessing glucose metabolism in tumor and normal tissues for patients with lung cancer following fractionated radiotherapy

Azadeh Abravan

Faculty of Mathematics and Natural Sciences

Department of Physics

Biophysics and Medical Physics

UNIVERSITY OF OSLO

September 2014

IV

Year 2014

Assessing glucose metabolism in tumor and normal tissues for patients with lung cancer following fractionated radiotherapy

Azadeh Abravan

"Wisdom is not a product of schooling but of the lifelong attempt to acquire it."

Albert Einstein.

Abstract

Medical imaging is an integral part of cancer management. Conventional medical imaging such as computed tomography provides anatomical images, which together with functional imaging may be used for depicting tumor properties of biological relevance. Positron Emission Tomography is one of the functional imaging methods which visualize metabolically active tissues. ^{18}F-fluorodeoxyglucose (FDG) is the most common PET tracer in oncology. FDG-PET depicts glucose metabolism, which increases in most tumors because many cancer cells undergo a metabolic shift during tumor development towards increased glucose metabolism. In addition to cancer, normal healthy tissue will also accumulate FDG. This accumulation may change with cancer treatment, as normal tissues are expected to respond to both radiotherapy and chemotherapy.

This project included 22 patients with advanced-stage non-small cell lung cancer, participating in a phase II trial on combined radiation and erlotinib (Tarceva)-therapy. The patients underwent three PET-CT examinations; at pre-therapy (prior to radiotherapy), mid-therapy, and post-therapy (six weeks after therapy). In addition, the patients underwent a complete CT-based digital radiotherapy planning. For each patient, the tumor, lymph nodes, lung, heart, esophagus, and bone marrow were delineated in the planning CT. The FDG-uptake distribution, in terms of the standardized uptake value (SUV), was obtained for tumor and organs at risk (OAR's) from all PET-CT examinations.

The maximum of the SUV distribution was used to monitor tumor's response to treatment. The median of the SUV was used to monitor treatment induced changes in the OAR's. Then, Mann-Whitney's U-test was employed to compare groups of data. We also tried to identify any correlation between OARs' SUV and radiation dose at mid-therapy and post-therapy. Linear regression was used to extract trends. We also investigated the effect of the Tarceva drug by separating into a Tarceva receiving group and a non-Tarceva receiving group. A further refinement was that we investigated the correlation between density changes in the lung, obtained from CT, and dose.

A significant (p = 0.05) decrease in the maximal tumor metabolic activity was observed from pre-therapy to post-therapy session. No significant changes were found in SUV between sessions in OAR's. Also, by looking at tumors and OAR's, no significant differences were found between the Tarceva receiving group and the non-Tarceva receiving group in each session.

Linear relationships were identified between SUV and radiation dose in both mid- and post-therapy sessions based on mean FDG uptake in given dose bins. The correlation was positive for lung and esophagus and was negative for bone marrow in both sessions. However, for heart a positive correlation was identified followed by a negative correlation from mid- to post-therapy sessions. A positive linear relationship was also observed between lung density and radiation dose. The effect of Tarceva on the FDG uptake in the lungs was significant in both sessions.

Overall, the results of this study lead us to the conclusion that ^{18}F-FDG PET-CT may identify changes in tumor glucose metabolism six weeks after radiotherapy. FDG uptake responses were also seen in normal tissue with respect to dose.

Preface

This thesis is submitted for the degree of Master of Science at the section for Biophysics and Medical Physics.

This thesis is dedicated to patients recruited in this study.

Oslo, September 2014

Azadeh Abravan

List of Abbreviations

^{18}F-FDG PET-CT	^{18}F- Fluoro-2-DeoxyGlucose Positron Emission Tomography integrated with Computed Tomography
BR	Breathing Rate
CI	Confidence Interval
CT	Computed Tomography
FOV	Field Of View
GTV	Gross Tumor Volume
HU	Hounsfield Unit
NSCLC	Non-Small Cell Lung Cell
PET	Positron Emission Tomography
PMT	Photo multiplier tube
RILT	Radiation Induced Lung Toxicity
RP	Radiation Pneumonitis
RT	Radio-Therapy
SUV	Standardized Uptake Value

Contents

1. Introduction

Cancer refers to a group of diseases characterized by uncontrolled growth and spread of mutated cells. If the spread is not controlled, it can result in death of the host. Cancer is caused by both external factors (such as tobacco, infectious organisms, chemicals, and radiation) and internal factors (such as inherited mutations, hormones, immune conditions, and novel mutations). Cancer treatment includes surgery, radiotherapy, chemotherapy, hormone therapy, and targeted therapy.

Cancer treatment has improved significantly over the past decade. Up to this point, many cancer types have become chronic diseases rather than terminal illnesses. This significant achievement owes to, among many factors, the effective means of radiotherapy and chemotherapy. Despite improvements in radiotherapy and chemotherapy, the outcome of patients suffering from a number of cancer types such as lung cancer remains quite poor. Lung cancer is the most fatal cancer worldwide (1). In Norway 2902 patients were diagnosed in 2012. Lung cancer is mostly diagnosed after presentation of clinical symptoms of the patient. Non-small cell lung cancer (NSCLC) accounts for about 80% of the lung cancer cases. It is an aggressive form of cancer and patients with NSCLC usually diagnosed with advanced disease (stage III- IV). Only minor gains have been made over the past decade in the treatment of advanced non-small cell lung cancer for patients in terms of prolonging survival and improving quality of life (2).

Radiotherapy uses ionizing radiation and delivers prescribed amounts of radiation to the malignant tumor usually over the multiple fractions. Radiation is a way of carrying energy in the form of particles or electromagnetic waves such as x-rays or gamma-rays. Ionizations occur when cells are exposed to ionizing radiation. Radiation kills or controls cancer cells, but can also damage the healthy cells in the area being irradiated. Radiotherapy is a common treatment for various cancer types such as NSCLC. It is sometimes combined with other treatments such as targeted therapy.

Targeted therapies are developed to block cellular pathways involved in cancer cell survival, proliferation, and metastasis. Gefitinib and Erlotinib (Tarceva) have been demonstrated to be

effective in front-line therapy in patients with inoperable NSCLC harboring epidermal growth factor receptor (EGFR) activating mutations (3). Tarceva is recommended after failure of previous chemotherapy and as a maintenance therapy for patients with progressive disease (4) (5).

Imaging plays an important role within the field of medicine and oncology. The ability to visualize changes occurring in the body helps physicians to make a better diagnostics and to perform a better treatment. Advances in computed tomography (CT) and positron emission tomography (PET) have contributed significantly to medical imaging. These contributions were not possible without fully exploiting the diagnostic information provided by PET-CT, which in turn requires a deep knowledge of both PET and CT. CT is an imaging modality which measures x-ray attenuation within the bodily tissues while PET uses radiotracers to observe specific physiological processes such as glucose uptake. PET was realized in the 1970's by Phelps and colleagues and became clinically available in the 1990's (6).

[18]F-fluorodeoxyglucose (FDG) PET-CT has become part of the standard protocol in the diagnosis, staging, and therapy response assessment for various types of cancers (7). It is well known that there is an increased transport of glucose into malignant cells and up-regulation of enzymatic activity which results in an increased tracer uptake. FDG uptake is not specific to cancer. Benign and inflammatory disorders have also been reported to take up FDG. Combined PET-CT is therefore essential in order to separate normal physiologic uptake from pathologic uptake. In other words, PET-CT provides us with accurate localization of functional abnormalities in the body. Furthermore, PET-CT scans before, during, and after treatment helps us to evaluate treatment by assessing the FDG uptake changes in the tumor as treatment progresses. It may also help us evaluate normal tissues response during and after the treatment.

This study evaluates FDG uptake and tissue density within the tumor and various organs at risk in 22 patients with NSCLC who have received fractionated radiotherapy. These patients have undergone three ^{18}F-FDG PET-CT examinations; prior to radiotherapy, at mid therapy (after typically 15 Gy), and six weeks after therapy. The major scientific goals of this study are:

Can ^{18}F-FDG PET-CT be used to detect metabolic changes in the tumor and normal tissues following radiotherapy? Can we identify any correlations or trends between glucose uptake in normal tissues and local dose? Can CT scans be used to assess changes in the lung density? Can we identify any trends between lung density and local dose? Is ^{18}F-FDG PET-CT a suitable biomarker in order to monitor Tarceva treatment over time? In order to answer these questions the first step would be to develop a computer program for reading and displaying PET and CT images of various organs and tumor and also to co-register the planning CT, dose, and a series of PET-CT images.

2. Background

2.1. Cancer

Malignancy arises from changes in cell regulation and tissue growth. To understand the process, it is important to appreciate the normal mechanisms by which growth is controlled in human tissues. Pathways are controlled in a way that cells are replaced or repaired with an appropriate rate and without altering the normal balance of different types of cells in a tissue. In other words, there is interplay between growth stimulants and suppressors in cells.

Damages to DNA can occur every day in the life of a cell. These may have different causes, such as infections, viruses, genetic instability, and chemical agents. However, in most cases damage will be repaired before it proceed to further changes or mutations. Cancer may be initiated when DNA damage occurs in an important part of the DNA sequence and left unrepaired. In such cases multiple subsequent changes in the DNA lead to failure in response to normal regulatory system, either an excess in growth factors or lack of the tumor suppressors. As a result, a transformed cell will be produced which will proliferate excessively until a potentially malignant clone of cells is produced. These progressive changes accumulate in the genome and make this progression irreversible.

2.1.1. Lung cancer

Lung cancer is described by the excessive growth of malignant cells in one or both lungs. It can start in the cells lining the bronchi, bronchioles, and alveoli (Figure 56). Changes in the lung cells' DNA can make them grow faster. In this phase of the disease, cells do not form a mass; yet it is not possible to see any abnormalities—for instance from chest x-ray. Overtime, these cells may have further mutations and become cancerous. Formation of new blood vessels from pre-existing vessels (angiogenesis) provides cancerous cells with nutritions and oxygen. This results in formation of a tumor that can be observed by medical imaging modalities.

Lung cancer is categorized by how cancerous cells look like under microscope. The two main types of the lung cancer are non-small cell lung cancer (NSCLC) and small cell lung cancer (SCLC). The prognosis of lung cancer is poor because the lungs are large and tumors can grow in them for a long time before they are found. Some symptoms, such as coughing and fatigue, are usually mistaken by people as being caused by other means. For this reason, early-stage lung cancer (stages I and II)[1] is difficult to detect. Most people with lung cancer are diagnosed at stages III and IV.[2] In this aggressive disease, blood-borne metastasis can occur to all sites of the body, especially in the bone, liver and central nervous system (CNS).

Lung cancer is the leading cause of cancer death for both men and women in the world. The incidence of lung cancer in Norway was about 2902 in 2012 (1602 in men and 1300 in women) (8). The number of deaths from this disease is similar in number to the incidence, reflecting the poor prognosis.

It is clear that smoking is the primary risk factor for lung cancer and accounts for more than 85% of all lung cancer-related deaths. The occurrence of lung cancer is correlated to the number of cigarettes smoked per day and the number of years spent smoking. Second-hand smoke is also known as a cause of developing lung cancer. Exposure to radon gas[3] also increases the risk for lung cancer. Other, less probable, causes have also been identified.

2.1.2. Non-Small Cell Lung Cancer

About 80% to 90% of lung cancers are non-small cell lung cancers. Among them are three sub-groups called Adenocarcinoma, Squamous cell carcinoma, and Large cell carcinomas. These

---

[1] Stage I: The cancer is located only in the lungs and has not spread to any lymph nodes.

Stage II: The cancer is in the lung and nearby lymph nodes.

[2] Stage III: Cancer is found in the lung and in the lymph nodes in the middle of the chest.

Stage IV: This is the most advanced stage of lung cancer, when the cancer has spread to both lungs, to fluid in the area around the lungs, or to another part of the body, such as the liver or other organs.

[3] Radon is a radioactive gas that is produced by the decay of radium 226.

cells differ in size, shape, and genetic make-up. However, the prognosis and treatment of such tumors are very similar. Surgery can be curative when the disease is localized, but most of the newly diagnosed patients have their disease widely spread and thus palliative treatment is the only option for such patients.

In order to deliver an appropriate treatment to the patient diagnosed with lung cancer, the doctor must determine the type and stage of cancer. This can be done by examining the lung tissue with, for example, biopsy. Biopsy is a way to remove a small piece of tissue for examination under a microscope. Other tests such as computed tomography and positron emission tomography may be performed in order to optimize the treatment and see how effective an ongoing treatment is during and after treatment.

2.2. Computed Tomography (CT)

A Computed Tomography (CT) combines computer and x-ray technology to produce 3 dimensional images of internal organs. CT scanner consists of a rotating x-ray tube and detectors on opposite sides of the patient to acquire cross-sectional images. CT is based on a measurement of x-ray attenuation through a desired section. CT scanners originate back in 1895 and exploration of x-rays by Wilhelm Conrad Röntgen. Modern CT scanners have a stationary or rotating detector array with a fan beam x-ray tube which is rotating around patient.

In helical (spiral) CT scanners which are widely used, the patient's table moves continuously while the x-ray tube acquires a series of projection images (Figure 1). A slice of the CT image is composed of voxels (volume elements). The numeric value in each voxel represents physical property of the tissue, called x-ray attenuation, or tissue density. These numbers are called Hounsfield units or CT numbers. The linear attenuation values normalized to the attenuation of water. This normalization is given by following equation:

$$HU = 1000 \times \frac{\mu_x - \mu_{water}}{\mu_{water}}$$

Here, μ_x is the linear attenuation coefficients of tissue x and μ_{water} is the linear attenuation coefficients of water.
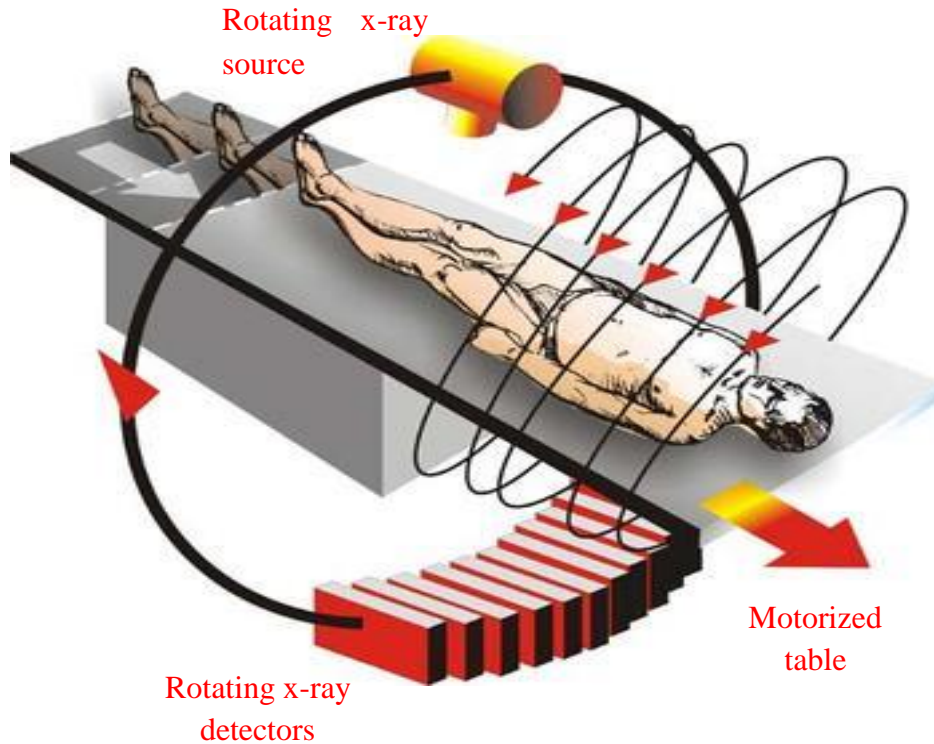
Figure 1: Spiral CT scan demonstration.

CT number gives an indication of the type of tissue. Water has a CT number of zero. Negative CT numbers are typical for air spaces, lung tissues and fat tissue (Figure 2). Radiologists occasionally make critical diagnostic decisions based on CT number of particular regions of interest.
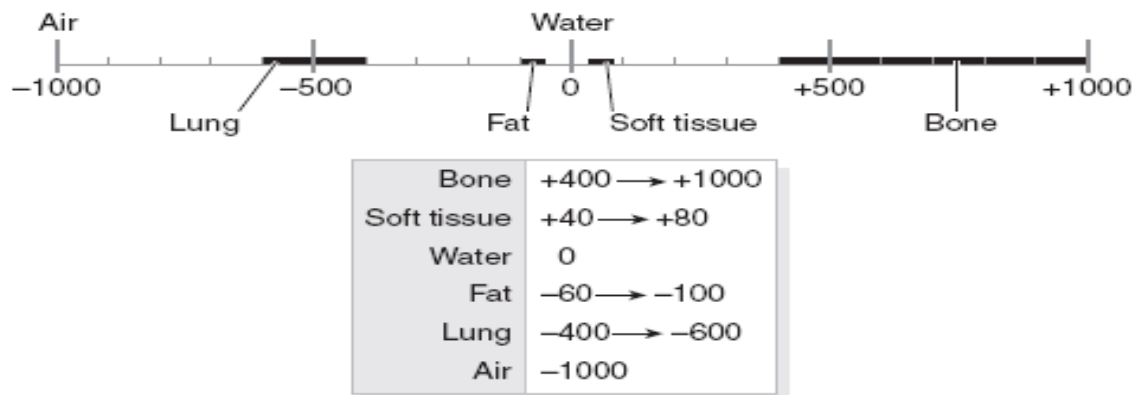

*Figure 2: The Hounsfield scale of CT numbers* **(9)**.

2.3. Positron Emission Tomography (PET)

PET scan is an important and valuable modality in radiotherapy. This imaging tool is growing faster than any other imaging modalities, and oncology is by far the most common field of application (10).

PET is a functional imaging technique that uses positron labelled tracers to produce three-dimensional, color images of the metabolic activities within the human body. The process is as follows: first, a radioactive tracer is injected and then gamma rays that are emitted from the patient's body are detected with a camera. PET tracers are usually a positron-emitting radionuclides placed on a biologically active molecule. Reconstructed PET images, along with CT images, give nuclear medicine specialists structural and functional information of the organs. In the next paragraphs we will talk in more detail about radionuclide and basic physics of the positron interactions as they play an important role in PET scan.

2.3.1. Radionuclide and positron decay

A positron emitter is a radioactive atom, or radionuclide, with an excess number of protons which may decay through the emission of positron. In positron decay an excess proton from a radionuclide is converted into a neutrino and a positron[4]. Positron decay is shown in the equation below:

$$^{A}_{Z}X \rightarrow ^{A}_{Z-1}Y + e^{+} + \nu$$
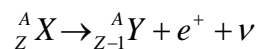
Here, X is the original radionuclide of mass number A and atomic number Z, Y is the daughter nuclide, e^{+} is the positron, and ν is a neutrino. Neutrinos that are produced in positron decay rarely interact in tissue and are almost impossible to detect. However, they influence the energy and range of the positrons, and as a result, the positron can have a spectrum of kinetic energies from zero up to a maximum value (E_{max}). The distance the positron travels in matter is determined by its kinetic energy.

---

[4] A positron has the same mass as an electron but has a positive electric charge.

2.3.2. Positron annihilation and PET

Because positron has a very short range in tissue (a few millimeters); it cannot escape from the body. Instead it slows down through multiple collisions with atomic electrons and then combines with an electron to form a positronium[5]. The short-live positronium annihilates to produce two photons with the same energy of 511 keV, which are emitted back-to-back in opposite directions according to the following equation:

$$e^- + e^+ = \gamma + \gamma$$
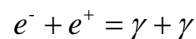
These two photons (γ) must escape the patient's body and then be detected simultaneously in two of the PET detectors.

A PET camera contains several rings of detectors (usually made of scintillation crystals) which are coupled with photo multiplier tubes[6] (PMTs). Whenever two opposed detectors receive two photons with a right energy (around 511 KeV) and within a temporal proximity (few nanoseconds), they'd likely came from the same annihilation. These two photons are recorded by the PET computer system as a "coincidence." Annihilation occurs on the line between each coincidence event (Figure 3).

---

[5] An unstable exotic atom contains an electron and a positron.

[6] Where photons are converted into an electrical signal to be later processed into an image
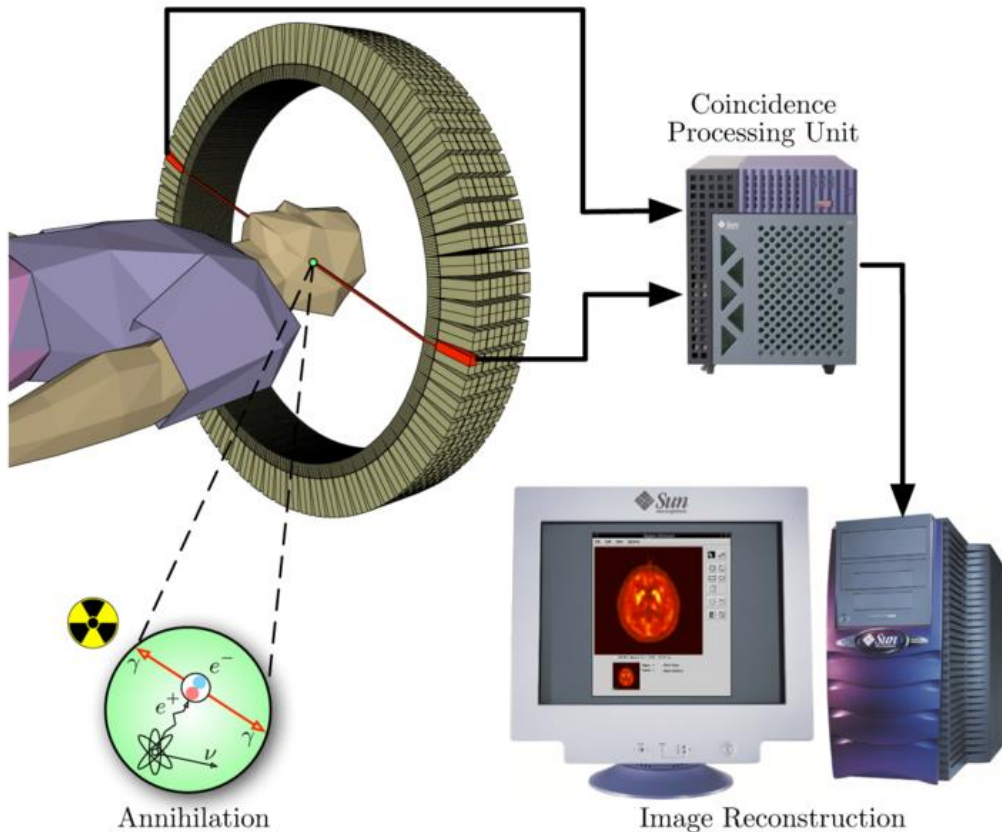
Figure 3: Schematics for a PET acquisition process **(11)**.

An event line records the approximate position of an entry. The lines are then summed up to make a representation of the activity. Because summing up the lines is in fact an averaging operation, the resulting picture would be vague or blurry. In order to improve the picture, a sharpening filter is applied through the process of "filtered back projection." All data is stored in a three-dimensional matrix where each element of the matrix is a cube called a "voxel." A voxel is the smallest element of visualization and represents the average of measurements taken at a point in space.

2.3.3. Tracer

A tracer is a molecule labeled by an appropriate positron emitter isotope and is usually introduced to the patient's body through a vein before image acquisition. This molecule should be of a type that is easily taken up by the cells in a given organ or by a pathological condition.

The preferred radionuclides (Table 1) in PET imaging are those that decay primarily by positron emission and not by electron capture[7] (i.e. that have a high atomic number). These nuclides should also have suitable half-lives. Radionuclides can be artificially produced in a cyclotron and be employed for making a PET tracer.

Table 1: lists the properties of radionuclides that are commonly used in positron emission tomography.

Nuclide	Half-life (min)	E_{max}(MeV)	β^+ fraction	Positron range in water (mm)
^{11}C	20.4	0.96	1.00	3.9
^{13}N	9.97	1.19	1.00	5.1
^{15}O	2.1	1.73	1.00	8.0
^{18}F	109.8	0.63	0.97	2.3
^{64}Cu	762	0.65	0.29	2.3
^{68}Ga	67.8	1.89	0.89	9.0
^{82}Rb	1.27	2.60	0.97	18.0
^{122}I	3.6	1.09	0.77	7.4

Currently, ^{18}F- fluorodeoxyglucose [^{18}FDG] is the most widely used tracer in nuclear medicine. By removing second hydroxyl group from glucose and replacing it with 18-Flourine isotope,

---

[7] When a proton rich nuclide captures its own electron, the electron combined with a proton and creates a new neutron. The atomic number goes down by one.

[18]FDG is produced (Figure 4). The half-life of [18]F (109.8 min; Table 1) is long enough that it makes it possible to be employed efficiently, while at the same time it is short enough not to expose the patient and the surroundings to excessive amounts of radiation after the examination.
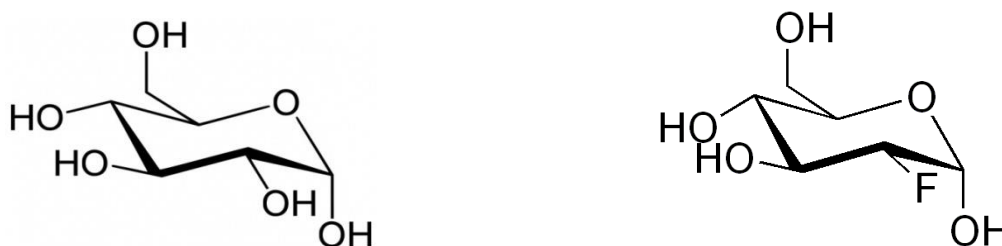
Figure 4: left: Chemical structure of D-glucose monohydrate, right: Chemical structure of [18]FDG.

Glucose is one of the primary sources of energy for cells. It is distributed through the blood and the cellular uptake is regulated by insulin. Molecular weight of FDG is quite close to that of the glucose molecule. This implies that FDG is actively accumulated in most tissues and tumors. The glucose transport mechanism carries the FDG into the intracellular environment where it undergoes enzymatic phosphorylation. Once FDG is phosphorylized, it cannot be further metabolized and is trapped within the cell. Therefore, FDG uptake, as reflected in [18]FDG-PET images, is a good indication of glucose uptake distribution in the cells and can be marker of the degree of anaerobic glucose metabolism. Hence, FDG is useful to identify and characterize tumors.

However, not all tissues with elevated rates of glucose uptake are indicative of malignancy. The FDG-PET scan may also reveal uptake in normal, healthy tissues. For instance, the brain, even at rest, is the dominant site of glucose utilization. Also the heart, particularly the left ventricle, is always in need of energy. Adenomas, fibroids, and inflammatory tissues also have shown intense uptake on FDG-PET scan. Furthermore, the inflammatory response to therapy, either radiation therapy or chemotherapy, will be associated with increased FDG accumulation.

2.4. PET-CT

PET scan is a functional imaging technique and the anatomical information of such a scan is limited. In order to get useful data, combination of PET scan with a structural imaging such as CT scan plays an important role in medical imaging. Almost all PET scanners today are combined with a Computed Tomography (CT) scanner so that the PET images can be fused with the CT images. As mentioned earlier, CT reflects the x-ray attenuation properties in tissue, and is often used as a proxy for tissue density. It reflects the patient anatomy, and is useful for identifying different tissues such as the heart, lungs, muscle, and fat. This information is not reflected in PET images, and so it is common to combine the two in PET-CT scans (Figure 5). This combination provides adequate anatomical detail to improve the anatomic placement of observations and accuracy of the test.

*Figure 5: A PET-CT system (**12**).*

2.5. Standardized Uptake Value (SUV)

^{18}F-FDG PET-CT makes it possible to study the metabolic and anatomic response to therapy in a given patient. Changes in tumor tissue uptake of FDG are frequently reported as change in "SUV$_{max}$". SUV is a semi quantitative value that is independent of patient's size and amount of FDG administered before examination. Although there is some source of bias and variance in estimating of FDG uptake, SUV is still most commonly used in FDG-PET imaging and is mathematically derived from the following formula:

$$SUV = \frac{radioactivity\ concentration\ \left[\frac{Bq}{kg}\right] \cdot Body\ mass\ [kg]}{Injected\ activity\ [Bq]}$$

Activities in the body that cause changes in glucose metabolism can affect the SUV and make the scan interpretations even more complex.

2.6. Radiotherapy

Radiotherapy or radiation therapy generally refers to cancer treatment with high energy particles or electromagnetic waves. Ionizing radiation such as x-rays traverses through the cells of an organ, causing DNA damage. As cancer cells often have less efficient DNA repair, fractionated radiotherapy may give a higher cellular effect in tumor compared to normal tissue. Linear accelerator or Linac (Figure 6) is a device mostly used for external beam radiation therapy. Linacs are based on the acceleration of electrons using strong microwaves and can provide x-rays at various megavoltage energies. The produced x-ray beams may range from 4 to 25 MeV, and can penetrate more or less all parts of the body.

Figure 6: An illustration of Linac system.

Radiotherapy is classified into three branches: curative, adjuvant, and palliative radiotherapy. Curative radiotherapy is prescribed by a radiation oncologist for those patients who have a localized tumor. Sometimes radiotherapy can be used as an adjuvant therapy to other treatments like surgery to ensure sterilization of the residual tumor or tumor bed. For patients with very advanced disease, e.g. with metastasis (distant spread), radiotherapy can be employed as a palliative therapy.

The aim of palliative radiotherapy is to relieve pain and improve the quality of life in patients with a limited survival time. Treatment is rather simple using a single or two opposed treatment beams and is done over a short period of time. Lower doses (compared to curative and adjuvant radiotherapy) are given to patients who received palliative care in order to minimize the side effects.

When the total dose is given to the patient in fractions over a period of time, it is called fractionated radiotherapy. Fractionated radiotherapy is beneficial in some aspects, for example it gives to normal tissue time to repair, and it also lets tumor cells move on to a more sensitive phase of the cell cycle.

2.7. Unwanted Side-Effects of Radiation

It is almost impossible to treat cancer using radiation without exposing healthy tissues. In other words, damage to the normal tissues, especially to those that are close to the tumor, is inevitable. The mammalian tissues respond to radiation in forms of cell death and cell damage together with repair capacity. While the severity of radiation-induced damage in a tissue depends on the RT dose, the onset of damage mostly depends on cell kinetics of the tissue. Tissue's ability to repopulate after irradiation is one of the most important factors in order to determine radiation-induced normal tissue injury. In 1906 Bergonié and Tribondeau reported that the sensitivity of a tissue to radiation is related to its mitotic activity, and decreases with cells' degree of differentiation [cited in (13)]. Non-dividing differentiated cells, such as the ones that build up muscle and lungs, are classified as radio-resistant and relatively unaffected by radiation and continue to function and die at their normal rate. In contrast, bone marrow cells which rapidly proliferate are categorized as radiosensitive cells.

Although radiotherapy represents a good approach to treat a cancer patient, radiation induced toxicity needs to be considered. Such toxicities range from early to late effects and depend on the treatment and organs being treated. Early effects of radiation may be seen a few days or weeks after treatments have started and may go on for several weeks after treatments have ended. Other effects may not show up until months, or even years, later.

2.8. Tarceva or Erlotinib

As we previously discussed cancer originates from a malignant cellular transformation, leading to uninhibited cell growth. Overexpression of Epidermal Growth Factor Receptors (EGFR's), which allow cells to divide and grow uncontrollably, have been found in many cancer types such

as lung cancer[8]. Some studies have shown that certain types of drugs, like tyrosine kinase inhibitors (TKIs), can help treat these kinds of cancers.

The use of TKIs belongs to a new class of treatments called targeted therapy. Generally, targeted therapy targets specific genes prevent cancerous cells from growing. TKIs block EGFR from working, resulting in a stop or slowing down tumor growth. The drug Tarceva (Figure 7) is an EGFR inhibitor. A series of trials have shown that Tarceva improves the survival of patients with advanced incurable NSCLC who have failed standard therapy (14). Therefore, Tarceva is an approved medication therapy in lung cancer.
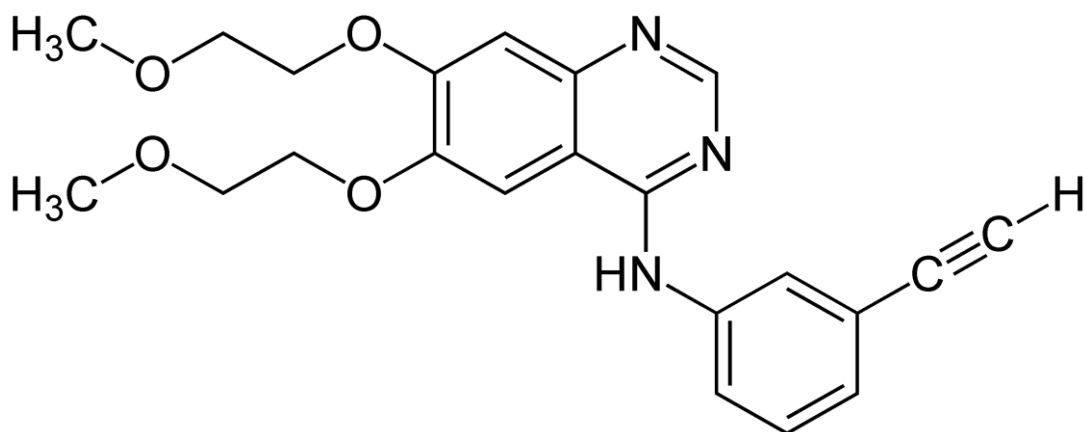

*Figure 7: Tarceva chemical structure (**15**).*

The material in this chapter was also adapted from (16) (17) (18).

---

[8]*EGFR testing helps us move toward our goal of tailoring treatments for the patient.*

3. Material and Methods

3.1. ^{18}F-FDG PET-CT scanning and data preprocessing

3.1.1. Acquisition

This project includes 22 patients with advanced non-small cell lung cancer who have received fractionated palliative radiotherapy (3×10 Gy) at Oslo University Hospital. The patients have been recruited into the ThoRaT (Thoracal Radiotherapy and Tarceva) study, which has been approved by the regional committee for health ethics and is currently running. A written informed consent was obtained from all patients. The current study, which focuses on data analysis, has no consequence for the patients whatsoever. The patients included have undergone at most three ^{18}F-FDG PET-CT examinations using a Biograph 16-scanner (Siemens, Germany); one prior to radiotherapy, one at mid therapy (after typically 15 Gy), and one six weeks after therapy.

Thirteen of these patients who have undergone thoracal radiotherapy also received oral Tarceva[9], once every day, from the day before start of radiotherapy. Nine of the 13 patients finished with the Tarceva in the last day of radiotherapy and the remaining 4 patients had Tarceva maintenance treatment until disease progression.

Before the treatment started, patients underwent a pre-treatment CT scan (CT simulation) using a light speed ultra-scanner (GE medical systems, USA). The CT image series is then sent to a radiotherapy planning program, in this case Oncentra Planning (Oncentra ® External Beam, Elekta, Sweden). Here, the treatment is planned on the basis of the tumor location and anatomy of the given patient, as reflected in the CT images. Treatment plan include two opposed 6 MV photon beams and the fractionation is 3 Gy × 10. For the purpose of the current study, the planning CT is used to delineate various parts of the thoracic area such as Gross Tumor Volume

---

[9] 150 mg p.o. (independent of the patient's body surface)

(GTV), lymph nodes, Ipsilateral Lung (IL), Contralateral Lung (CL), heart, bone marrow, and esophagus.

In oncology, a routine ^{18}FDG-PET acquisition protocol consists of several steps. Since tumor uptake of FDG is not insulin dependent, FDG-PET imaging is augmented in the fasting state. Blood glucose is lower in fast patients and the image is less contaminated with muscle activities. In this regard, patients should not eat and drink liquid containing fat or sugar (for instance milk) at least six hours prior to the examination. An appropriate hydration is required for FDG secretion and patients are told to drink water before examination is performed.

Blood glucose level should be determined prior to FDG administration. If blood glucose is too high[10] the quantitative measurements are not considered valid and depending on this level the examination could be postponed. Tracer is administered at least one hour before data acquisition and patients are examined with CT scan followed by PET scan. The amount of FDG may vary from scanner to scanner, at the Radiumhospital, adults receive approximately 400 MBq.

After injection of FDG, patients should avoid excess movement and exercises both mentally and physically. She/he has to lie down in a quiet room and relax. Also, it is important that the patient feel warm and comfortable. All these precautions are to avoid unspecific FDG uptake in the muscles and brown fat.

3.1.2. PET-CT images

In this project, PET and CT images are acquired in the same scanner and are produced in the DICOM[11] (Digital Imaging and Communications in Medicine) file format. The images can be displayed and further analyzed with the help of Interactive Data Language (IDL).

A DICOM file consists of image and also patient and image data which are placed in the header. The DICOM header consists of different variables that are extracted from the data object and can

---

[10] Fasting blood glucose range is between 5.1-6.8 mMol/L.

[11] A standard for file exchange in medical imaging developed by NEMA, National Electrical Manufacturers Association

be read by the program called eFilm DICOM Dump. Two numbers correspond to each of these variables and are called hex codes. Some of the important properties of such variables are listed in Table 2.

Table 2: List of Dicom hex codes. The two leftmost columns are the identification tag. The Dicom value is the value returned by the IDLffDICOM object when the GetValue (hex1, hex2) is called.

Hex codes		Dicom value
0028	0010	Rows
0028	0011	Columns
0028	0030	Pixel spacing
0018	0050	Slice thickness
0028	1053	Rescale slope
0020	0032	Image position
0018	1072	Radionuclide start time
0018	1074	Radionuclide total dose
0020	0013	Instance number
0008	0032	Acquisition time
07FE	0010	Pixel data
0028	1053	Rescale slope
3004	000E	Dose grid scaling

3.2. IDL

Interactive data language is platform independent, array-oriented program for scientists and can be used in the analysis and visualization of multi-dimensional data sets. It has grown out of programs written for analysis of various NASA mission's data such as Mariner. IDL is a computing environment which can help visualize and analyze any modality of medical imaging.

This program has extensive coding rules and syntax. In the current project, one of the main tasks was to create a program in IDL that can read DICOM files and co-register different image modalities.

3.2.1. Reading medical imaging data

In order to open and read arbitrary DICOM files from the specified disk file, IDLffDICOM must be used. IDLffDICOM object is one of the several file reader classes that contains the data of the image embedded in a DICOM file and can only read DICOM tags. Below are example code lines:

```
obj= OBJ_NEW('IDLffDICOM')

files= FILE_SEARCH ('*', count= nct)

read=obj->Read(files(0))

dim_x=obj->GETVALUE('0028'x, '0011'x,/NO_COPY)
```

The *OBJ_NEW* allocates the memory needed to store the data read from the file. The *GETVALUE* function uses appropriate set of hex numbers that belong to desired variable. The '*x*' after these two numbers implied that they should be read as hex values.

The *FILE_SEARCH* function returns a string array containing the names of all files matching the input path directory. The returned array contains pointers to all elements in the object. This function returns -1 if no matching element is found. The keyword *No_copy* is used when we want the pointers returned point to the actual data (not copied data) in the object for the specified DICOM tags.

Columns and rows give the number of pixels, or matrix size, in x and y direction. For example in this project, number of pixels in the CT images is 512×512 and in the PET images is 168×168. The number of image slices (in the z direction) is equal in both image series, but can vary between patients. The slice thickness is 5mm for both CT and PET images, while the difference between the two consecutive z-positions is 3 mm. This implies that there is an overlap between the two consecutive slices. Z-position together with x and y position can be found in image

position variable. Image position is such a variable stored in the DICOM header as a string point array. In order to get the floating point array the *STRSPLIT* function were used (following lines) which splits image position string argument into separate substrings. The *FLOAT* function then converts substrings into a single-precision floating-point value.

ct_pos=obj->GETVALUE('0020'x, '0032'x,/NO_COPY)

ct_pos=*ct_pos(0)

ct_pos = FLOAT(STRSPLIT(ct_pos,'\', /EXTRACT))

3.2.2. Displaying medical imaging data

After reading the desired data in IDL, the next step is to visualize image data. There are several methods to perform this task. The most commonly used methods for displaying static medical images is "direct graphics". This method provides with number of commands[12] for quickly displaying images which are stored as two dimensional arrays in IDL. Medical images separate into gray scale and RGB. Gray scale images are represented by a two dimensional array of numbers which are proportional to pixel intensity or brightness. On the other hand, in three dimensional RGB images, each pixel is labeled with mix of three colors, red, green, and blue which represent the resulting color of the certain pixel.

To evaluate the right SUVs for different delineated organs of our interest in thoracic area, we need to first be sure that all images are precisely overlaid. This has been done in several steps that will be discussed in the following paragraphs. However, before introducing co-registration of the images, some corrections must be done in order to get a right data value for PET, CT, and dose images.

In PET image decay correction is needed before convert image data to SUV map. The decay constant λ is equal to $\lambda = \dfrac{\ln 2}{t_{1/2}}$; which $t_{1/2}$ is the half-life of the radioactive material (i.e. 109.771 for FDG). The decay correction, *A,* is then derived by the equation below:

---

[12] Such as TVSCL, TV, etc.

$$A = \exp[\lambda.(t_1 - t_0)]$$

Where t_0 is the radionuclide's start-time and t_1 is acquisition time and they were extracted from the PET images' header and converted to decimal system before they used in decay correction. Radionuclide activity, rescale slope, and patient's body weight[13] are the other parameters that need to be considered in SUV calculation. Rescale slope is a conversion factor to map the values stored in the data array to the actual units in MBq/ml in PET.

Pixel value in CT image represents mean attenuation of the tissue, ranging between 0 and 4000. In order to get a Hounsfield Unit (HU) from image data the following linear transformation is applied:

$$HU = pixel\ value * Rescale\ slope + Rescale\ intercept$$

Both rescale slope and rescale intercept can be found in DICOM header and are equal to 1 and -1024 respectively. Accordingly, the HU range is from -1024 to 2976 or more.

The third consideration that we need to take into account is how to manipulate RT dose image in order to get the right dose response for different organs. The RT Dose module is used to convey 3D array of radiation dose data generated from treatment planning systems and gives us the information about amount of dose received in various parts of irradiated tissues. In the current study the attributes defined within the module support dose for single beam comprising a complete treatment plan. In order to get the whole dose over thoracic area we summed two opposed beams. It is important to multiply each dose frame by dose grid scaling before summation. Pixel value in RT dose image is a relative dose to an implicit reference point and is not in Gray units. Dose grid scaling value is a factor for converting dose data from pixel value to Gray.

---

[13] In this project, patient's weights are lost in the header after the patients' identities are removed. We entered this data into the program manually.

3.2.3. Co-Registration of images

Accurate alignment between CT and PET images is vital especially when it comes to analysis glucose uptake value of GTV and organ at risk. This is done by visualizing both CT and PET images simultaneously in the same window and applying an appropriate program to minimize the misalignment. The best parts to consider if these images are aligned or not are bone and rib cage. CT and PET images from each session were not always overlaid precisely. In order to remove a shift that causes this problem, one can calculate the shift in x and y directions[14] (code line below) and apply it on the PET image.

diff=[round((pt_pos(0)-ct_pos(0))/ref_res(0)),round((pt_pos(1)-ct_pos(1))/ref_res(1))]

Pt_pos are positions of PET image and *ct_pos* are positions of CT image, index 0 and 1 correspond to x and y direction respectively. This adjustment was minimal since each ^{18}F-FDG PET-CT scans was done in the same machine and may affect only the borders.

PET and CT images have different resolutions. PET scan usually has a poorer resolution compared to CT scan. In PET-CT fusion display, PET slice interpolated to the same resolution as the CT to get a smooth image. Image fusion for all the patients in three different slices; transversal, sagittal, and coronal had been checked to validate the IDL program that is made in this respect (Figure 8-A).

Since radiotherapy treatment planning was made based on planning CT, co-registration of planning CT image and RT Dose image had been done by employing an appropriate positional shift. Validation of this co-registration was acquired with the help of fused planning CT image and RT Dose image for all of the patients (Figure 8-B).

---

[14] There is no need to shift PET in z-direction because all CT and PET images are sorted.
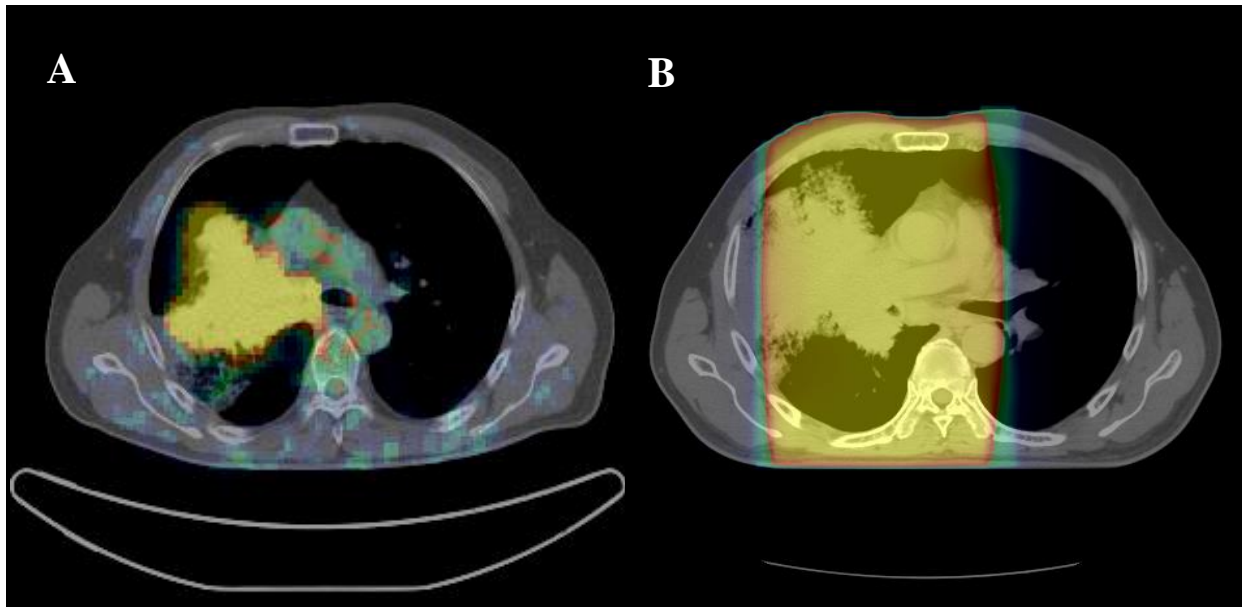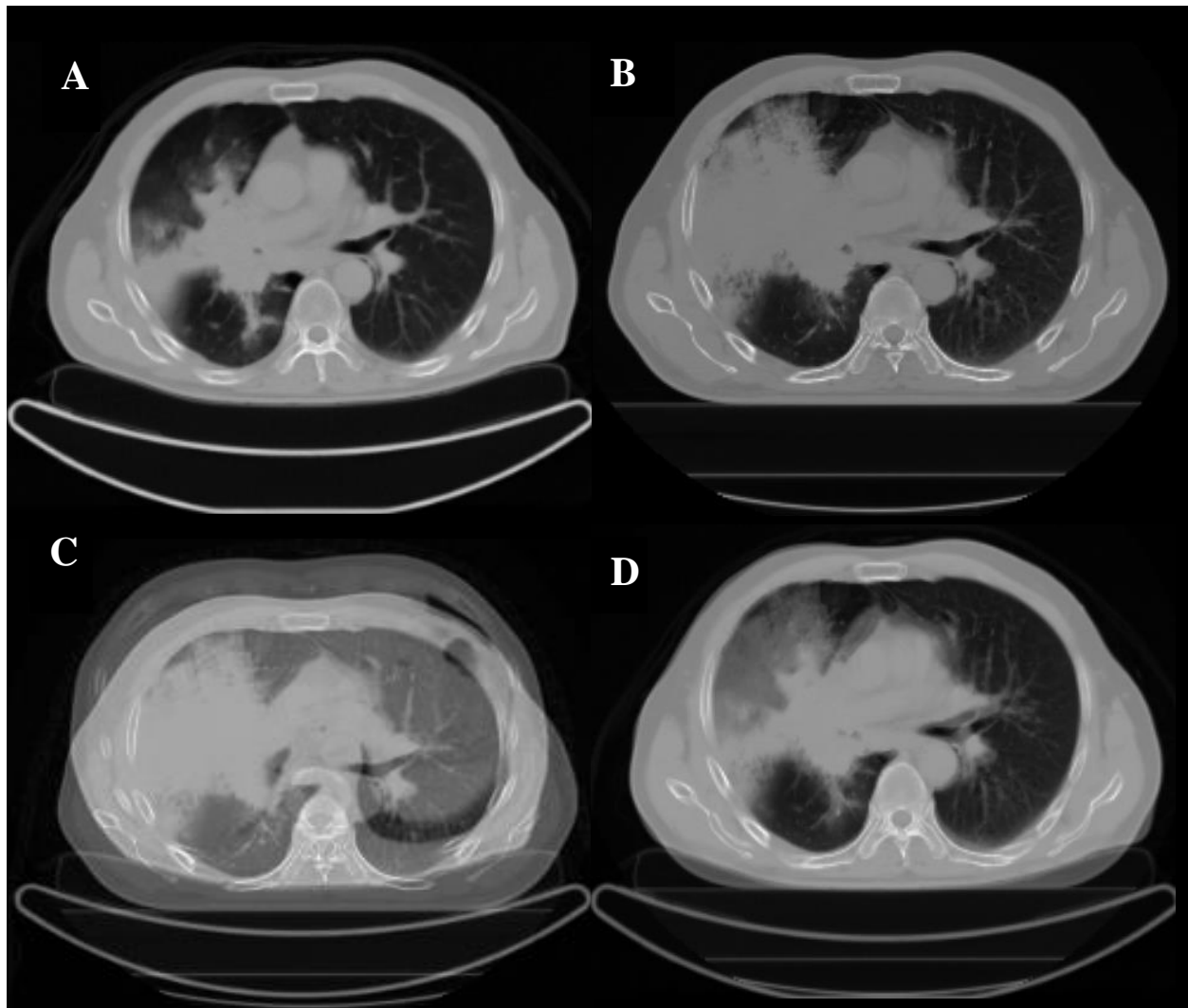
Figure 8: A transversal slice chosen from patient 3 at mid-therapy session. A: Co-registered PET-CT is demonstrated. B: Co-registered planning CT and radiotherapy dose distribution is demonstrated.

Up to now all PET-CT scans and planning CT-RT dose are co-registered. Since all the radiologist's delineations have been done based on the planning CT, all available sets of PET-CT images need to be co-registered with planning CT. Considering that CT and planning CT scans are acquired in a different machine, they don't have the same reference coordinate and hence FOV (Field Of View) is different for these two images. In order to deal with this registration, the IDL codes in this subroutine search for the maximum correlation between each sets of CT image and planning CT image and the calculated shift in x, y, and z directions is then applied on CT sets (Figure 9). Once each sets of CT image co-registered with planning CT image, we can use the same shift on PET sets to have planning CT and PET sets co-registered. All the excess data, out of the thoracic area, in PET-CT scans was cut-off with the help of the calculated shift in the z-direction.

In this part of the program when correlation was applied, we encountered a memory problem; because arrays were too big. In order to deal with memory problem and also get unify resolution for all the images, we introduced a reference resolution (*ref_res*) and interpolated all the

resolutions to this resolution. From now on all of the images (PET-CT, planning CT and RT dose images) have 3mm resolution in x, y, and direction.

Figure 9: A transversal slice chosen from patient 3. A: CT image from mid-therapy session, B: Planning CT image, C: Un-shifted CT and planning CT, D: Co-registered CT and planning CT.

After this final adjustment, all the images were overlaid precisely on the planning CT. The delineations from the planning CT can be used to extract desired data from different PET-CT sessions to see how these data change, for example, with dose value and time. The following images were registered PET images from different sessions on planning CT image (Figure 10). Data from these registrations together with contours in planning CT provide us with useful

standard uptake value in various organs and how the SUV of such organs change with time and dose.
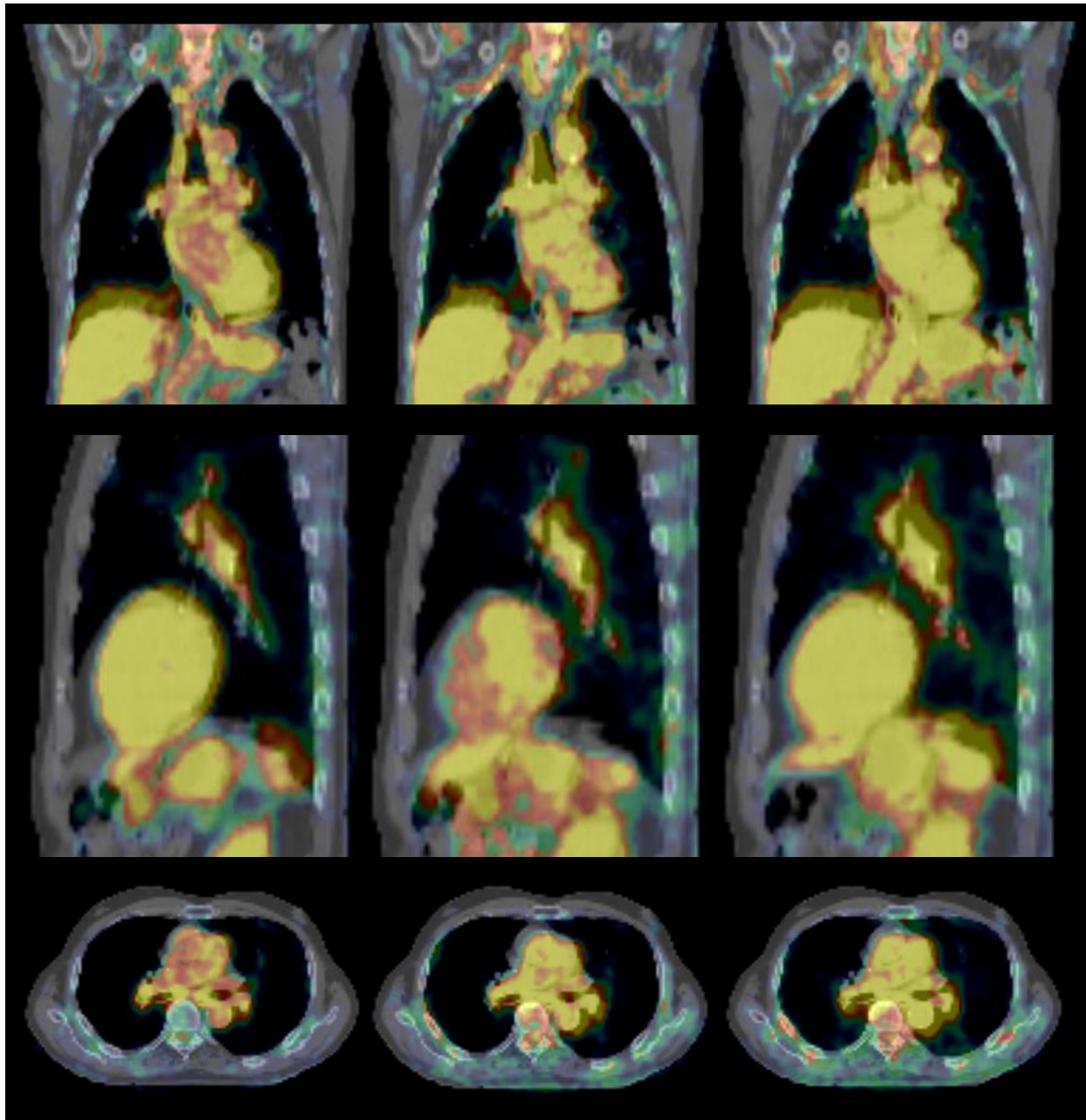
Figure 10: Co-registered planning CT and PET scans of patient 6 at different time points. The left column corresponds to prior to treatment, the middle to mid-treatment and the right to post-treatment. The upper, middle, and lower images correspond to the coronal, sagittal, and axial plane, respectively.

In this phase of the project, different contours were used as an index both on CT and PET data to extract SUV and CT number belonging to these contours (Figure 11). Because there is usually some error on registration of images and in order to be sure that glucose uptake in GTV and lymph nodes does not affect the other organs of interest, dilate command was applied on GTV and lymph nodes delineation to make a margin around it and then to use this new object carved out of other organs. In addition, for lungs, margined contour of heart, esophagus, and bone marrow had been carved out. Also we used a CT number window between value of 100 and 800 for lung in all CT sessions in order to make sure that all of the voxels included in the lungs are indeed lungs.
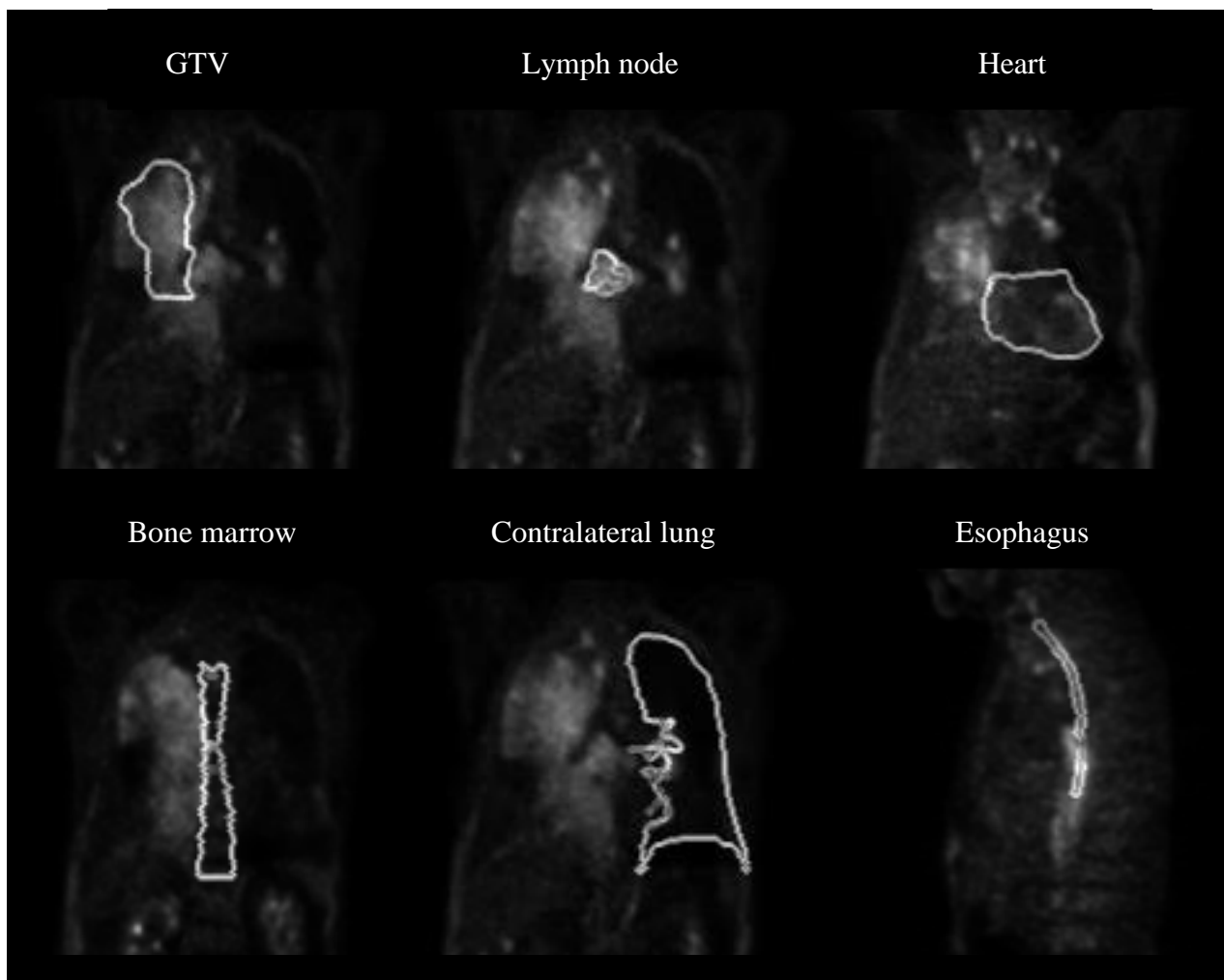
Figure 11: Illustration of various delineations, laid over mid-therapy PET scan slices from patient 1

3.3. Data analysis

The SUVs of various organs which are stored in voxels and come in 3D matrix can be presented in histograms. In this study, the histogram refers to a graph that is generated from the number of voxels in an image containing values of a specified intensity range. The signal intensity may be expressed as Becquerel's per voxel or as a Standardized Uptake Value. The total value range, the maximum value of the data points minus the minimum value of the data points, is divided into bins with equal lengths. Larger bins draw a coarse representation and eliminate the noise while smaller bins provide higher resolution. For each bin, the voxels in the region of interest that have a value within the bin range are counted. This value is then normalized to the total number of tumor voxels.

In order to have an overview of how SUV in different organs change with sessions, it is common to reduce SUV of patients to the mean value. Mean includes all data points but gives a dependency on the definition of the border and as such introduces inter observer variability. If the delineation of organs is done in a strict way less of the surrounding tissue is included and a higher mean will be calculated. The value is however robust and rather independent of noise. Furthermore, the tumor and lymph nodes could also be represented with their single highest value, which is maximum value (SUV$_{max}$). This value represents the most active part of the tumor or affected lymph nodes.

Can we identify any changes in SUV of OAR's with dose? In order to answer this question, first total dose was binned to the size of 0.5 Gray in order to have clear trance of SUV. Second, SUV$_{mean}$ was calculated over each dose bins and SUV versus dose is plotted (Axis x shows the delivered percentage of dose). Example below shows such a plot for ipsilateral lung of patient 4 in mid-therapy and post-therapy since pre-therapy PET scan is not linked to RT dose (Figure 12). The same technique was applied to plot density response versus RT dose in the lung tissue.
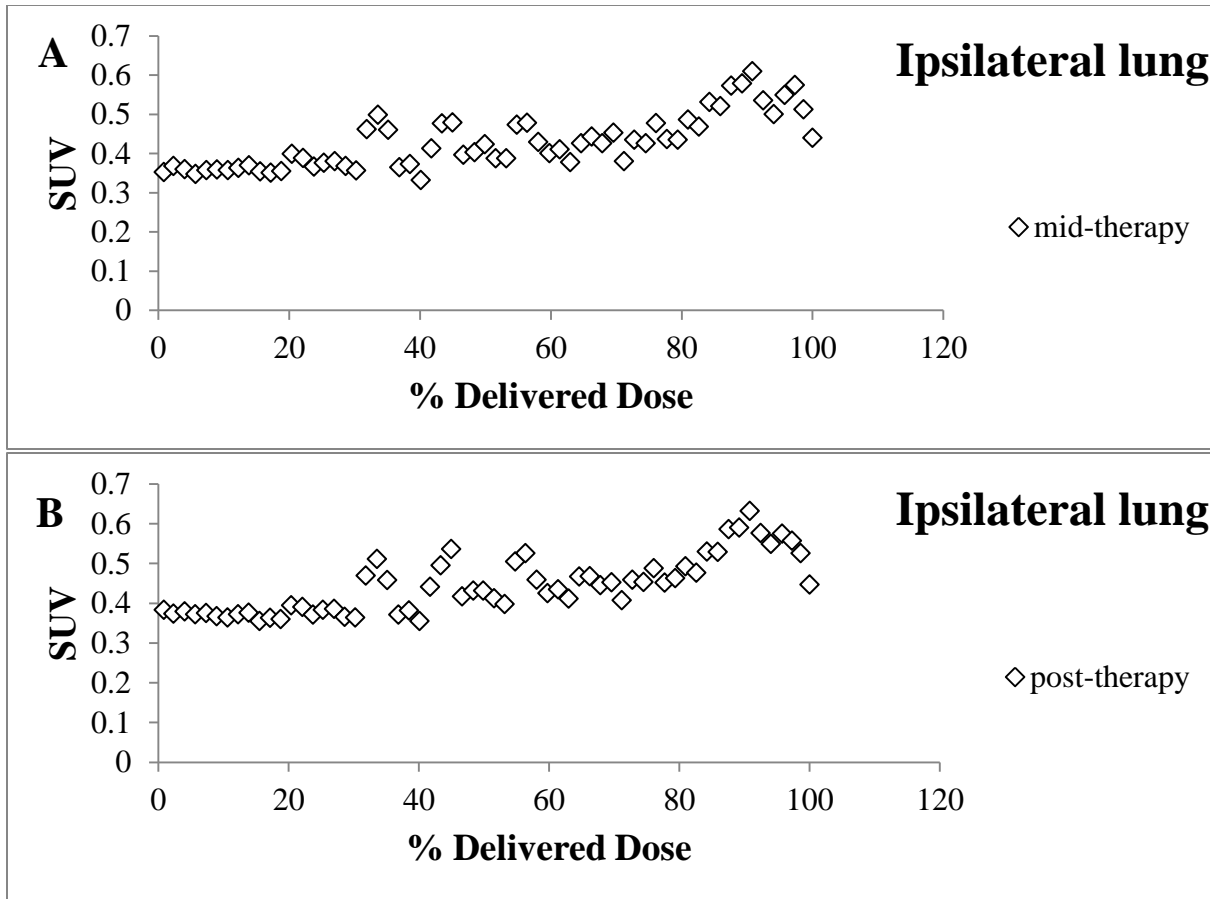
Figure 12: SUV in the ipsilateral lung versus percentage delivered dose from patient 4. A: at mid-therapy, B: at post-therapy session.

3.4. Box-Whisker plot

Box-whisker plot is an exploratory graphic and is a helpful way to display the distribution of the data. The box plot displays data broken down into three quartiles, each with an equal number of data values. Furthermore, the lines extending vertically from the box are called whiskers, showing the variability outside the upper and lower quartiles. The plot also shows where the mean of the data lies. Below is a formal description of the statistics:

Q1 – quartile 1: the median of the lower half of the data set (25th percentile).

Q2 – quartile 2: the median of the entire data set.

Q3 – quartile 3: the median of the upper half of the data set (75th percentile).

Mean Value: the average value of the entire data set.

Extreme Values: the smallest and largest values in a data set.

3.5. Statistical Inference

3.5.1. Mann-Whitney U-Test

In order to identify significant difference in glucose uptake level between two sessions, Mann-Whitney U-test (Also known as the Mann-Whitney-Wilcoxon (MWW) or Wilcoxon Rank-Sum Test) was applied. This test is a great substitute for two-sample t-test, since the distributions of data in this project are unknown and they do not necessarily come from a normally distributed population. On the other hand, Mann-Whitney U-test is suitable for a sample size smaller than 20. This test is used to test the null hypothesis that two populations have identical distribution functions against the alternative hypothesis that the two distribution functions differ only with respect to their medians.

In order to calculate the U statistics, the combined set of data is first arranged in ascending order with tied scores receiving a rank equal to the average position of those scores in the ordered sequence. If R_1 and R_2 denote the sum of ranks for the SUV level of patients included in 2 different sessions for certain organ, The Mann-Whitney test statistic (U) is then calculated using the following formulas:

$$U_1 = N_1.N_2 + N_1(N_1+1)/2 - R_1$$
$$U_2 = N_1.N_2 + N_2(N_2+1)/2 - R_2$$
$$U = Min(U_1, U_2)$$

Here, N_1 and N_2 are the sizes of the two samples (sessions).

We next compare the value of calculated U with the value given in the Tables of Critical Values (Table 6) for the Mann-Whitney U-test, where the critical values are provided for given N_1 and N_2, and accordingly accept or reject the null hypothesis (p = 0.05).

Sample size in different sessions was equal to the number of patients examined in pre-therapy, mid-therapy, and post-therapy session which was 14, 19, and 7, respectively (patient 12 and 24 were missing contralateral lung structures, and delineations for heart and esophagus of patient 15 were not available).

3.5.2. 95% confidence interval

SUV levels are measurements of uptake values and are subject to errors of measurement. These instrumental and human errors can be considered as a source of noise (with a random nature). We assumed SUV levels (relative to dose) in each session were samples taken from the unknown variable of "glucose uptake relative to dose." Then, the two unknown variables are different with 95% accuracy if their 95% confidence–intervals are completely separate (no joint interval).

The variables discussed in this work (for example, glucose uptake values for mid-therapy and post-therapy) are not directly observable, instead, the results of the measurements of SUVs show "samples" taken from these variables. In order to see if the uptake values (relative to dose) in mid-therapy and post-therapy are indeed different, we need to perform a statistical significance test. A 95% significance test of the difference determines if the difference in two variables is due to naturally occurring phenomenon and not contributed to chance alone.

The same test was used to identify significant differences between Tarceva receiving patients and non-Tarceva receiving patients at mid-therapy and post-therapy session.

The material in this chapter was also adapted from (19) (20) (21).

4. Results and analysis

4.1. Visual inspection

In this study, morphological changes in normal lung tissue and tumor tissue varied between patients. In Figure 13 and Figure 14, there are two extreme examples of patients with respect to anatomical changes during the examination period. These changes are presented from the planning CT acquisition to the last session of ^{18}F-FDG PET-CT examination.

Figure 13 shows transversal and coronal slice including GTV for patient 1. Changes in lung anatomy over time are obvious. It appears that the lung is progressively occupied by tumor tissue and possibly also some pleural fluid. The patient died before reaching the post-therapy session.
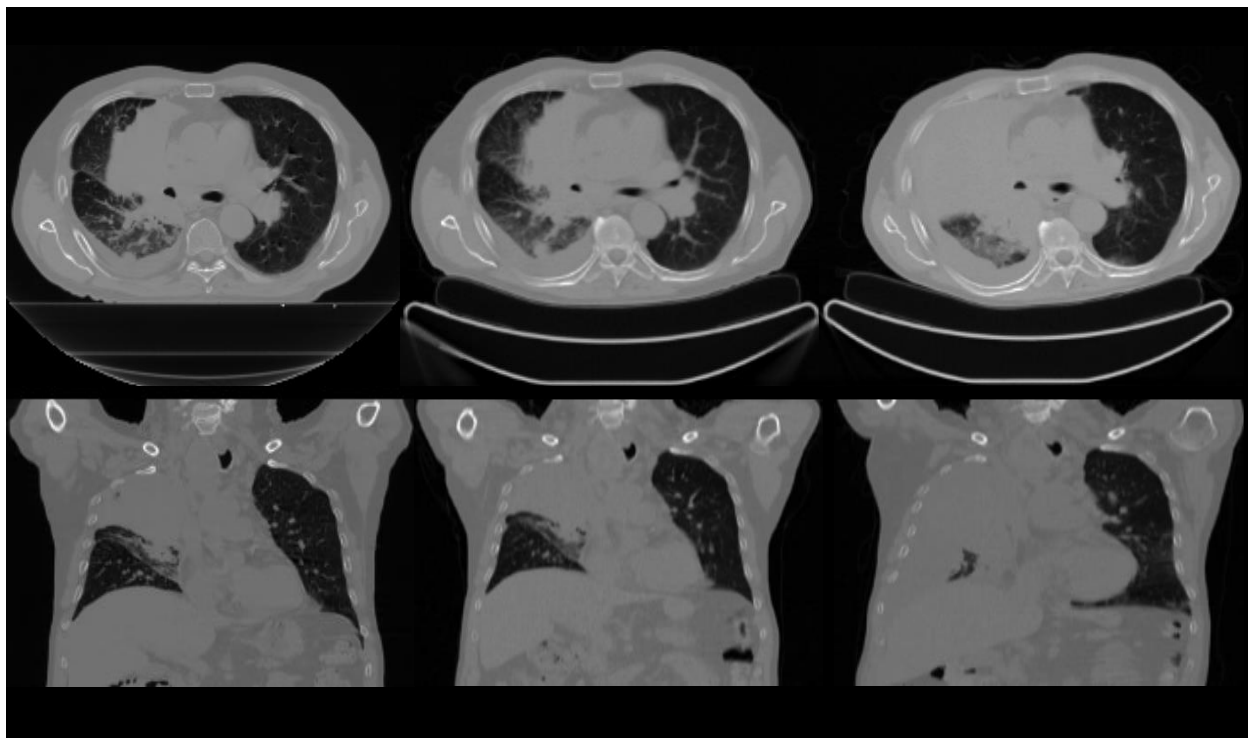
Figure 13: CT scans of patient 1 at different time points. The left column corresponds to planning CT, the middle to pre-treatment, and the right to mid -treatment. The upper and lower images correspond to the axial and coronal plane, respectively.

Figure 14 shows transversal and coronal slices for patient 4. As opposed to patient 1 above, the lung anatomy is more stable over time. The patient lived 14 months after post-therapy examination.
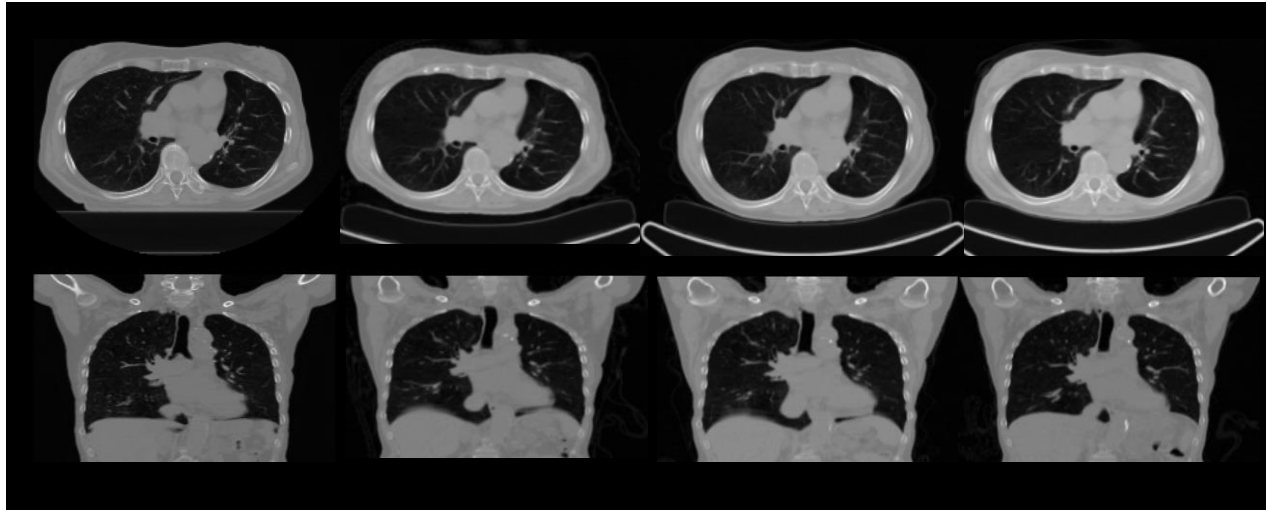
Figure 14: CT scans of patient 4 at different time points. The first column from left corresponds to planning CT, the second to pre-treatment, the third to mid-treatment, and the forth to post-treatment. The upper and lower images correspond to the axial and coronal plane, respectively.

PET images can be condensed, as explained in section 3.3, to histograms for further analysis. As an example, histograms of the GTV of patient 21 (Figure 15) were plotted for three sessions. By looking at pre-therapy histogram, we realize that SUV_{max} was about 21. The histogram was shifted towards the lower values as large parts of the tumor have values close to 2. In the histogram plotted for the mid-therapy, SUV_{max} increased to 23. The histogram has more or less the same shape as for pre-therapy with a slight shift towards higher values. In the histogram plotted for post-therapy, SUV_{max} decreased to 14.
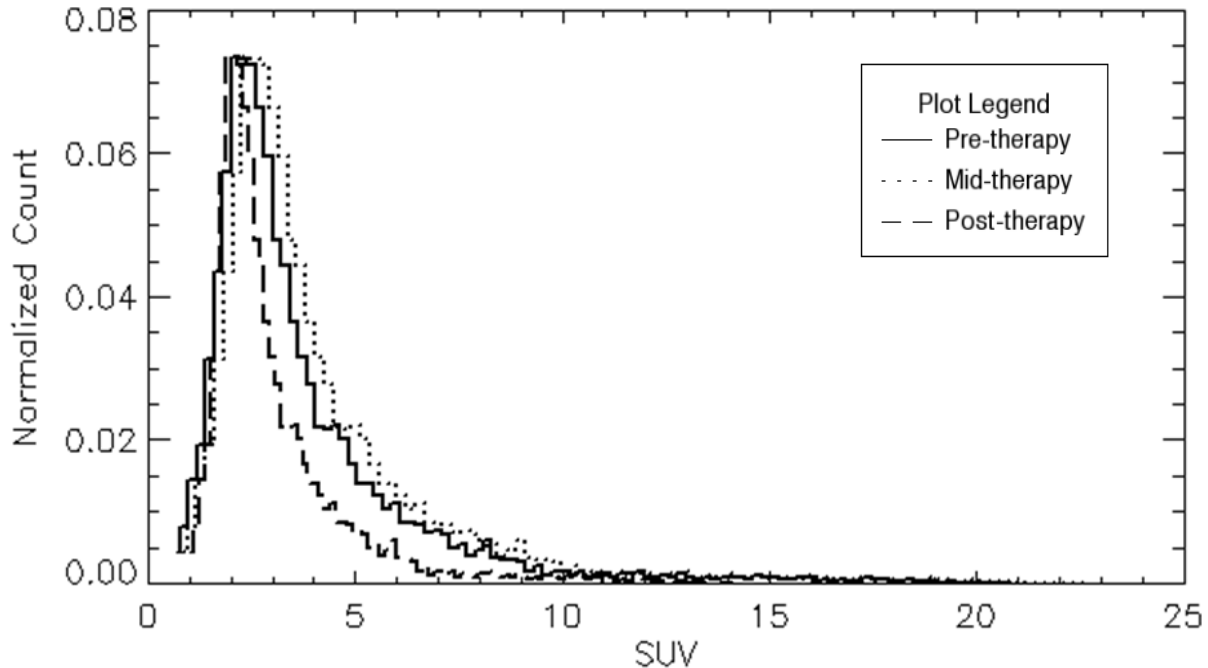
Figure 15: GTV histograms plotted for patient 21.

4.2. Glucose metabolism

4.2.1. Temporal characteristics

In this part, box plots for SUVs were generated to demonstrate the spread of the glucose uptake value across all available sessions for GTV and various organs such as lung, esophagus, heart, and bone marrow. These plots demonstrate how SUVs are distributed in each session and whether there are potential unusual observations in the data set.

The Box-whisker plot (Figure 16) shows an overall distribution of SUVs in GTV for the available sessions across all patients. The mean value was greater than the median value, this expresses that data was "skewed" towards the lower SUV values. The difference between mean and median was quite apparent for some patients. For instance, in patient 7, we observed $SUV_{mean}–SUV_{median}=2.7$ in both sessions. The reason for such a large difference could be the observation of very large SUV_{max} for this patient; the SUV distribution for this patient is more skewed compared to other patients. Other notable patients with large differences in SUV_{mean} and

35

SUV$_{median}$ were patient 21 and patient 16. Comparably, some patients (such as patient 6) have had more symmetrical SUV distributions.

Figure 16: Box-whisker plot showing the overall distribution of SUVs in the tumor for the available sessions across all patients.

The Box plot in Figure 17 shows the SUV distribution in the heart. It was evident that SUV$_{min}$ was about 0.2 for all patients while SUV$_{max}$ differed dramatically across patients (from 3.2 to 21.5). The SUV distribution was rather narrow for most of the patients and small differences between mean and median of SUV implied a symmetrical distribution of glucose uptake in the heart. Again, SUV$_{mean}$ > SUV$_{median}$ showed a skewed distribution towards lower values. Relatively large SUV$_{mean}$ − SUV$_{median}$ in few patients was a result of high maximum in SUVs.
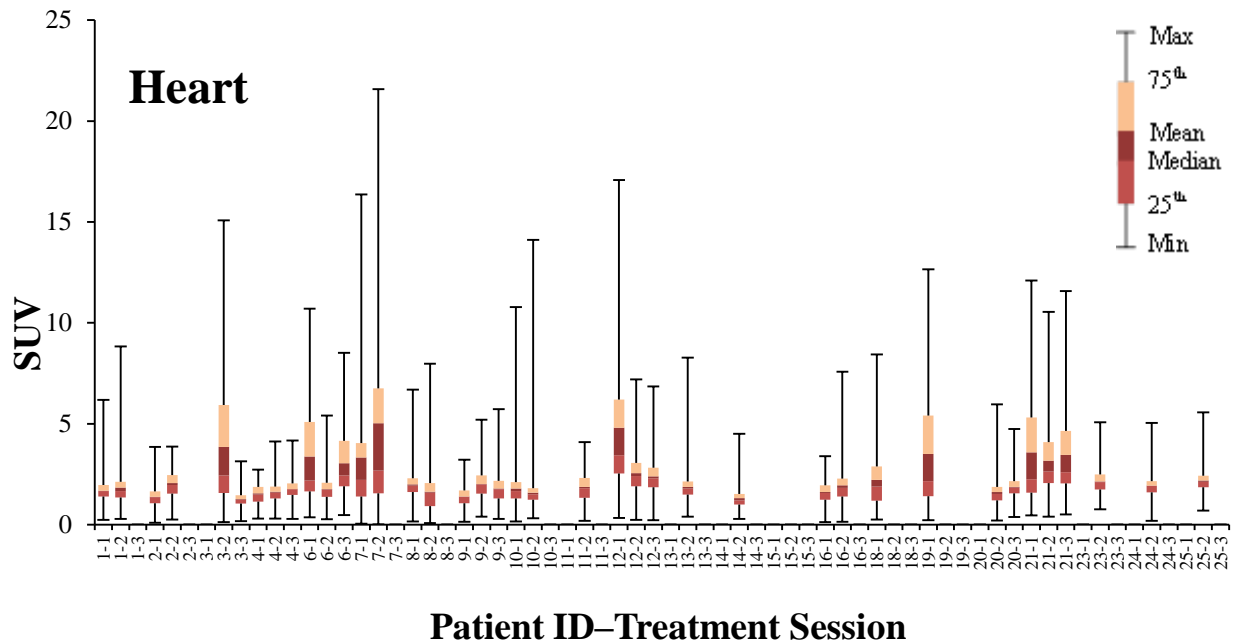
Figure 17: Box-whisker plot showing the overall distribution of SUVs in heart for the available sessions across all patients.

SUV distribution in esophagus is plotted against the session of a given patient's examination in a Box plot (Figure 18). SUV_{min} was between 0.1 and 0.5 for all data. SUV_{max} ranged between 2 and 7 for most patients. Patient 10 again had a very high SUV_{max} (over a value of 15) compared to other patients.
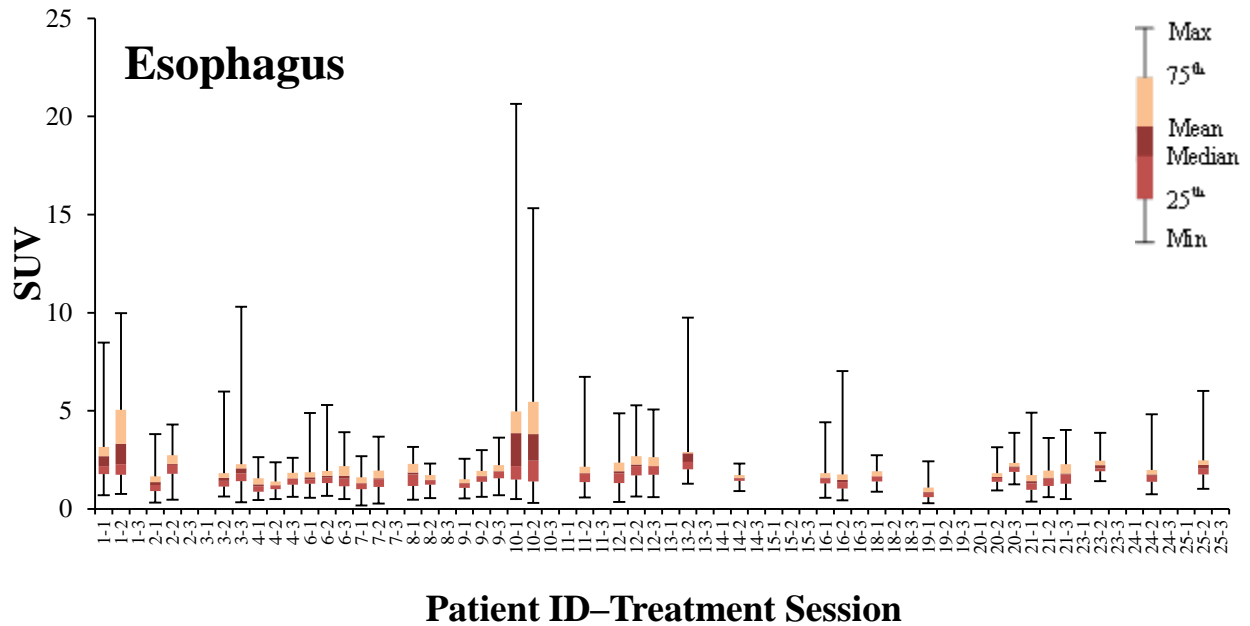
Figure 18: Box-whisker plot showing the overall distribution of SUVs in esophagus for the available sessions across all patients.

The Box plot in Figure 19 shows the SUV distribution in the bone marrow. The difference between first and third quartiles (or interquartile) was relatively narrow. $SUV_{max} - SUV_{min}$ was less than 7 for most patients. SUV_{min} was close to 0.2 for most patients. Patients 10 and 21 had a SUV_{max} that is dramatically larger than for the other patients.
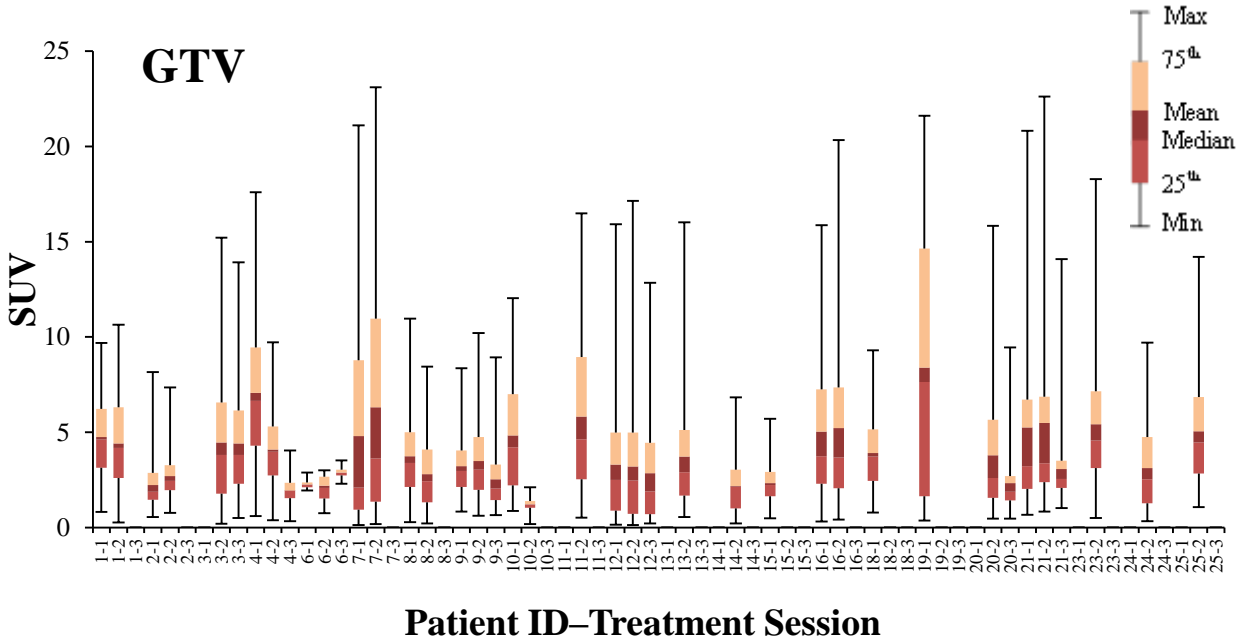
Figure 19: Box-whisker plot showing the overall distribution of SUVs in bone marrow for the available sessions across all patients.

The Box plot in Figure 20 shows the SUV distribution in the ipsilateral lung. In this plot a wide range of SUV_{max} can be seen. The interquartile was relatively small. Patient 21 (at pre-therapy session and post-therapy session) and patient 10 (at pre-therapy session) had the largest value of SUV_{max}, which was approximately 18.
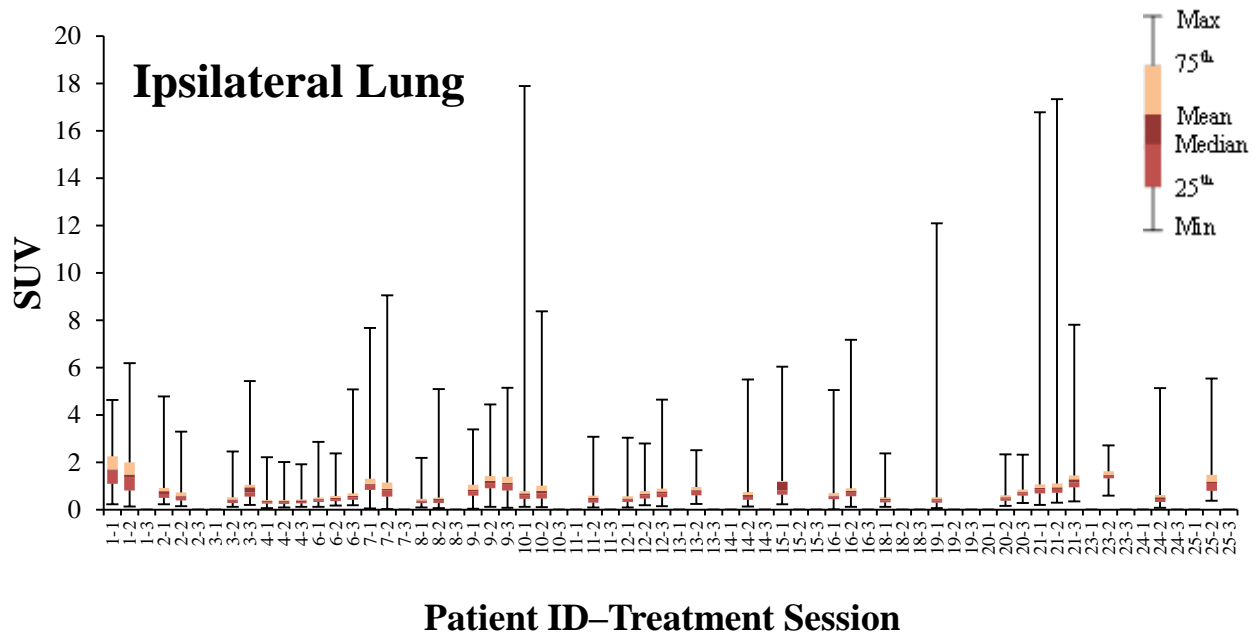
Figure 20: Box-whisker plot showing the overall distribution of SUVs in ipsilateral lung for the available sessions across all patients.

The Box plot in Figure 21 shows the SUV distribution in the contralateral lung. It can be observed that SUV_{min} was close to 0.1 for most patients, while SUV_{max} differed from patient to patient and across sessions. The two highest SUV_{max}'s of 9 and 10 belonged to patient 11 and 10 at mid-therapy session, respectively. Patient 1 had the largest interquartile compared to other patients.
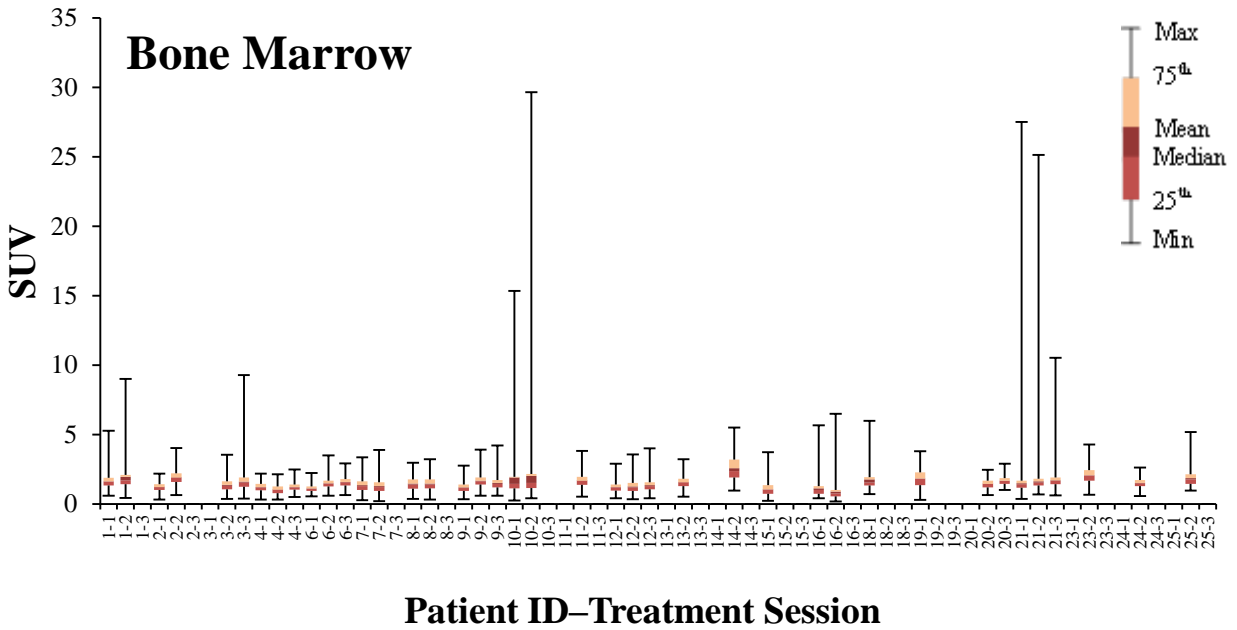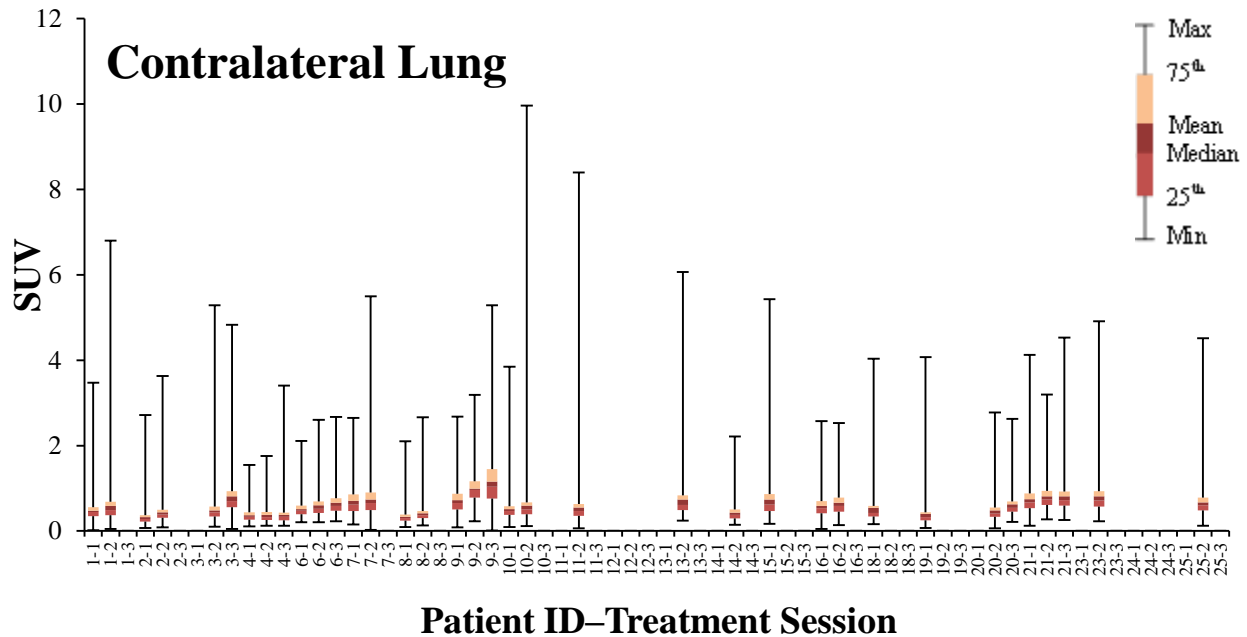
Figure 21: Box-whisker plot showing the overall distribution of SUVs in contralateral lung for the available sessions across all patients.

4.2.2. Time trends

In the following, the temporal changes observed in SUVs are presented. The following plots were made based on different statistical values such as SUV_{mean}, SUV_{median} and SUV_{max} for patients in various sessions. The average of the data points was also shown (as a red square) in the diagrams. Results were further expressed as SUV_{mean} ±SD (Standard Deviation) for all patients across sessions. Mann-Whitney U-test then was used when searching for significant differences between these two groups in each session (Table 7).

In Figure 22, SUV_{max} from patients' GTV were plotted across sessions. A large heterogeneity in the changes of SUV_{max} for GTV was observed during radiotherapy for the patients. The SUV_{max} was 12.6±6.0 before start of radiotherapy (pre-therapy session), which slightly increased to 13.0±6.1 at mid-therapy session. Six weeks after radiotherapy (post-therapy), SUV_{max} decreased to 9.5±4.4. Analyzing the subset of patients (n = 5), who underwent ^{18}F-FDG PET-CT scan at all three sessions, a progressive decrease were observed: the SUV_{max} at pre-therapy was 13.1±7.3

(range: 2.9–20.9), at mid-therapy it was 12.5±7.6 (range: 2.7–22.6), and at post-therapy it was 8.7±4.9 (range: 3.5–14.1).

Figure 22: SUV$_{max}$ in GTV plotted versus session (before start of RT, mid therapy and 6 weeks after RT) for all individual patients. The population-based mean is given by a red square.

In Figure 23 the progressive decrease was also observed for SUV$_{mean}$ in the GTV across the sessions for all patients and subset of patients who underwent ^{18}F-FDG PET-CT scan at all three sessions (n=5).

Figure 23: SUV$_{mean}$ in GTV plotted versus session (before start of RT, mid therapy and 6 weeks after RT) for all individual patients. The population-based mean is given by a red square.

In Figure 24, SUV$_{max}$ for all delineated lymph nodes were plotted across sessions. Some patients did not have any delineated lymph nodes while others have up to 11 lymph nodes (Table 9). A large heterogeneity in lymph nodes' SUV$_{max}$ was observed during the radiotherapy between patients. The SUV$_{max}$ was 9.7 ± 8.6 at pre-therapy, which slightly decreased to 8.8 ± 6.9 at mid-therapy. At post-therapy, SUV$_{max}$ further decreased to 6.0 ± 8.7.

Figure 24: SUV$_{max}$ in lymph nodes plotted versus session (before start of RT, mid therapy and 6 weeks after RT) for all individual patients. The population-based mean is given by a red square.

In Figure 25, SUV$_{median}$ from patients' lung were plotted across sessions. SUV$_{median}$ in the lung was 0.57±0.2 at pre-therapy session, which increased to 0.62±0.2 at mid-therapy session. SUV$_{median}$ further increased to 0.70±0.2 at post-therapy session. Analyzing the subset of patients (n = 5), who underwent ^{18}F-FDG PET-CT scan at all three sessions, a similar trend were obtained: the SUV$_{max}$ at pre-therapy was 0.53±0.2, at mid-therapy it was 0.65±0.3, and at post-therapy it was 0.71±0.3.
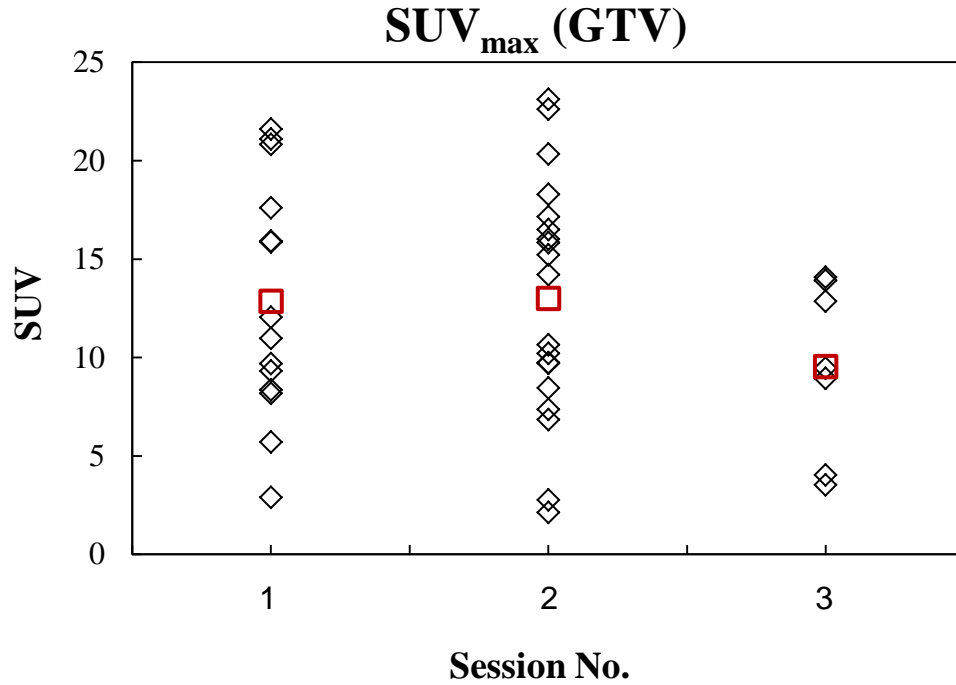
Figure 25: SUV_median in lung plotted versus session (before start of RT, mid therapy and 6 weeks after RT) for all individual patients. The population-based mean is given by a red square.

Classifying the lung into ipsilateral and contralateral lung also showed a progressive increase. The SUV_{median} for contralateral lung (Figure 26) was 0.47±0.1 at pre-therapy, 0.54±0.2 at mid-therapy, and 0.65±0.2 at post-therapy. For ipsilateral lung (Figure 27), SUV_{median} at pre-, mid-, and post-therapy sessions was 0.67±0.3, 0.71±0.3, and 0.74±0.3, respectively.

Figure 26: SUV$_{median}$ in contralateral lung plotted versus session (before start of RT, mid therapy and 6 weeks after RT) for all individual patients. The population-based mean is given by a red square.
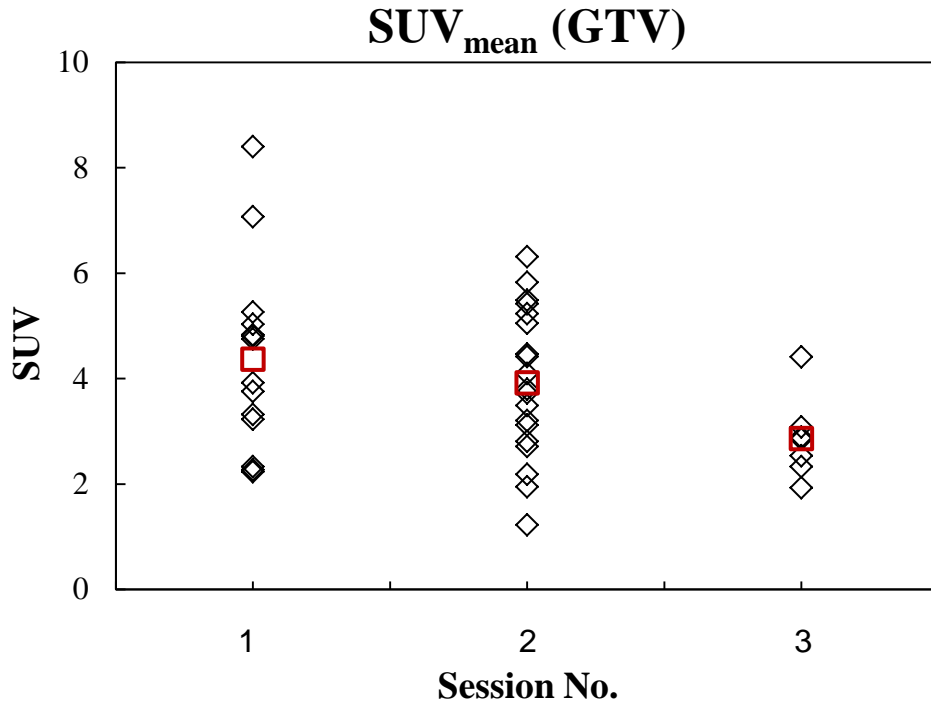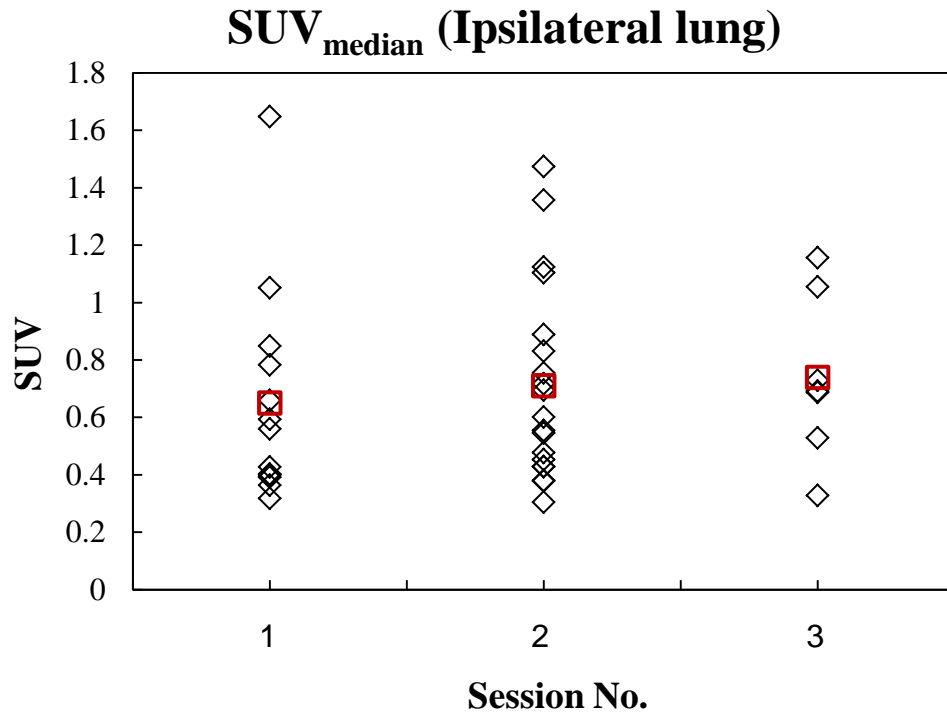
Figure 27: SUV_median in ipsilateral lung plotted versus session (before start of RT, mid therapy and 6 weeks after RT) for all individual patients. The population-based mean is given by a red square.

In Figure 28, SUV_{median} from patients' bone marrow were plotted across sessions. SUV_{median} For the bone marrow at pre-therapy was 1.3 ± 0.2. This value increased to 1.5 ± 0.4 at mid-therapy session. Likewise at post-therapy session, SUV_{median} was 1.5 ± 0.2. Analyzing the subset of patients ($n = 5$), who underwent ^{18}F-FDG PET-CT scan at all three sessions; similar results were obtained. Here, SUV_{median} at pre-therapy session was 1.2 ± 0.1, at mid-therapy it was 1.4 ± 0.2, and at post-therapy it was 1.4 ± 0.2.
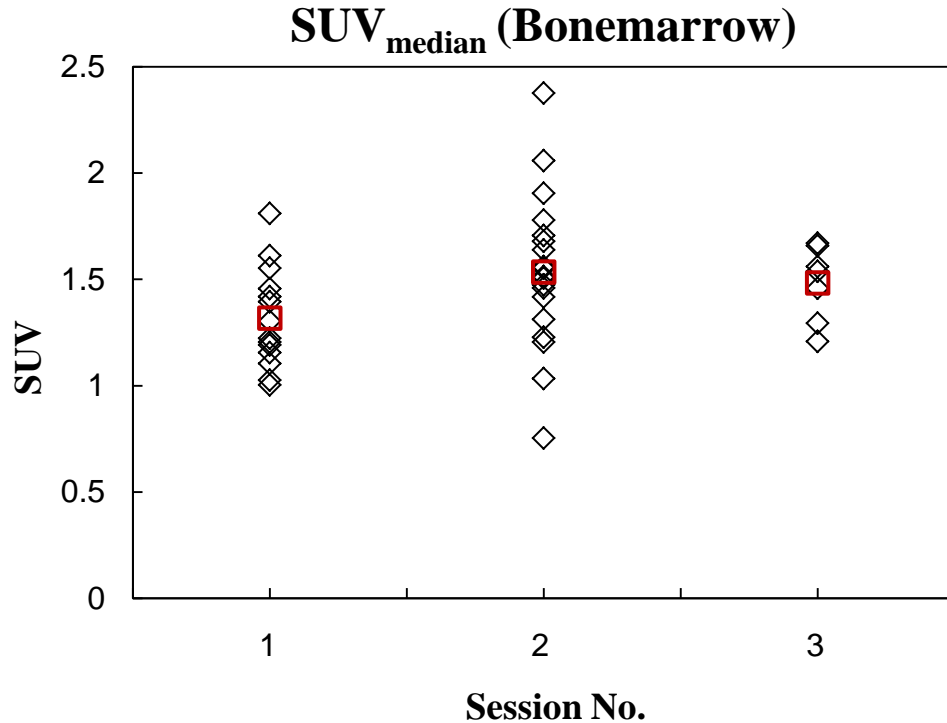
Figure 28: SUV$_{median}$ in bone marrow plotted versus session (before start of RT, mid therapy and 6 weeks after RT) for all individual patients. The population-based mean is given by a red square.

In Figure 29, SUV$_{median}$ from patients' esophagus were plotted across sessions. SUV$_{median}$ in the esophagus was 1.5 ± 0.4 at pre-therapy. This value increased to 1.8 ± 0.4 at mid-therapy session. Likewise at post-therapy session, SUV$_{median}$ was 1.8 ± 0.2. A progressive increase was observed by analyzing the subset of patients ($n = 5$) who underwent ^{18}F-FDG PET-CT scan at all three sessions. The SUV$_{median}$ at pre-therapy session was 1.4 ± 0.2, at mid-therapy it was 1.6 ± 0.3, and at post-therapy it was 1.8 ± 0.3.
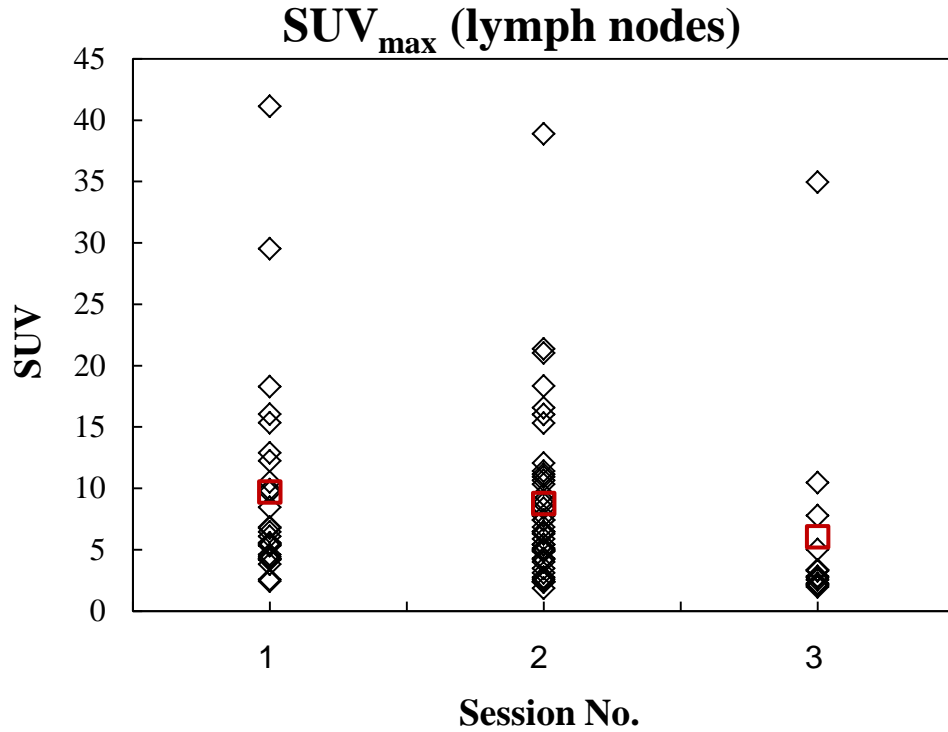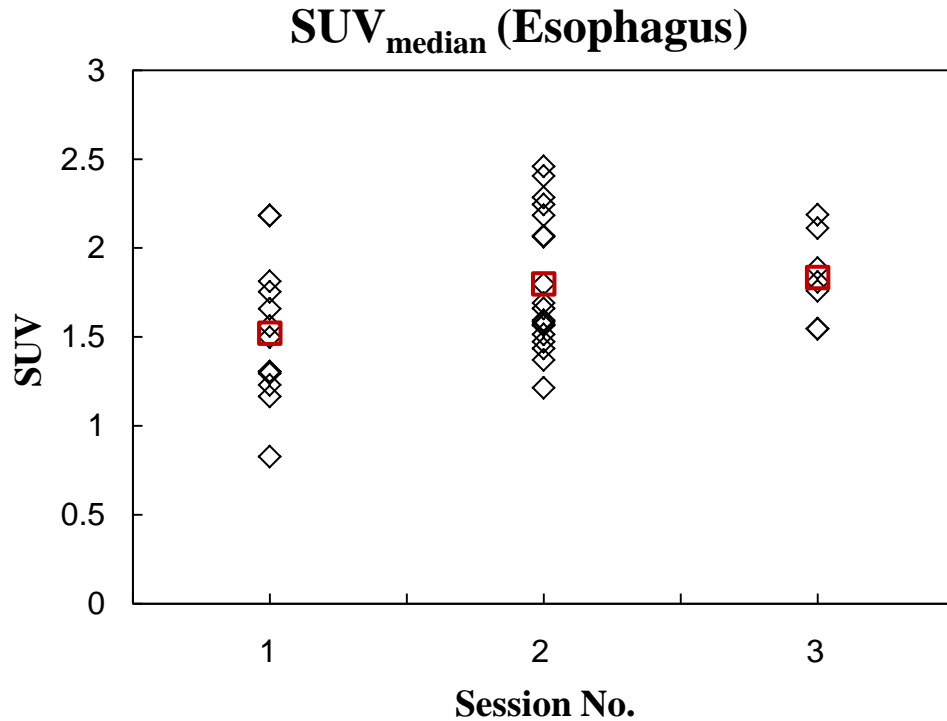
Figure 29: SUV_{median} in esophagus plotted versus session (before start of RT, mid therapy and 6 weeks after RT) for all individual patients. The population-based mean is given by a red square.

In Figure 30, SUV_{median} from patients' heart were plotted across sessions. SUV_{median} for the heart at pre-therapy was 1.9±0.5. Likewise this value was 1.9±0.4 at mid-therapy and reached 2.0±0.5 at post-therapy session. The same trend was observed by analyzing the subset of patients (n = 5), who underwent ^{18}F-FDG PET-CT scan at all three sessions. SUV_{median} before radiotherapy (pre-therapy session) was 2.1±0.8, at mid-therapy it was 2.1±0.4, and at post-therapy it was 2.2±0.4.
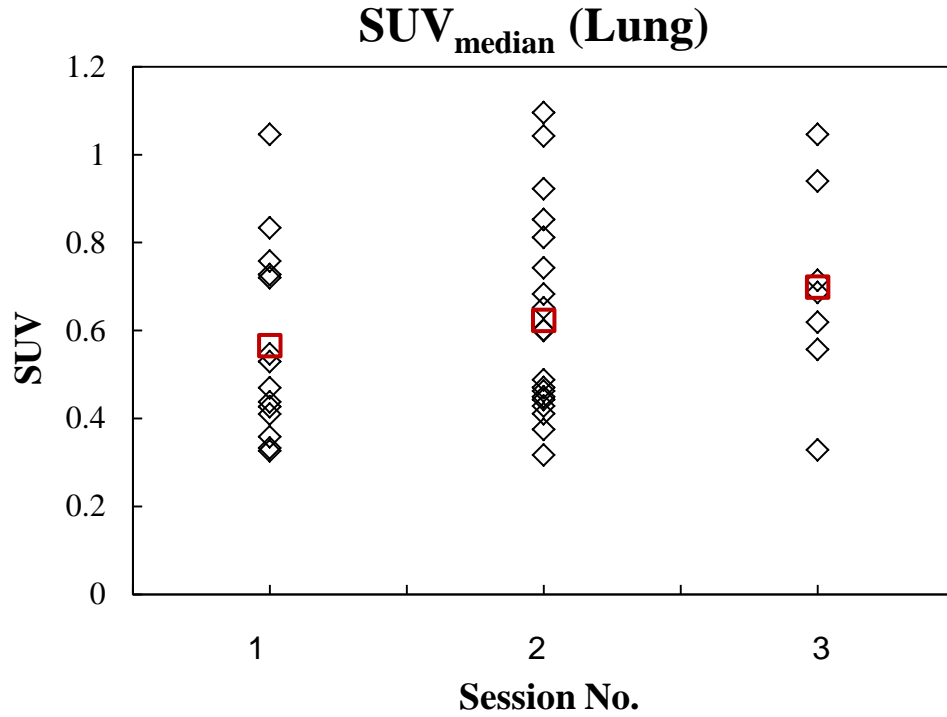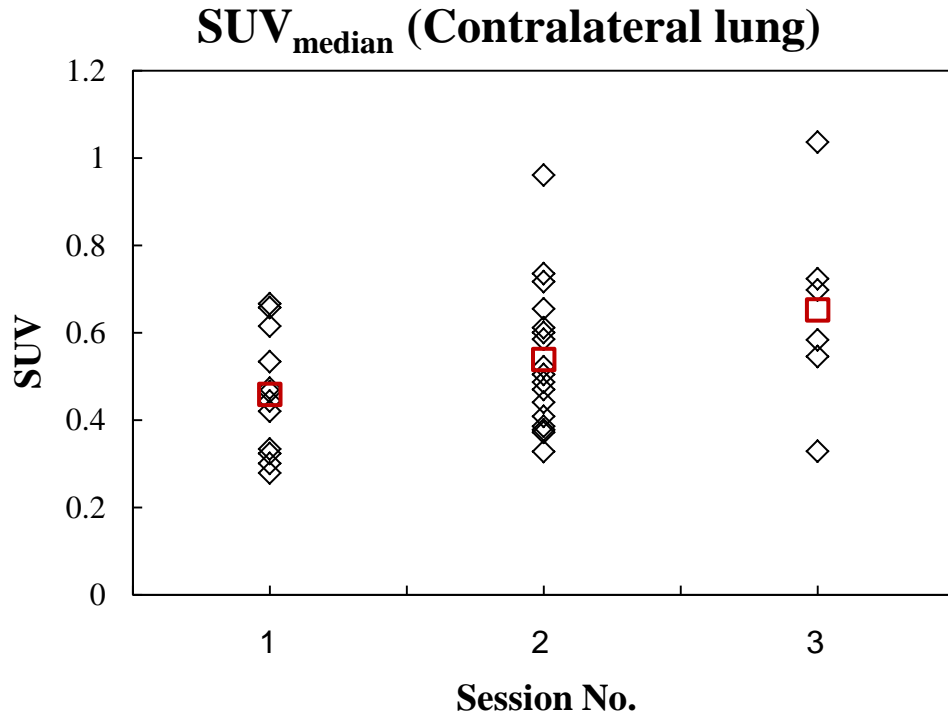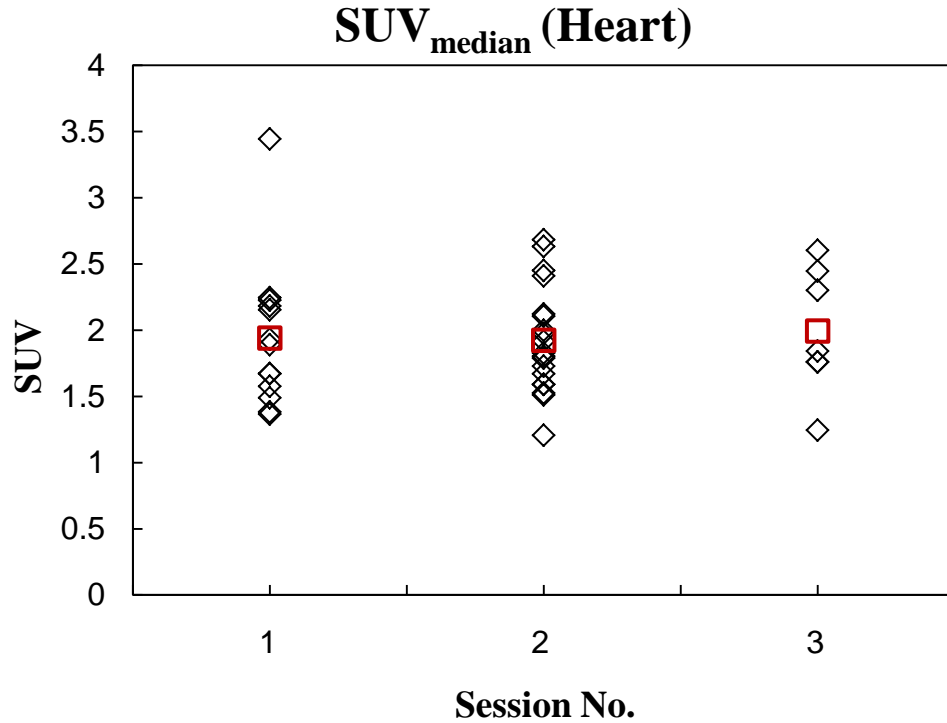
Figure 30: SUV_{median} in heart plotted versus session (before start of RT, mid therapy and 6 weeks after RT) for all individual patients. The population-based mean is given by a red square.

4.2.3. FDG uptake response versus dose

This part of the study was focused on how SUV changes with dose in the mid-therapy and the post-therapy sessions and whether we can identify any trends in SUV_{mean} level with RT dose. SUV_{mean} was calculated in dose bins of 0.5 Gy for all patients and the mean value of SUV_{mean} from all patients that belongs to each dose bin was then calculated. Because only half of the total RT dose was delivered at mid-therapy, the dose ranged between 0 and 15 Gy in this session. On the other hand, the dose was between 0 and 30 Gy at post-therapy session. Thus, data was shown in terms of % of delivered dose. 100% of delivered dose corresponds to 15 Gy and 30 Gy at mid- and post-therapy, respectively. A linear regression model was used to investigate the correlation between FDG uptake and dose at mid- and post-therapy. In the following plots the slope and intercepts are reported as an estimate ± SE (Standard Error). We also looked for statistical significance, both with respect to the dose response relationship and with respect to differences in FDG-uptake between the two imaging sessions. 95% confidence intervals were used for

assessing significance. Because the GTV received quite homogeneous RT doses, SUV versus dose plots were shown only for the OAR's.

Figure 31 shows SUV in the lung across all patients against percentage delivered dose at mid-therapy and post-therapy sessions. The straight lines represent fitted regression lines for these sessions. The lines have positive slopes and are almost parallel.

At mid-therapy the median of SUV_{mean} in the lung that received 0–5 Gy was 0.70 (range, 0.66–0.73), 5–10 Gy was 0.74 (range, 0.70–0.77), and >10 Gy was 0.77 (range: 0.74– 1.00). At post-therapy session, the median of SUV_{mean} in the lung that received 0–10 Gy was 0.79 (range, 0.71–0.86), 10–20 Gy was 0.87 (0.83–0.90), and >20 Gy was 0.87 (range, 0.82–1.02). Using linear regression the slope at mid-therapy and post-therapy was 0.0046±0.0005 and 0.0051±0.0005, with a 95% CIs [0.0037, 0.0056] and [0.0042, 0.0061], respectively. The intercept at mid-therapy and post-therapy was 0.67±0.01 and 0.77±0.01, with a 95% CIs [0.66, 0.69] and [0.75, 0.78], respectively.
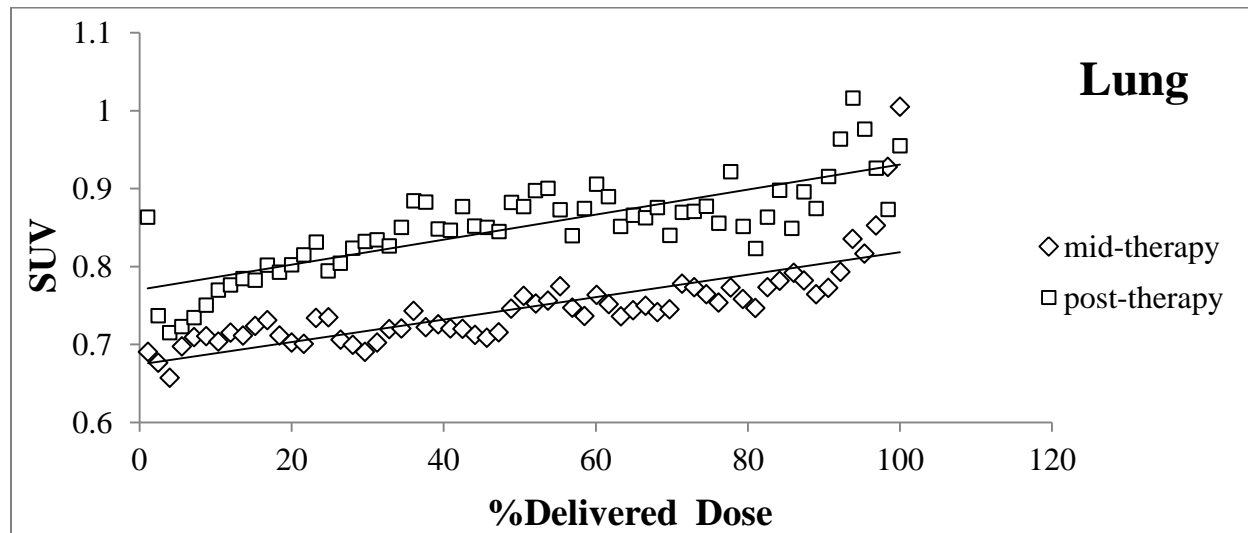
Figure 31: SUV in the lung versus percentage delivered dose at mid-therapy and post-therapy. The solid lines correspond to a linear regression.

The lung FDG uptake dose response curves corresponding mid-therapy and post-therapy from individual patients were generated; various slopes and their standard error were used to build up sensitivity plot across all available sessions (Figure 32). It can be observed that except for patient

3 (at mid-therapy) and for patient 21 (at mid- and post-therapy) relationship between FDG uptake and dose was positive. At mid-therapy, 17 patients with positive slopes had a mean of slopes range of 0.0018 to 0.0118. At post-therapy, 6 patients with positive slopes had a mean of slopes range of 0.0005 to 0.0146. Looking for patients with data in the mid-therapy and post-therapy, we found out that in all patients except patient 9, sensitivity was higher in post-therapy compare to mid-therapy.
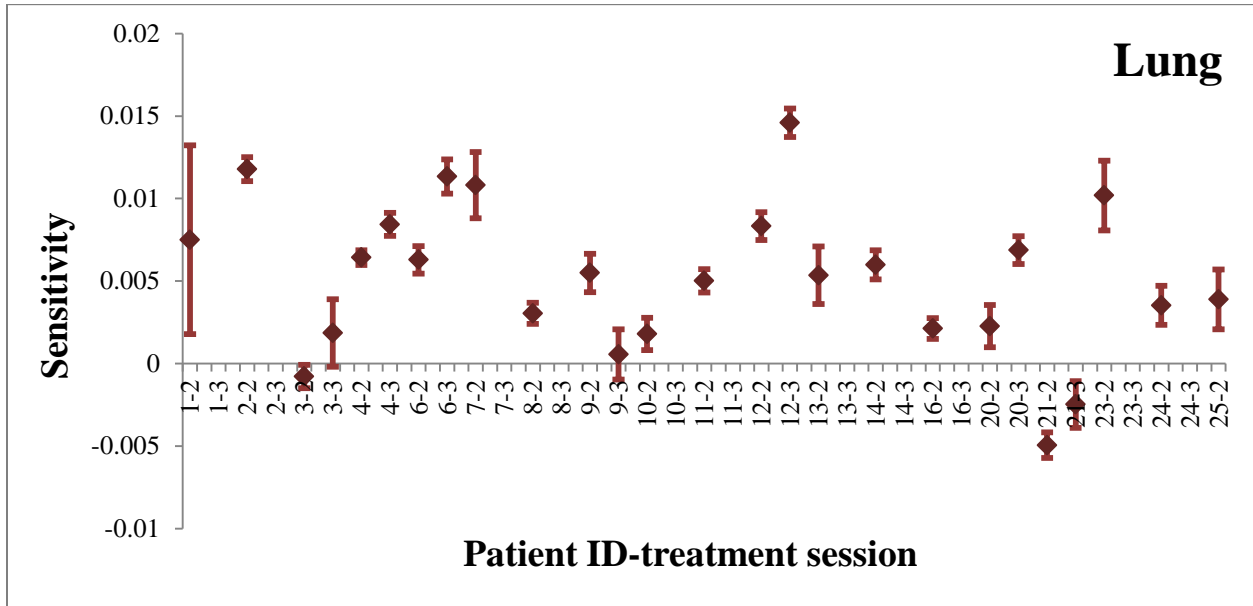
Figure 32: Lung sensitivity plotted for the available sessions across all patients.

The following organs along with their statistical properties of FDG response, SUV values for different dose intervals were reported in Table 3 at the end of this chapter.

Figure 33 shows SUV in the bone marrow across all patients against percentage delivered dose at mid-therapy and post-therapy sessions. The straight lines represent fitted regression lines for these sessions. The lines have negative slopes. Using linear regression the slope at mid-therapy and post-therapy was -0.004 ± 0.001 and -0.001 ± 0.001, with a 95% CIs [-0.006, -0.003] and [-0.004, 0.001], respectively. The intercept at mid-therapy and post-therapy was 1.66 ± 0.01 and 1.48 ± 0.02, with a 95% CIs [1.63, 1.69] and [1.44, 1.52], respectively.
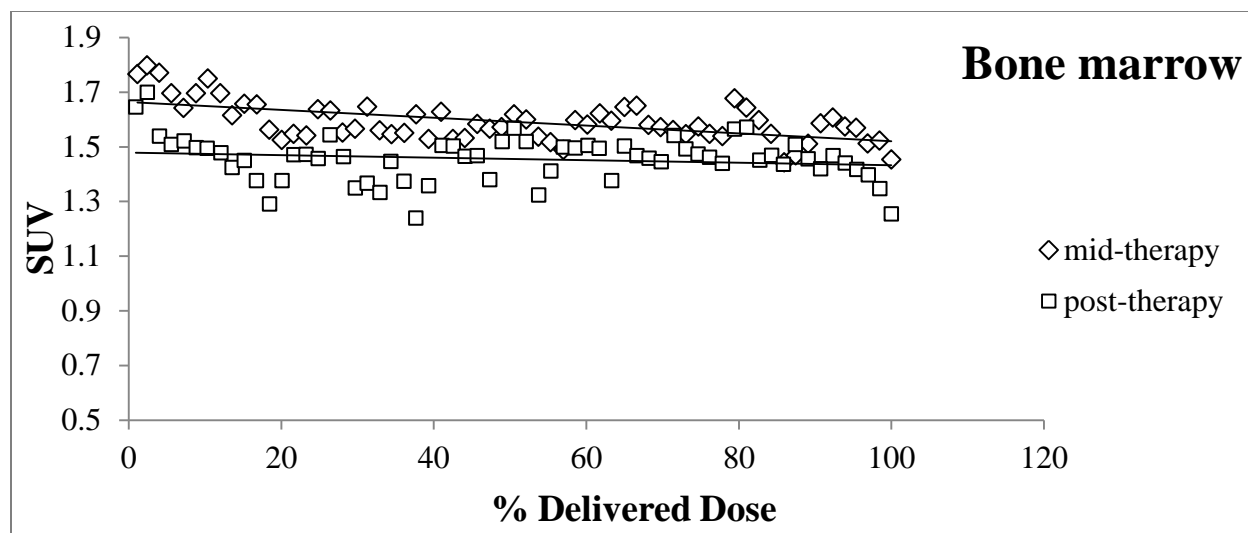
Figure 33: SUV in the bone marrow versus percentage delivered dose at mid-therapy and post-therapy. The solid lines correspond to a linear regression.

Figure 34 shows SUV in the esophagus across all patients against percentage delivered dose at mid-therapy and post-therapy sessions. The straight lines represent fitted regression lines for both sessions. The lines have positive slopes and are almost parallel. Using linear regression the slope at mid-therapy and post-therapy was 0.020 ± 0.002 and 0.019 ± 0.004, with a 95% CIs [0.016, 0.023] and [0.011, 0.026], respectively. The intercept at mid-therapy and post-therapy was 1.45 ± 0.31 and 1.59 ± 0.07, with a 95% CIs [1.39, 1.52] and [1.44, 1.73], respectively.
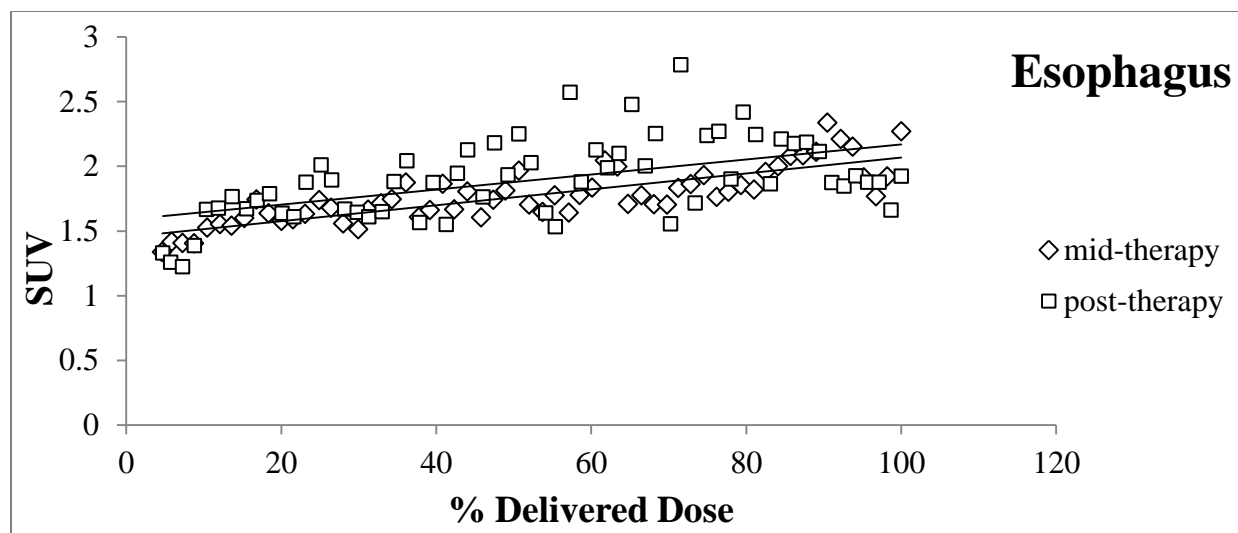
Figure 34: SUV in the esophagus versus percentage delivered dose at mid-therapy and post-therapy. The solid lines correspond to a linear regression.

Figure 35 shows SUV in the heart across all patients against percentage delivered dose at mid-therapy and post-therapy sessions. The straight lines represent fitted regression lines for both sessions. The line that belongs to mid-therapy has a positive slope while the line that belongs to post-therapy has a negative slope. Using linear regression the slope at mid-therapy and post-therapy was 0.008 ± 0.001 and -0.004 ± 0.002, with a 95% CIs $[0.005, 0.011]$ and $[-0.008, 0.000]$, respectively. The intercept at mid-therapy and post-therapy was 1.97 ± 0.02 and 1.99 ± 0.04, with a 95% CIs $[1.93, 2.02]$ and $[1.91, 2.07]$, respectively.
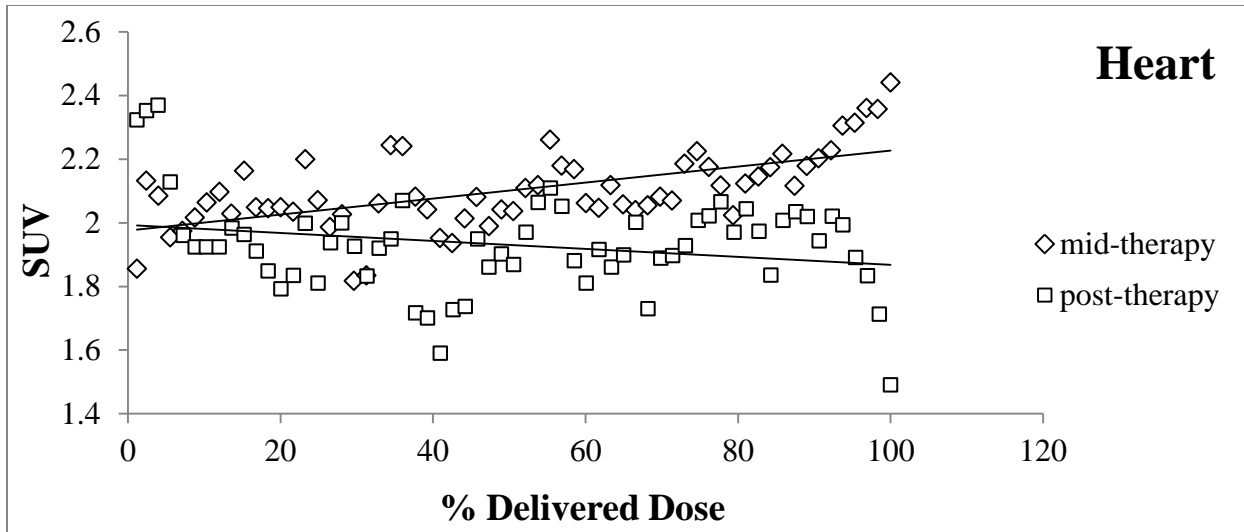
Figure 35: SUV in the heart versus percentage delivered dose at mid-therapy and post-therapy. The solid lines correspond to a linear regression.

4.3. Influence of Tarceva on glucose metabolism

4.3.1. Time trends

In total 13 patients received Tarceva, of which only 3 patients underwent all examinations. Eight patients were examined in the pre-therapy, 10 in the mid-therapy, and 5 in the post-therapy. In order to compare Tarceva receiving group of patients with the non-Tarceva receiving group, we calculated normalized SUV (NSUV) to measure the activity of GTV and OAR's and to improve the reproducibility of this measure. NSUV (for GTV) was derived from the following equation for individual patients:

$$NSUV = \frac{SUV_{\max}(mid-therapy)}{SUV_{\max}(pre-therapy)}$$

For other organs SUV_{median} was used instead of SUV_{max}. Mann-Whitney U-test was used when searching for significant differences between these two groups in each session (Table 8).

Figure 36 shows SUV_{max} in GTV plotted versus sessions and for patient separated into Tarceva and non-Tarceva receiving groups. For patients treated with both RT and Tarceva the SUV_{max} in

the tumor was 11.0±6.8 (range: 2.9–21.6) before start of radiotherapy (pre-therapy). This value increased to 12.5±5.8 (range: 2.7–22.6) at mid-therapy session. At post-therapy session, SUV_{max} decreased to 10.0±4.3 (range: 3.5–14.0). Analyzing the subset of patients (n = 3), who underwent ^{18}F-FDG PET-CT scan in all three sessions, similar results were obtained: the SUV_{max} at pre-therapy was 10.7±9.1 (range: 2.9-20.8), at mid-therapy it was 11.9±10.0 (range: 2.7–22.6), and at post-therapy it was 8.8±5.2 (range: 3.5–14.1). Furthermore, a progressive decrease as followed was seen for patients enrolled for RT arm alone: the SUV_{max} was 15.4±4.0 (range: 9.7–21.1) at pre-therapy, which decreased to 13.6±6.7 (range: 2.1–23.1) at mid-therapy. This value further decreased to 8.4±6.2 (range: 4.0–12.8) at post-therapy session.

Figure 36: SUV_{max} in GTV plotted versus sessions (before start of RT, mid therapy, and 6 weeks after RT) for all individual patients separated into Tarceva receiving and non-Tarceva receiving groups. The population-based mean is given by a red square.

Figure 37 shows SUV_{mean} in GTV plotted versus sessions and for patient separated into Tarceva and non-Tarceva receiving groups. For patients treated with both RT and Tarceva the SUV_{mean} in the tumor was 3.9±2.1 at pre-therapy, 3.8±1.2 at mid-therapy, and 3.0±0.8 at post-therapy.

Analyzing the subset of patients (n = 3), who underwent ^{18}F-FDG PET-CT scan in all three sessions, the SUV_{median} at pre-therapy was 3.6±1.5, at mid-therapy it was 3.6±1.7, and at post-therapy it was 2.8±0.2. For patients treated with radiotherapy alone, SUV_{mean} was 5.0±1.2 at pre-therapy, 4.0±1.7 at mid-therapy, and 2.4±0.6 at post-therapy session.

Figure 37: SUV_{mean} in GTV plotted versus session (before start of RT, mid therapy and 6 weeks after RT) for all individual patients separated into Tarceva receiving and non-Tarceva receiving groups. The population-based mean is given by a red square.

Figure 38 shows SUV_{median} in lung plotted versus sessions and for patients separated into Tarceva and non-Tarceva receiving groups. For patients treated with both RT and Tarceva, SUV_{median} in the lung was 0.5±0.2 at pre-therapy, 0.6±0.3 at mid-therapy, and 0.8±0.2 at post-therapy session. Analyzing the subset of patients (n = 3), who underwent ^{18}F-FDG PET-CT scan in all three sessions, the SUV_{median} at pre-therapy was 0.6±0.2, at mid-therapy it was 0.8±0.3, and at post-therapy it was 0.9±0.2. For patients treated with radiotherapy alone, SUV_{median} was 0.6±0.3 at pre-therapy, 0.6±0.2 at mid-therapy, and 0.5±0.2 at post-therapy session.

Figure 38: SUV$_{median}$ in lung plotted versus session (before start of RT, mid therapy and 6 weeks after RT) for all individual patients separated into Tarceva receiving and non-Tarceva receiving groups. The population-based mean is given by a red square.

Figure 39 shows SUV$_{median}$ in ipsilateral lung GTV plotted versus sessions and for patient separated into Tarceva and non-Tarceva receiving groups. For patients treated with both RT and Tarceva, SUV$_{median}$ in the ipsilateral lung was 0.6±0.2 at pre-therapy, 0.7±0.4 at mid-therapy, and 0.8±0.3 at post-therapy session. Analyzing the subset of patients (n = 3), who underwent ^{18}F-FDG PET-CT scan in all three sessions, the SUV$_{median}$ was 0.7±0.2 at pre-therapy session, 0.8±0.3 at mid-therapy session, and 0.9±0.3 at post-therapy session. For patients treated with radiotherapy alone, SUV$_{median}$ was 0.8±0.5 at pre-therapy, 0.7±0.3 at mid-therapy, and 0.5±0.2 at post-therapy session.

SUV_median (Ipsilateral lung)

Figure 39: SUV_median in ipsilateral lung plotted versus session (before start of RT, mid therapy and 6 weeks after RT) for all individual patients separated into Tarceva receiving and non-Tarceva receiving groups. The population-based mean is given by a red square.

Figure 40 shows SUV_{median} in contralateral lung plotted versus sessions and for patient separated into Tarceva and non-Tarceva receiving groups. For patients treated with both RT and Tarceva, SUV_{median} in the contralateral lung was 0.5±0.2 at pre-therapy, 0.6±0.2 at mid-therapy, and 0.7±0.2 at post-therapy. Analyzing the subset of patients (n = 3), who underwent ^{18}F-FDG PET-CT scan in all three sessions, the SUV_{median} was 0.6±0.1 at pre-therapy, 0.7±0.2 at mid-therapy, and 0.8±0.2 at post-therapy session. For patients treated with radiotherapy alone, SUV_{median} was 0.5±0.1 at pre-therapy, 0.5±0.1 at mid-therapy, and 0.3 at post-therapy session.
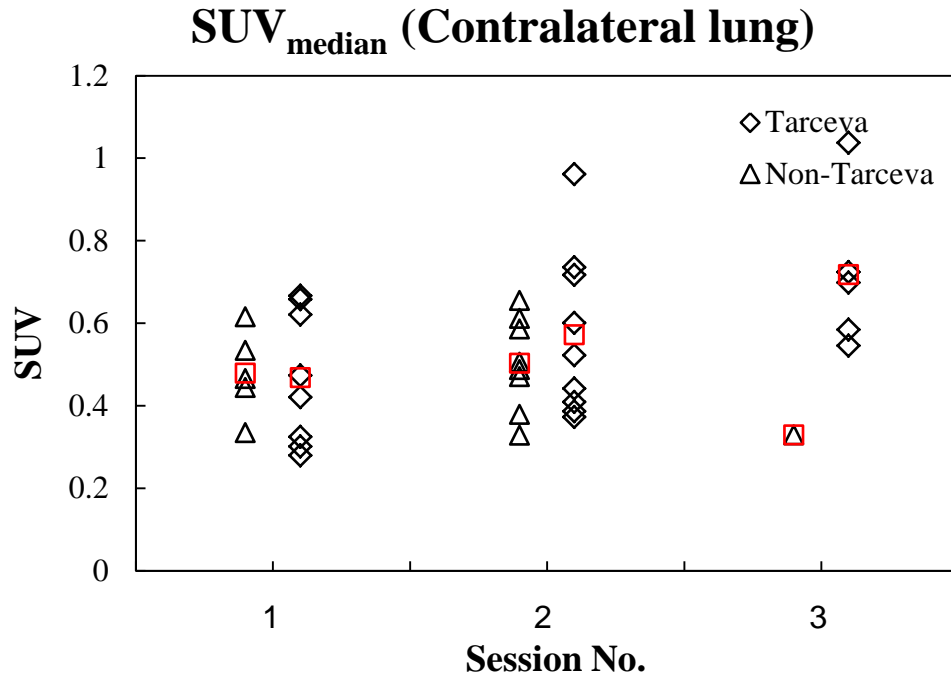
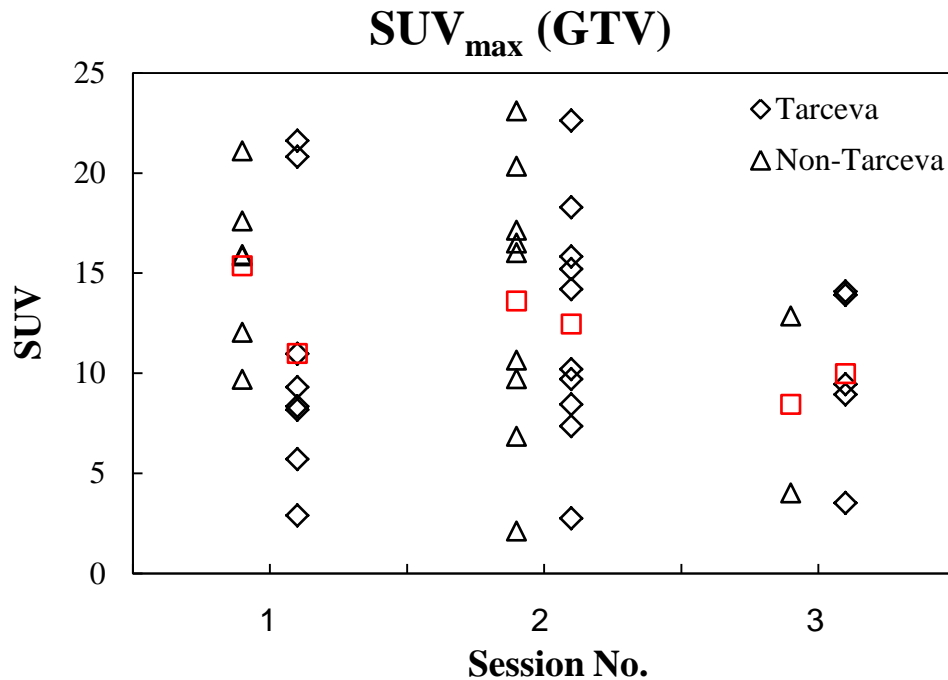*Figure 40: SUV_{median} in contralateral lung plotted versus session (before start of RT, mid therapy and 6 weeks after RT) for all individual patients separated into Tarceva receiving and non-Tarceva receiving groups. The population-based mean is given by a red square.*

Figure 41 shows SUV_{median} in bone marrow plotted versus sessions and for patient separated into Tarceva and non-Tarceva receiving groups. For patients treated with both RT and Tarceva, the SUV_{median} in the bone marrow was 1.3 ± 0.3 at pre-therapy, 1.6 ± 0.2 at mid-therapy, and 1.6 ± 0.1 at post-therapy session. Analyzing the subset of patients (n = 3), who underwent ^{18}F-FDG PET-CT scan in all three sessions, the SUV_{median} at pre-therapy was 1.2 ± 0.2, at mid-therapy and post-therapy it was 1.5 ± 0.1. For patients treated with radiotherapy alone, SUV_{median} was 1.3 ± 0.2 at pre-therapy, 1.4 ± 0.5 at mid-therapy, and 1.2 ± 0.1 at post-therapy session.
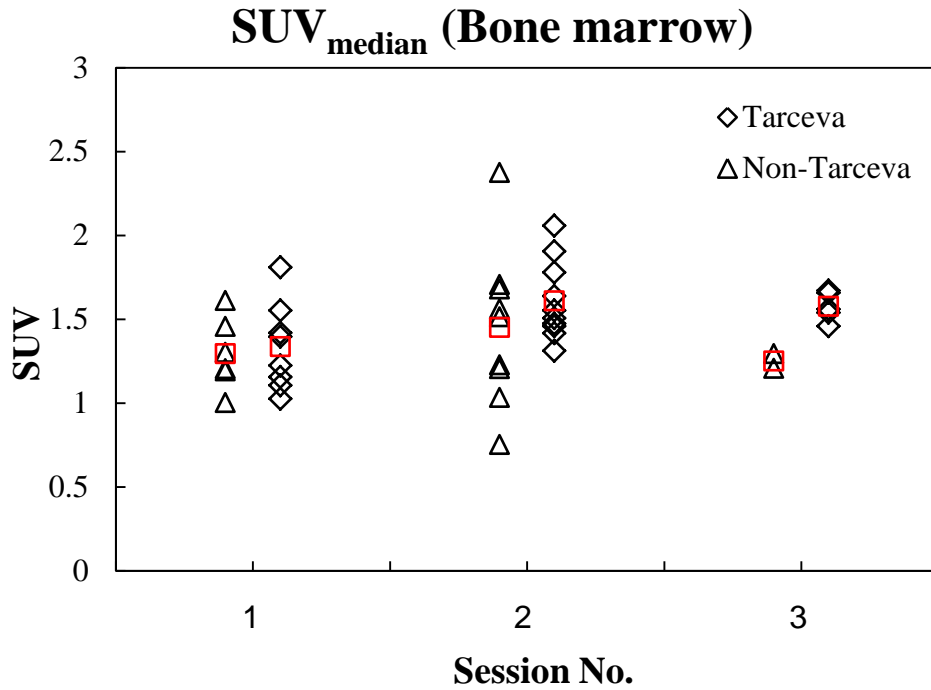
Figure 41: SUV$_{median}$ in bone marrow plotted versus session (before start of RT, mid therapy and 6 weeks after RT) for all individual patients separated into Tarceva receiving and non-Tarceva receiving groups. The population-based mean is given by a red square.

Figure 42 shows SUV$_{median}$ in esophagus plotted versus sessions and for patient separated into Tarceva and non-Tarceva receiving groups. For patients treated with both RT and Tarceva, the SUV$_{median}$ in the esophagus was 1.4±0.3 at pre-therapy, 1.7±0.2 at mid-therapy, and 1.8±0.2 at post-therapy session. Analyzing the subset of patients (n = 3), who underwent ^{18}F-FDG PET-CT scan in all three sessions, the SUV$_{median}$ at pre-therapy was 1.4±0.1, at mid-therapy it was 1.6±0.1, and at post-therapy it was 1.7±0.2. In patients treated with radiotherapy alone, SUV$_{median}$ was 1.7±0.4 at pre-therapy, 1.9±0.5 at mid-therapy, and 1.9±0.4 at post-therapy session.
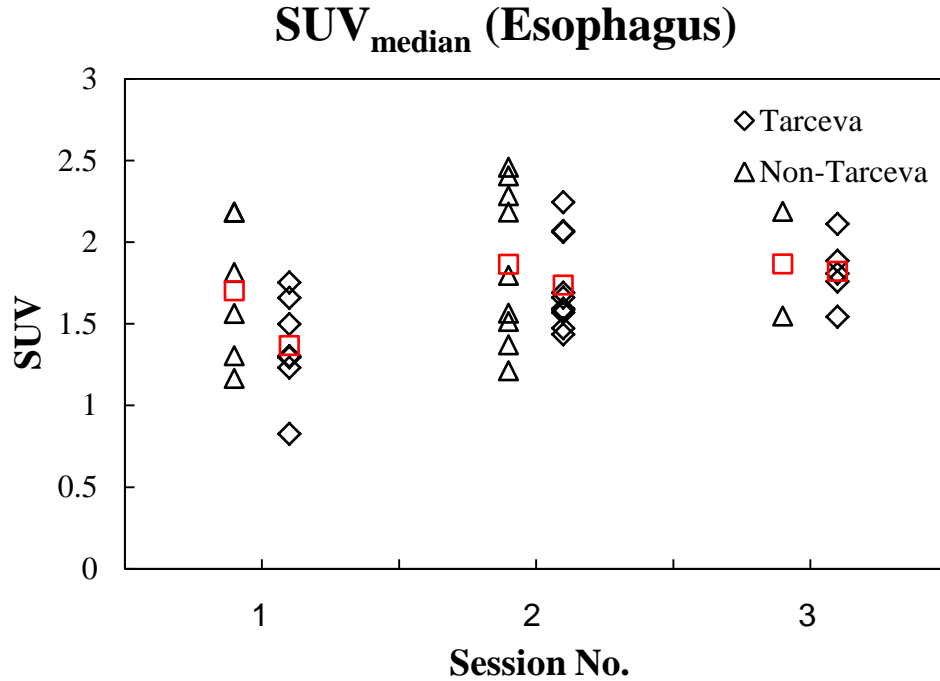
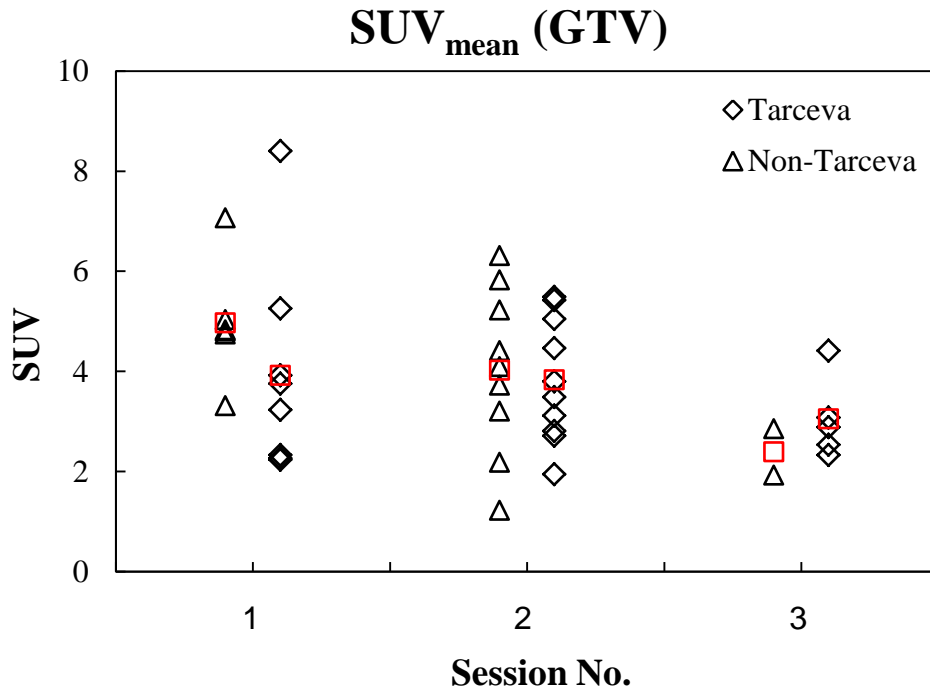*Figure 42: SUV_{median} in esophagus plotted versus session (before start of RT, mid therapy and 6 weeks after RT) for all individual patients separated into Tarceva receiving and non-Tarceva receiving groups. The population-based mean is given by a red square.*

Figure 43 shows SUV_{median} in heart plotted versus sessions and for patient separated into Tarceva and non-Tarceva receiving groups. For patients treated with both RT and Tarceva, the SUV_{median} in the heart was 1.9 ± 0.4 at pre-therapy, 2.0 ± 0.3 at mid-therapy, and 2.0 ± 0.5 at post-therapy session. Analyzing the subset of patients ($n = 3$), who underwent ^{18}F-FDG PET-CT scan in all three sessions, the SUV_{median} before radiotherapy (pre-therapy) was 1.9 ± 0.5, at mid-therapy it was 2.1 ± 0.5, and in post-therapy it was 2.3 ± 0.4. For patients treated with radiotherapy alone, SUV_{median} was 2.0 ± 0.7 at pre-therapy, 1.8 ± 0.4 at mid-therapy, and 2.0 ± 0.4 at post-therapy session.
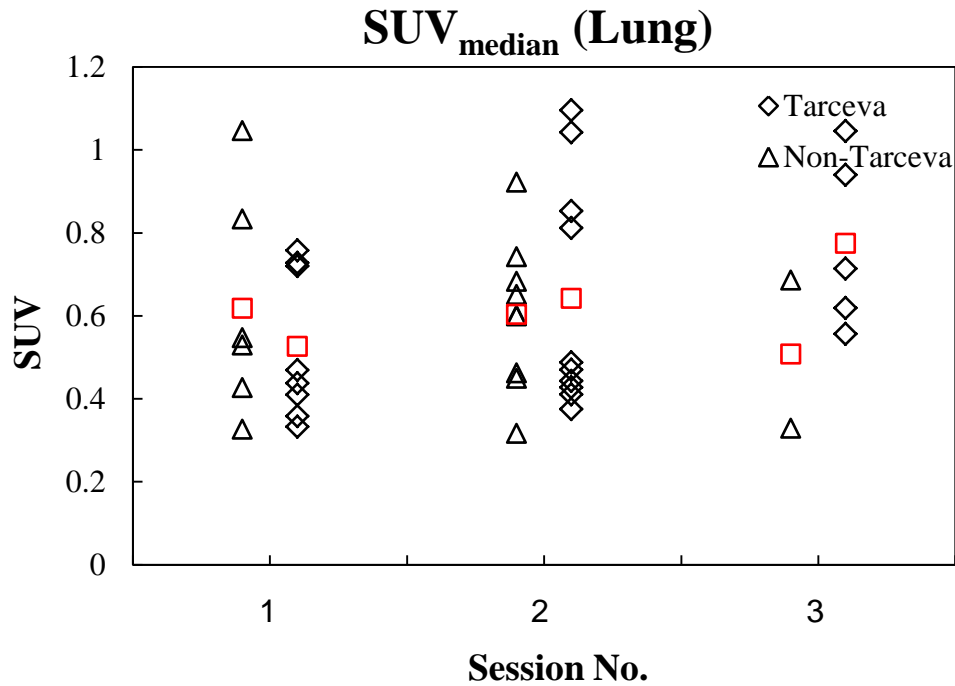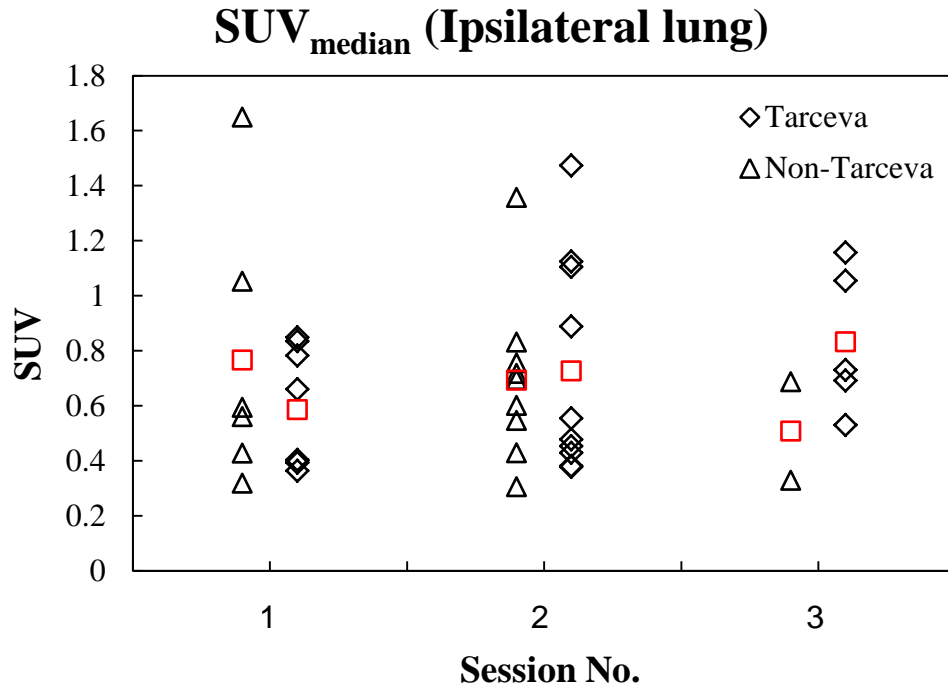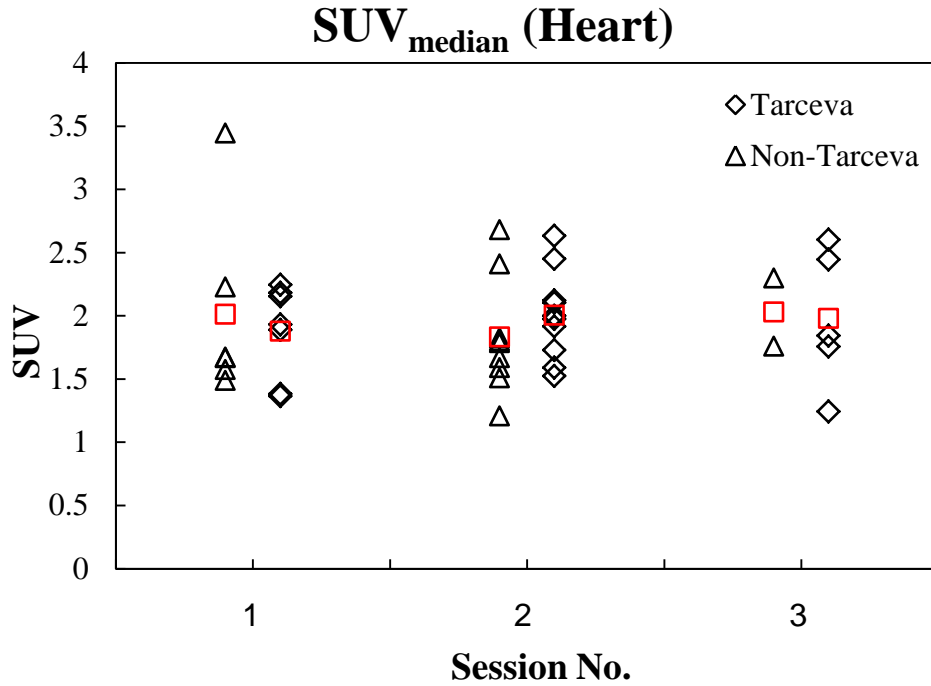
Figure 43: SUV$_{median}$ in heart plotted versus session (before start of RT, mid therapy and 6 weeks after RT) for all individual patients separated into Tarceva receiving and non-Tarceva receiving groups. The population-based mean is given by a red square.

4.3.2. FDG uptake response versus dose

This part of the study was focused on how SUV changes with dose at mid-therapy or at post-therapy sessions when Tarceva receiving patients and non-Tarceva receiving patients were separated. SUV$_{mean}$ was calculated in each dose bin of 0.5 Gy for all patients and the mean value of SUV$_{mean}$ that belongs to each dose bin was then calculated. A linear regression model was used to investigate the correlation between FDG uptake and dose. In the following plots the slope and intercepts are reported as an estimate $\pm$ SE (Standard Error). We also looked for statistical significance, both with respect to the dose response relationship and with respect to differences in FDG-uptake between the two groups of patients (Tarceva receiving and non-Tarceva receiving) in each session (mid-therapy and post-therapy). 95% confidence intervals were used for assessing significance. The following organs along with their statistical properties of FDG response were reported in Table 4 at the end of this chapter.

Figure 44 shows SUV in the lung across all patients against delivered dose at mid-therapy session. These plotted data are separated into two groups, Tarceva receiving patients and non-Tarceva receiving patients. The straight lines represent fitted regression lines for these groups. The lines have positive slopes and are almost parallel.

At mid-therapy, the SUV in the lung that received 0-15 Gy was ranging between 0.59 and 0.83 for patients who were treated with radiotherapy alone. This value was between 0.69 and 0.87 for patients who were treated with both Tarceva and radiotherapy. Using linear regression the slope for non-Tarceva patients and Tarceva patients was 0.005 ± 0.001 and 0.004 ± 0.000, with a 95% CIs [0.003, 0.006] and [0.003, 0.005], respectively. The intercept for non-Tarceva patients and Tarceva patients was 0.622 ± 0.010 and 0.722 ± 0.001, with a 95% CIs [0.599, 0.646] and [0.708, 0.736], respectively.
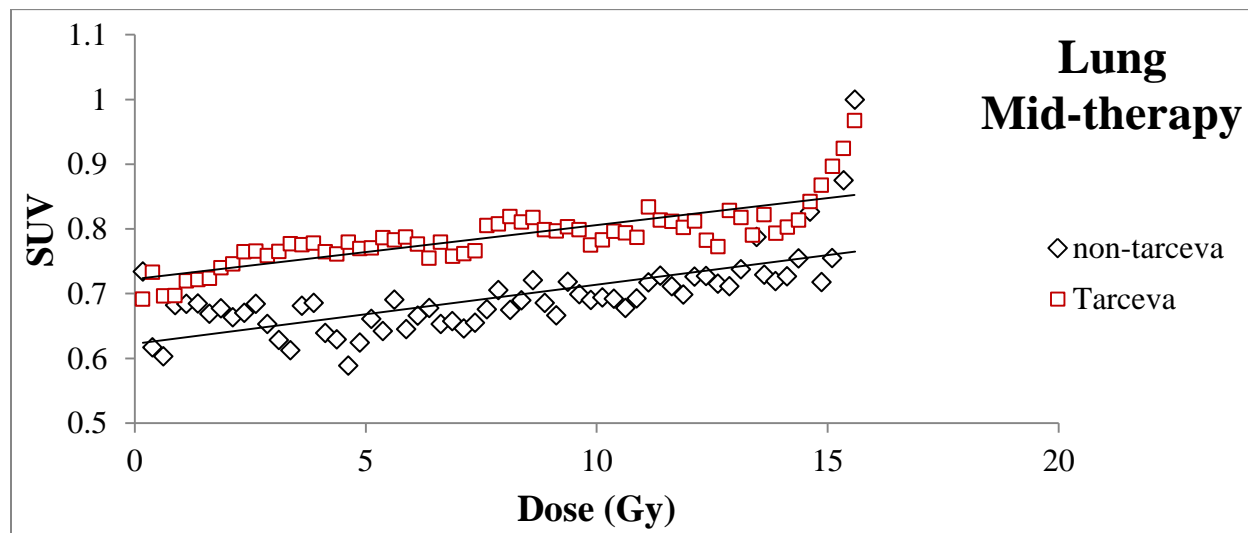
Figure 44: SUV in the lung versus delivered dose at mid-therapy across patients separated into Tarceva receiving and non-Tarceva receiving groups. The solid lines correspond to a linear regression.

Figure 45 shows SUV in the lung across all patients against delivered dose at post-therapy session. The plotted data are separated into two groups, Tarceva receiving patients and non-Tarceva receiving patients. The straight lines represent fitted regression lines for these groups. The lines have positive slopes but the line fitted on non-Tarceva group is much steeper.

At post-therapy, the SUV in the lung that received 0-30 Gy was ranging between 0.37 and 0.88 for patients who were treated with radiotherapy alone. This value was between 0.79 and 1.05 for patients who were treated with both Tarceva and radiotherapy. Using linear regression the slope for non-Tarceva patients and Tarceva patients was 0.010±0.001 and 0.003±0.001, with a 95% CIs [0.009, 0.011] and [0.002, 0.004], respectively. The intercept for non-Tarceva patients and Tarceva patients was 0.40±0.01 and 0.88±0.01, with a 95% CIs [0.38, 0.42] and [0.86, 0.90], respectively.
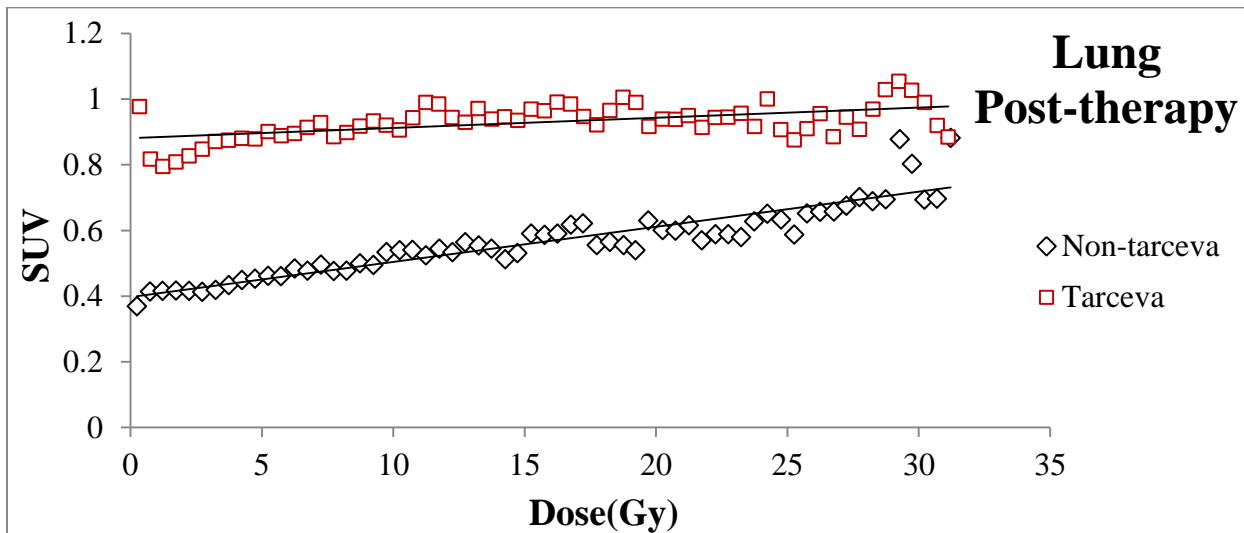
Figure 45: SUV in the lung versus percentage dose at post-therapy across patients separated into Tarceva receiving and non-Tarceva receiving groups. The solid lines correspond to a linear regression.

Figure 46 shows SUV of the bone marrow across all patients against delivered dose at mid-therapy session. These plotted data separated into two groups, Tarceva receiving patients and non-Tarceva receiving patients. The straight lines represent fitted regression lines for these groups. The lines have negative slopes. The line fitted on non-Tarceva group is much steeper than for Tarceva group.

At mid-therapy session, the SUV in the bone marrow that received 0-15 Gy was ranging between 1.30 and 1.92 for patients who were treated with radiotherapy alone. This value was between 1.40 and 1.82 for patients who were treated with both Tarceva and radiotherapy. Using linear

regression the slope for non-Tarceva patients and Tarceva patients was –0.006±0.001 and –0.003± 0.001, with a 95% CIs [–0.009, –0.003] and [–0.005, –0.001], respectively. The intercept for non-Tarceva patients and Tarceva patients was 1.66±0.03 and 1.66±0.02, with a 95% CIs [1.60, 1.73] and [1.62, 1.70], respectively.
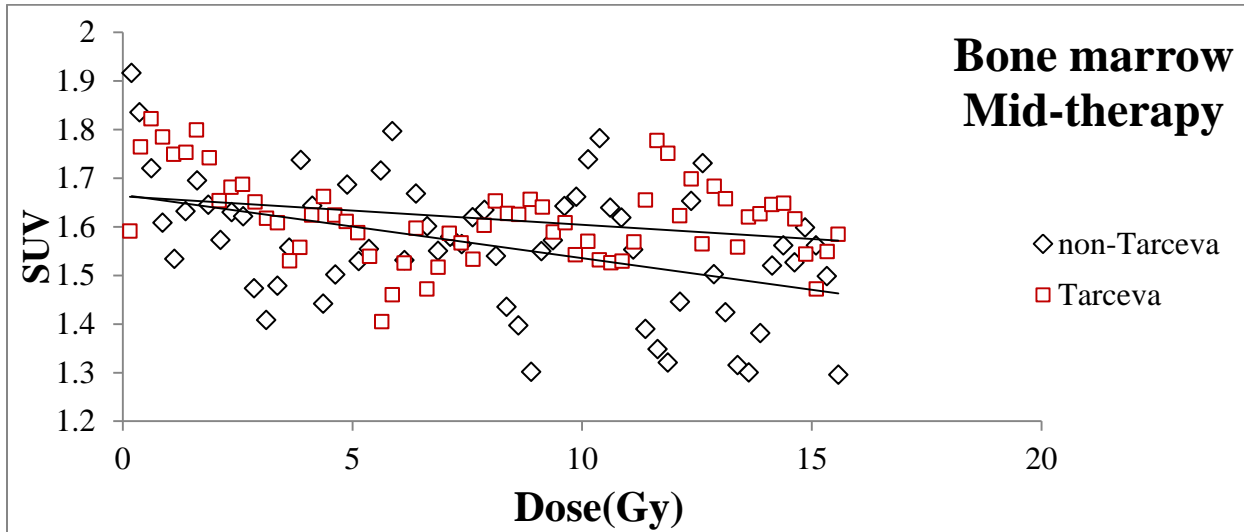
Figure 46: SUV in the bone marrow versus delivered dose at mid-therapy across patients separated into Tarceva receiving and non-Tarceva receiving groups. The solid lines correspond to a linear regression.

Figure 47 shows SUV in the bone marrow across all patients against delivered dose at post-therapy session. These plotted data separated into two groups, Tarceva receiving patients and non-Tarceva receiving patients. The straight lines represent fitted regression lines for these groups. These lines have negative slopes.

At post-therapy, the SUV in the bone marrow that received 0-30 Gy was ranging between 1.09 and 1.69 for patients who were treated with radiotherapy alone. This value was between 1.19 and 1.82 for patients who were treated with both Tarceva and radiotherapy. Using linear regression the slope for non-Tarceva patients and Tarceva patients was –0.003±0.001 and –0.001±0.001, with a 95% CIs [–0.006, 0.000] and [–0.004, 0.002], respectively. The intercept for non-Tarceva patients and Tarceva patients was 1.37±0.03 and 1.53±0.03, with a 95% CIs [1.30, 1.43] and [1.47, 1.59], respectively.
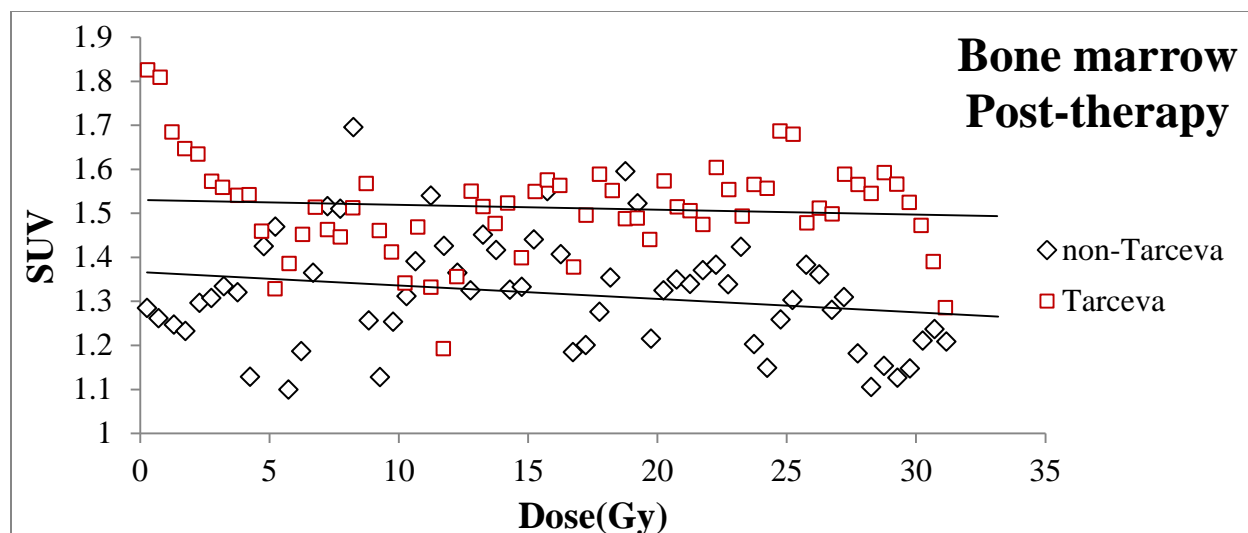
Figure 47: SUV in the bone marrow versus delivered dose at post-therapy across patients separated into Tarceva receiving and non-Tarceva receiving groups. The solid lines correspond to a linear regression.

4.4. Tissue density

4.4.1. Temporal characteristics

Box plot of HUs were generated to demonstrate the density distribution across three sessions for GTV and lung. These plots display data broken down into three quartiles, which was described in section 3.4.

The Box-whisker plot (Figure 48) showed an overall distribution of tumor density for the available sessions across all patients. The median value was greater than the mean value and express that data is "skewed" toward the higher density. Heterogeneity of the tumor was varied from patient to patient.
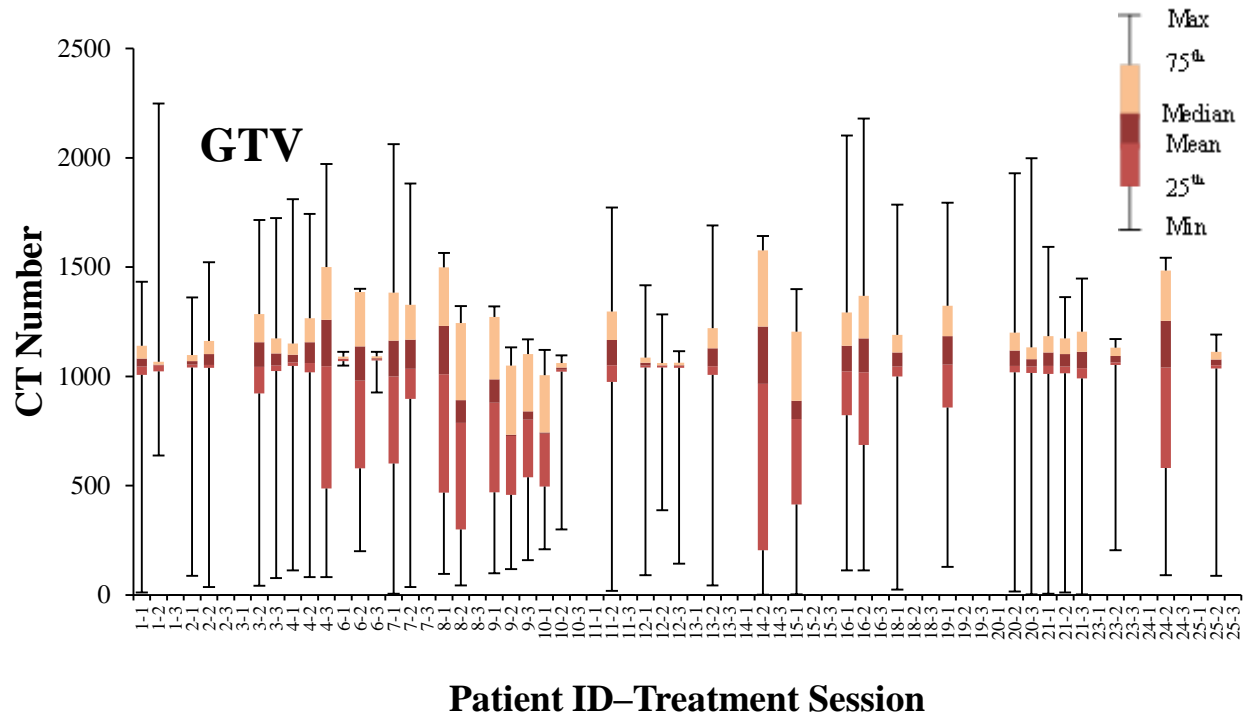
Figure 48: Box-whisker plot showing the overall distribution of density in GTV for the available sessions across all patients[15].

The Box-whisker plot (Figure 49) showed an overall distribution of lung density for the available sessions across all patients. In this plot we observed that the lung heterogeneity varied from patient to patient. All patients had the same CT Number$_{min}$ and CT Number$_{max}$ (100 and 800 respectively) because, as mentioned in section 3.2.3, we limited the CT number to these numbers.

---

[15] CT Numbers here are equal to the CT numbers which were extracted from the codes and were not converted to HU. For conversion formula in section 3.2.2 is used.
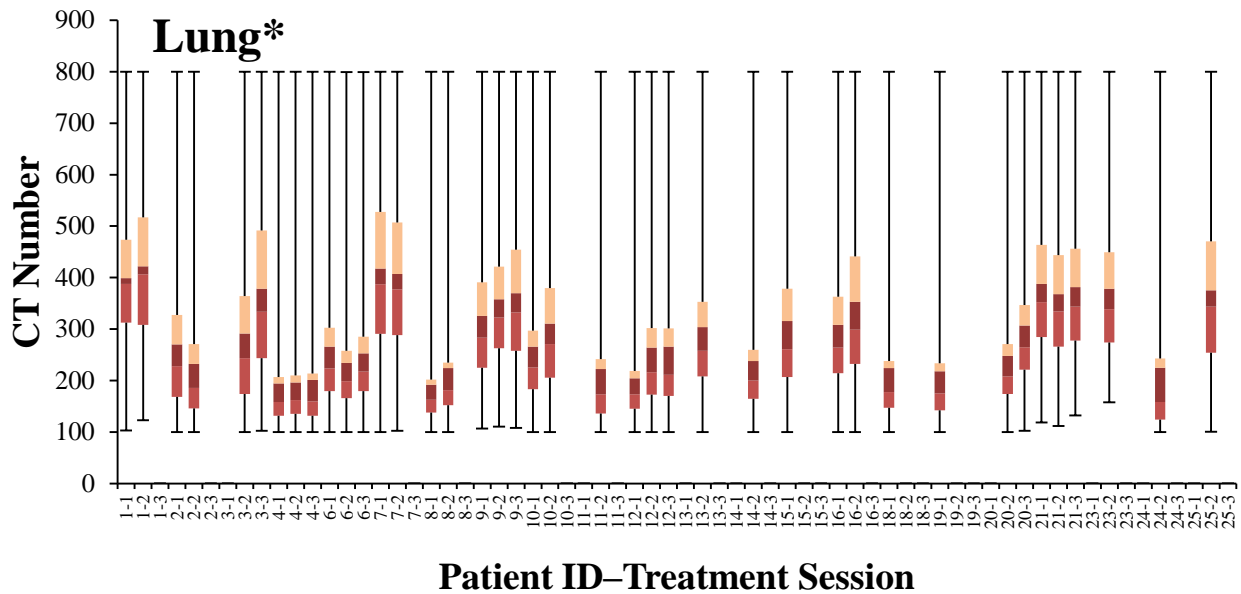
Figure 49: box-whisker plot showing the overall distribution of density in lung for the available sessions across all patients (*the legend is the same as for Figure 48).

4.4.2. Time trend

In Figure 50 HU_{median} in the lung for all patients were plotted across sessions. HU_{median} in the lung was −774.1 (range, −869.6 to −468.2) at pre-therapy, which increased to −763.4 (range, −865.7 to −471.2) at mid-therapy. This value further increased to −753.6 (range, −864.8 to −642.7) at post-therapy session.
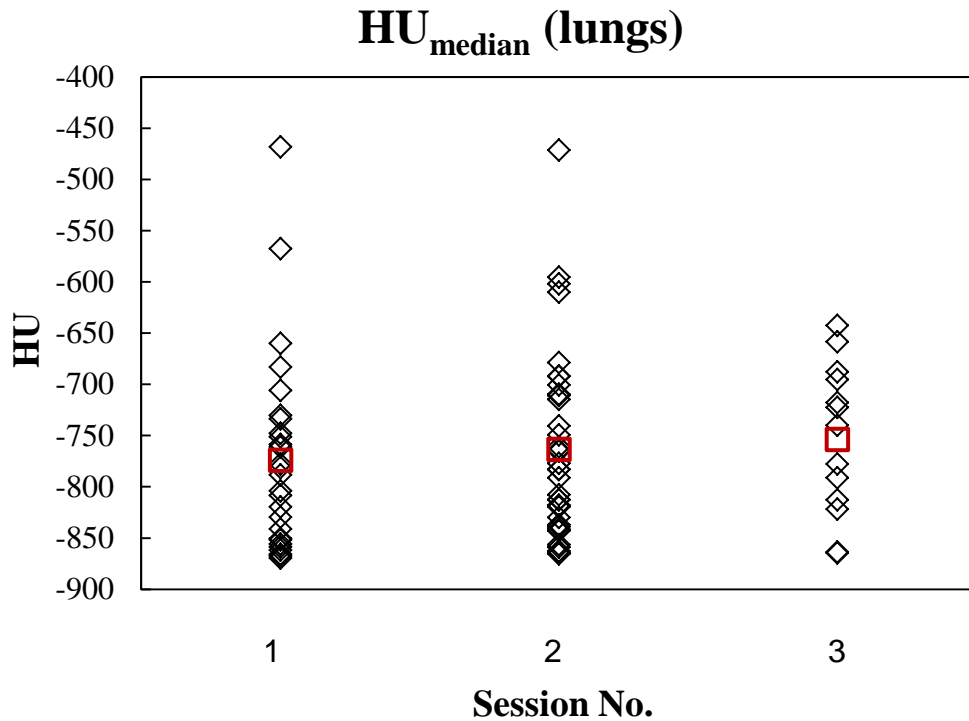
Figure 50: HU_median in the lung plotted versus time (before start of RT, mid therapy and 6 weeks after RT) for all individual patients with a CT-PET scans.

4.4.3. HU response versus dose

To determine the changes in lung density as a function of dose in the mid-therapy and in the post-therapy session HU_{mean} was calculated in each dose bin of 0.5 Gy for all patients and the mean value of HU_{mean} that belongs to each dose bin was then calculated. 100% delivered dose corresponds to 15 Gy for mid-therapy session and 30 Gy for post-therapy session. A linear regression model was used to investigate the correlation between HU and dose at mid- and post-therapy. In the following plots the slope and intercepts are reported as an estimate ± SE (Standard Error). 95% confidence interval statistical test was then used for validation of the significant differences between the two sessions.

Figure 51 shows HU in the lung across all patients against percentage delivered dose at mid-therapy and post-therapy sessions. The straight lines represent fitted regression lines for these sessions. The lines have positive slopes. The line that belongs to post-therapy has a steeper slope.

At mid-therapy, the median of HU_{mean} in the lung that received 0–5 Gy was –722.1, 5–10 Gy was –714.9, and >10 Gy was –711.6. At post-therapy session, the median of HU_{mean} in the lung that received 0–10 Gy was –710.1, 10–20 Gy was –701.1, and >20 Gy was –691.9.

Using linear regression the slope at mid-therapy and post-therapy was 0.66±0.10 and 1.55±0.2, with a 95% CIs [0.34, 0.98] and [1.11, 1.99], respectively. The intercept at mid-therapy and post-therapy was –725.2±2.9 and –718.6±3.9, with a 95% CIs [–731.0, –719.4] and [–726.6, –710.7], respectively.
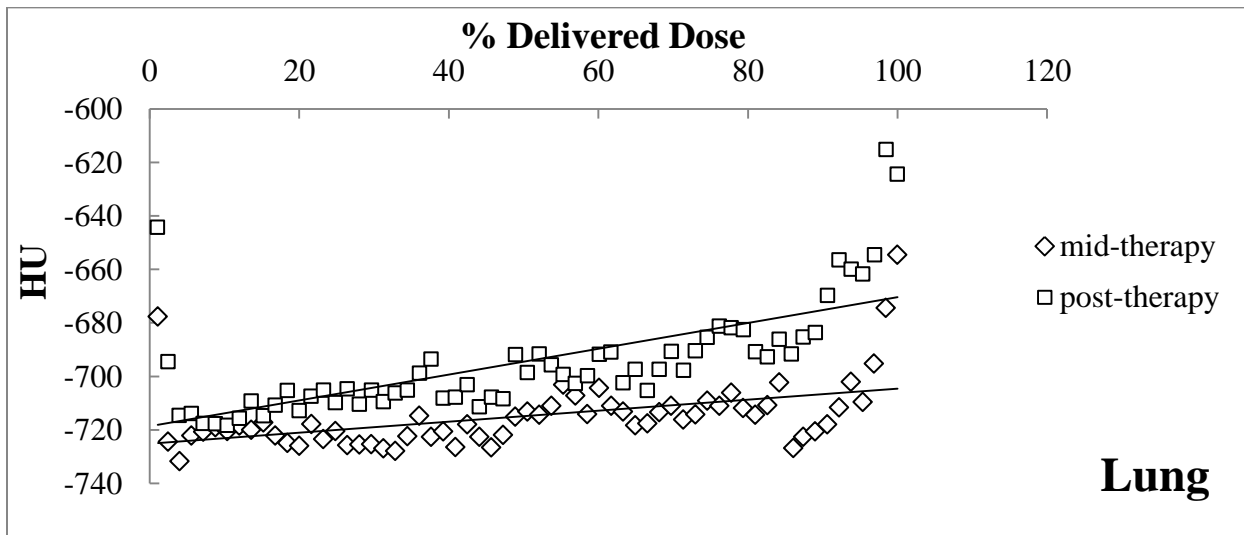
Figure 51: HU in the lung versus percentage delivered dose at mid-therapy and post-therapy. The solid lines correspond to a linear regression.

Table 3: SUV values at mid and post therapy with different dose levels in the organs at risk considered in the current study.

Organ	Session	Median of SUV_mean PDD* (0%-33%)	Median of SUV_mean PDD (33%-66%)	Median of SUV_mean PDD (>66%)	Slope**	95% CI For slope	Intercept**	95% CI For intercept
Lung	Mid-therapy	0.7	0.7	0.8	0.0046	0.0037, 0.0056	0.67	0.66, 0.69
	Post-therapy	0.8	0.9	0.9	0.0051	0.0042, 0.0061	0.77	0.75, 0.78
Bone marrow	Mid-therapy	1.6	1.6	1.6	−0.004	−0.006, −0.003	1.66	1.63, 1.69
	Post-therapy	1.5	1.5	1.5	−0.001	−0.004, 0.001	1.48	1.44, 1.52
Esophagus	Mid-therapy	1.6	1.8	1.9	0.020	0.016, 0.023	1.45	1.39, 1.52
	Post-therapy	1.7	1.9	2.0	0.019	0.011, 0.026	1.59	1.44, 1.73
Heart	Mid-therapy	2.0	2.1	2.2	0.008	0.005, 0.011	1.97	1.93, 2.02
	Post-therapy	1.9	1.9	2.0	−0.004	−0.008, 0.000	1.99	1.91, 2.07

* *Percentage delivered dose*
***From a linear regression of the SUV vs dose datasets, the slope and the intercept of the regression relation is obtained. The slope is given in units [Gy⁻¹], while the intercept is simply the estimated SUV level at zero dose.*

72

Table 4: The slope and the intercept of the linear regression at mid- and post-therapy based on Tarceva status.

Organ	Session	Tarceva status	Slope	95% CI For slope	Intercept	95% CI For intercept
Lung	Mid-therapy	Tarceva	0.004	0.003, 0.005	0.72	0.71, 0.74
		Non-Tarceva	0.005	0.003, 0.006	0.62	0.60, 0.65
	Post-therapy	Tarceva	0.003	0.002, 0.004	0.88	0.86, 0.90
		Non-Tarceva	0.010	0.009, 0.011	0.40	0.38, 0.42
Bone marrow	Mid-therapy	Tarceva	−0.003	−0.005, −0.001	1.66	1.62, 1.70
		Non-Tarceva	−0.006	−0.009, −0.003	1.66	1.60, 1.73
	Post-therapy	Tarceva	−0.001	−0.004, 0.002	1.53	1.47, 1.59
		Non-Tarceva	−0.003	−0.006, 0.000	1.37	1.30, 1.43

5. Discussion

5.1. Critical appraisal

In this study, twenty two patients with NSCLC, 6 women and 16 men at the average age of 70 years (range: 60–81), were included. Post ^{18}F-FDG PET-CT examination couldn't be performed on 15 patients due to rapid progression of disease, death, or that patients did not show up at the imaging session. Three patients were not examined at mid-therapy. Furthermore, eight patients missed their first ^{18}F-FDG PET-CT examination. The limited number of patients in this project and the missing data for sessions, especially for session three, introduces difficulties in drawing solid conclusions. Other issues to consider include: 1) the fact that blood sugar for patient 1 was higher than a normal range (above 8 mMol/L), 2) the time interval between pre-therapy and mid-therapy was too long for two patients (65 and 34 days for patient 6 and 8, respectively), 3) the incubation time was more than the normal range (60–80 min) for patient 3 and 19 at pre-therapy session and for patient 1 at mid-therapy.

Lung cancer patients may have other lung diseases such as Chronic Obstructive Pulmonary Disease (COPD). The involvement of inflammatory cells in the pathogenesis of COPD is well established and FDG uptake is greater in COPD than in normal subjects (22). SUV level from patients with COPD could be higher and this could be a source of error. COPD status was not recorded in the current investigation.

Another issue that should be taken into account is that, for some patients (Figure 13), a fluid accumulation in the lung (called pleural effusion) caused by the cancer was observable. The pleural fluid causes difficulties in scoring one-to-one voxel associations in the HU analysis of the lung.

Having only one set of delineations on planning CT may be problematic especially for patients with rapid disease progression. In other words, tumor volume changes from planning CT to the last ^{18}F-FDG PET-CT examination may occur, but only data from within the early tumor volume is scored. This also affects the lung volume, especially in ipsilateral lung. Still, error in lung data

74

is minimized by introducing the CT window for lung tissue at all sessions. Some patients may have tumor masses in both lungs, and spread of the cancer cells during the treatment. This can affect the data of ipsilateral and contralateral lungs, since the lung with the largest tumor volume is used as ipsilateral lung.

Originally, there were two Tarceva arms (+ one RT arm) in the clinical study. In one arm, patients were given Tarceva from the first to the last day of radiotherapy. In the second arm, patients kept receiving Tarceva after the end of the radiotherapy. In the analysis, these two trial arms are mixed together, which could give rise to uncertainties with respect to assessing the effects of Tarceva.

Correction for blood glucose level in individual patients is not performed in the estimated SUVs. However, the strong correlation between SUV and blood glucose concentration suggests that for non-diabetic fasted patients, lung tumor SUVs should not be adjusted for blood glucose level (23).

5.2. Gross Tumor Volume

5.2.1. Time trend in SUV

Hebert et al. (24) showed that in terms of measuring the response to radiotherapy, metabolic changes are more sensitive than morphological (structural) changes. This study focused on the effect of radiotherapy on FDG uptake from PET imaging of 20 patients who were examined before and after radiotherapy. It was one of the first studies to incorporate a larger sample of patients. This study has been followed up by several articles reporting that ^{18}F-FDG PET-CT detects metabolic alterations before morphologic ones (25) (26).

In 2007 two groups published results from repeated ^{18}F-FDG PET-CT before, during, and after radiotherapy. Baardwijk et al. (26) performed ^{18}F-FDG PET-CT scans on 23 patients with medically inoperable or advanced NSCLC, before start of radiotherapy, on day 7 and 14 during radiotherapy, and 70 days after radiotherapy. Radiotherapy was delivered twice a day with a fraction size of 1.8 Gy. Investigating the time trends, they observed an increase in SUV_{max} during the first week of RT, followed by a decrease in the second week and 70 days after treatment. A large heterogeneity in the SUV_{max} in repeated PET scans was also observed between the individual patients. Furthermore, Kong et al. (25) investigated changes in SUV in 15 patients with NSCLC (stages I to III) with ^{18}F-FDG PET-CT performed two weeks before RT, during RT (after delivery of 45 Gy), and 3 to 4 months after RT. Radiotherapy was delivered with 30 daily fractions with a fraction size ranging from 2.2 to 3.4 Gy. The authors observed a significant reduction in SUV_{peak} mid-therapy, with a further reduction in this value post-therapy.

Giovacchini et al. (27) performed four repeated ^{18}F-FDG PET-CT scans in 6 patients with NSCLC who were not amendable to surgical treatment. The scans were taken before RT, during radiotherapy (at the median of 14 days before the end of radiotherapy), and at two instances after radiotherapy (at a median of 28 and 93 days respectively). Radiotherapy was delivered with a total dose between 60-70.2 Gy with a fraction size ranging from 1.8 to 2.0 Gy. Radiotherapy induced a progressive decrease in SUV_{max}. The decrease was more evident three months after radiotherapy but could also be detected during the treatment. No significant differences in

76

SUV_{max} were found between the last two sessions. More recently, Massaccesi et al. (28) performed three series of ^{18}F-FDG PET-CT in 25 patients with NSCLC: before treatment, during the third week of concurrent chemo-radiotherapy, and four weeks after the end of treatment. A total dose of 50.4 Gy was delivered with a fractionation of 1.8 Gy per day. The authors observed that the tumor metabolic activity (SUV_{max}) significantly decreased during chemo-radiotherapy, and decreased even more at the post therapy session.

The aim of this part of the current study was to evaluate changes in the uptake of FDG on PET scans performed before, during, and after radiotherapy in patients with NSCLC. A large heterogeneity in tumor metabolic activity (SUV_{max} and SUV_{mean}) among the individual patients before treatment may suggest a large cellular heterogeneity between tumors. In our observation the average of SUV_{max} pre-therapy is much higher than that reported by Baardwijk (26), but more similar to those reported by Giovacchini (27) and Massaccesi (28). There are various mechanisms that could potentially affect the level of FDG uptake. Mechanisms such as the up-regulation of glucose transporters and hexokinase enzymes (29), hypoxia (30), and tumor aggressiveness and proliferation (31) (32) could enhance trapping of FDG in the tumor cells. We observed a significant ($p = 0.05$) reduction in SUV_{max} from the pre-therapy to the post-therapy session, in line with the studies previously mentioned. The insignificant decrease in maximal tumor metabolic activity from the pre-therapy session to the mid-therapy session may imply that the time window of 5 days is not appropriate (too small) to see changes in FDG uptake in the course of radiotherapy. However, the optimal time to perform ^{18}F-FDG PET-CT examination during the treatment is remained unclear. Massaccesi et al. (28) reported a significant decrease in the tumor metabolic activity after an RT dose of 23.4 Gy (total dose of 50.4 Gy, fractionation of 1.8 Gy/day). In contrast, Baardwijk et al. (26) did not observe any significant decrease in tumor metabolic activity after 14 days (1.8 Gy twice a day). Differences in the radiotherapy fractionation schedule, treatment time, concurrent chemotherapy administration, tumor biology, and pre-treatment SUV_{max} values might also have an impact on tumor FDG uptake during radiotherapy. Small sample size considerably limited the statistical inference to detect significant changes in glucose metabolism over time.

According to the Positron Emission Tomography Response Criteria in Solid Tumors (PERCIST) guidelines, a 30% reduction in tumor FDG uptake is defined as metabolic response (33). In addition, an absolute reduction of at least 0.8 SUV is also required. By calculating changes in tumor SUV_{max} between all available sessions for individual patients and using PERCIST criteria, tumor metabolic response was found in a few of patients (Table 5). On the other hand, no significant decrease was found in SUV_{mean}. This may imply that SUV_{max} was the more sensitive parameter to show metabolic modification induced by the treatment.

Table 5: Percentage change in tumor SUV_{max} between all available sessions for individual patients. Negative values represent a reduction in SUV_{max} while positive values represent an increase in SUV_{max}.

Patient's ID	% change, pre- to mid-therapy	% change, mid- to post-therapy	% change, pre- to post-therapy
1	9.9		
2	-9.9		
3		-8.5	
4	-44.7	-58.7	-77.1
6	-4.7	28.0	21.9
7	9.5		
8	-22.9		
9	22.1	-12.4	6.9
10	-82.4		
12	7.7	-25.0	-19.2
16	28.2		
20		-40.3	
21	8.6	-37.7	-32.3

5.2.2. Influence of Tarceva

Over the last decade, several molecular targeted agents, such as Tarceva or gefitinib[16] have emerged for treatment of NSCLC. Tarceva is one of the most widely studied targeted agents, and have been used in clinical trials for patients with NSCLC. However, research concerning response monitoring with ^{18}F-FDG PET-CT for targeted therapies is scare. The first report on the value of PET in evaluation of early response to targeted therapies emerged in 2003. Here, Stroobants et al. (34) reported that a PET response was observed in 13 out of 21 patients with gastrointestinal stromal tumors (GISTs) after 8 days of treatment with Imatinib.

Two groups has reported that ^{18}F-FDG PET-CT may detect tumor changes occurring as early as 2 days after start of Tarceva treatment, which can predict early response in NSCLC patients (35) (36). In contrast, Ullrich and colleagues (37) reported that ^{18}F-FDG PET-CT failed to robustly identify the responding tumors after two days of treatment (using PC9 and the HCC827 xenografts in nude mice). They suggest that glucose metabolism rather indirectly reflects tumor cell proliferation and therefore is not a suitable marker for Tarceva at early stage of treatment.

Aukema et al. (38) studied whether ^{18}F-FDG PET-CT could predict response to Tarceva for patients with NSCLC. In that study, 23 patients with non-small cell lung cancer who were eligible for surgical resection were evaluated. All patients received neoadjuvant Tarceva once daily for 3 weeks and two series of ^{18}F-FDG PET-CT were performed before and one week after the administration of Tarceva. 6 of 23 patients (26%) showed metabolic response[17] within one week of treatment, 16 patients (70%) showed stable disease and 1 patient (4%) showed progressive disease. This study suggested that during the early course of Tarceva therapy for NSCLC, ^{18}F-FDG PET-CT can identify response in most patients. In contrast, Hachemi et al. (39) performed three series of ^{18}F-FDG PET-CT on 12 patients with stage IIIA to IV NSCLC. Scans acquired before (5±4 days) and after (9±3 days and 60±6 days) Tarceva therapy, with a

---

[16] Another EGF Receptor blocker

[17] Metabolic response was defined as a decrease of at least 25% in SUV_{max} using European Organization or Research and Treatment of Cancer (EORTC).

median duration of 75 days. It was found that the tumor SUV_{max} did not vary significantly over time.

Based on our results, no significant changes were found in the tumors' SUV_{max} for patients receiving Tarceva during the imaging sessions. This could suggest that ^{18}F-FDG PET-CT is not a suitable biomarker to monitor Tarceva treatment. The other possibility might be that Tarceva did not significantly affect the tumor during mid- or post-therapy sessions. Furthermore, no significant differences were found in the tumor SUV_{max} between patients receiving and not receiving Tarceva in each imaging session. It could be that the patients included in the current study had such an aggressive disease that the tumors did respond to neither radiotherapy nor Tarceva therapy.

5.3. Lymph nodes

5.3.1. Time trend in SUV

Kong et al. (25) and Massaccesi et al. (28) also investigated the effect of radiotherapy on lymph nodes' metabolic activity before, during, and after treatment. Kong et al. (25) reported that FDG activity of metastatic lymph nodes decreased during radiotherapy, without any significant differences between mid-therapy and post-therapy. On the other hand, Massaccesi et al. (28) reported that lymph nodes' metabolic activity decreased at the end of treatment. Based on our results, no significant changes in SUV_{max} were observed between sessions. This could imply that lymph nodes are more resistant to treatment than tumors. It has been reported that neoplastic lymph nodes are a negative prognostic factor in patients with NSCLC (40).

5.4. Lung

Lung is one of the most relevant organs at risk in the treatment of thoracic cancer. The lung is a complex organ consisting of over 40 types of cells [reported by Sorokin et al. cited in (13)], and the mechanisms leading to radiation induced lung injury is not completely understood. A number of studies has attempted to determine the mechanisms leading to radiation induced lung injury. It has been reported that the early clinical phase of radiation effects in the lung becomes apparent at

about 1–3 months after radiotherapy, with congestion, cough, dyspnea, fever, and chest pain caused by inflammation (41).

5.4.1. Time trend in SUV

Hicks et al. (42) performed a qualitative evaluation of metabolic changes within the irradiated lung volume which was beyond the regions of tumor. ^{18}F-FDG PET-CT scans before treatment and post treatment were performed on 73 patients with NSCLC treated with radical RT or chemo irradiation. The authors found a positive correlation between the degree of radiation-induced change in irradiated normal tissues (lung and pleura), and the degree of both metabolic and CT response. These post treatment changes were most likely due to radiation pneumonitis (RP) and pleuritis[18]. Furthermore, a metabolic response in the normal lung and RP seemed to be associated with a higher probability of tumor response.

Kong et al. (25) performed a pilot study and investigated changes in SUV in 15 patients with NSCLC (stages I to III). ^{18}F-FDG PET-CT scans were performed two weeks before RT, during RT (after delivery of 45 Gy), and 3 to 4 months after RT. Radiotherapy was delivered with 30 daily fractions with a fraction size ranging from 2.2 to 3.4 Gy. The authors found that there was no significant increase in SUV_{peak} activity within irradiated lung between pre-RT and mid-RT, while the FDG uptake within irradiated lung was significantly higher on the post-RT scans.

Ruysscher et al. (43) performed three series of ^{18}F-FDG PET-CT scans, one before RT (on day 0) and two during RT (on days 7 and 14), on 18 patients with stage III non-small cell lung cancer. Radiotherapy (with a total dose range of 54.0 to 79.2 Gy) was delivered twice daily with a fraction size of 1.8 Gy. The authors observed that patients without RILT (Radiation Induced Lung Toxicity) had a stable SUV_{max} in the lungs between days 7 and 14; while patients with RILT had an increased SUV_{max} in the lungs during RT.

Based on our results there were no significant differences in SUV_{median} (Figure 25) and SUV_{max} (data not shown) in lung among different imaging sessions. We speculate that this could

---

[18] an inflammation of the pleura

probably be the result of using SUV data from the entire lung. For example the SUV level in Kong et al. (25) study came from the irradiated lung and not the whole lung. Since a palliative regime was used for treating patients, all parts of the lung have received a dose in the current study. Thus, we decided to exclude parts of the lung that received relatively small amounts of radiation. First we extracted the part of the lungs that received 10 Gy or more (V_{10}), and calculated the 90th percentile of the resulting SUV distribution (SUV_{90}). Then the lung volume receiving 20 Gy or more was extracted, and SUV_{90} was calculated. The data are shown in Figure 52 and Figure 53, using V_{10} and V_{20}, respectively. Even with this refinement, no significant differences were found in lung SUV_{90} using Mann-Whitney U-test on the modified data.
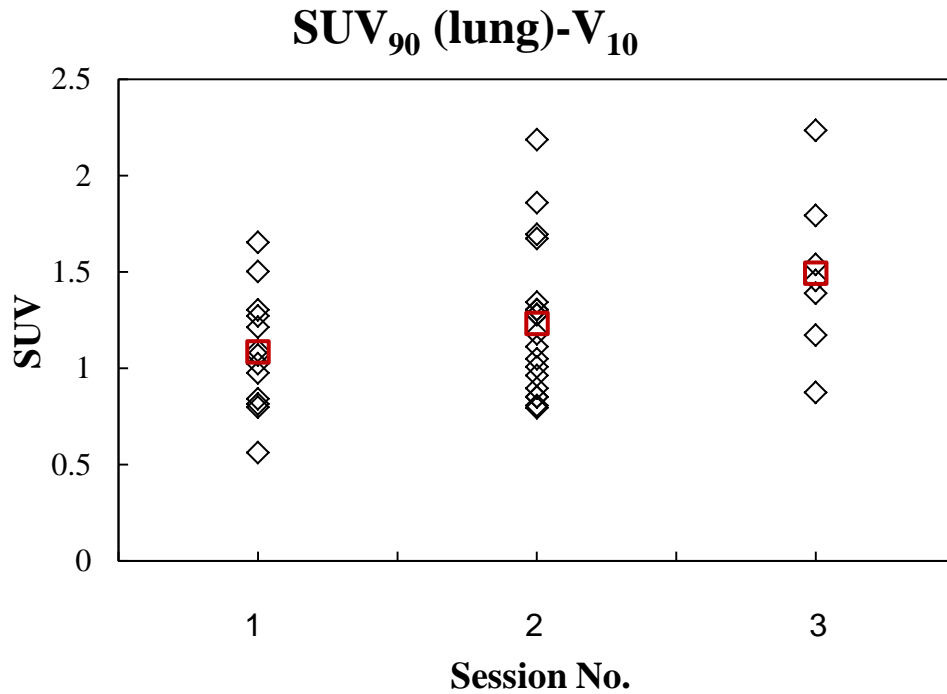
Figure 52: SUV_{90} in lung plotted versus imaging session (before start of RT, mid therapy and 6 weeks after RT) for all individual patients, using SUV data from voxels which received 10 Gy or higher.

82
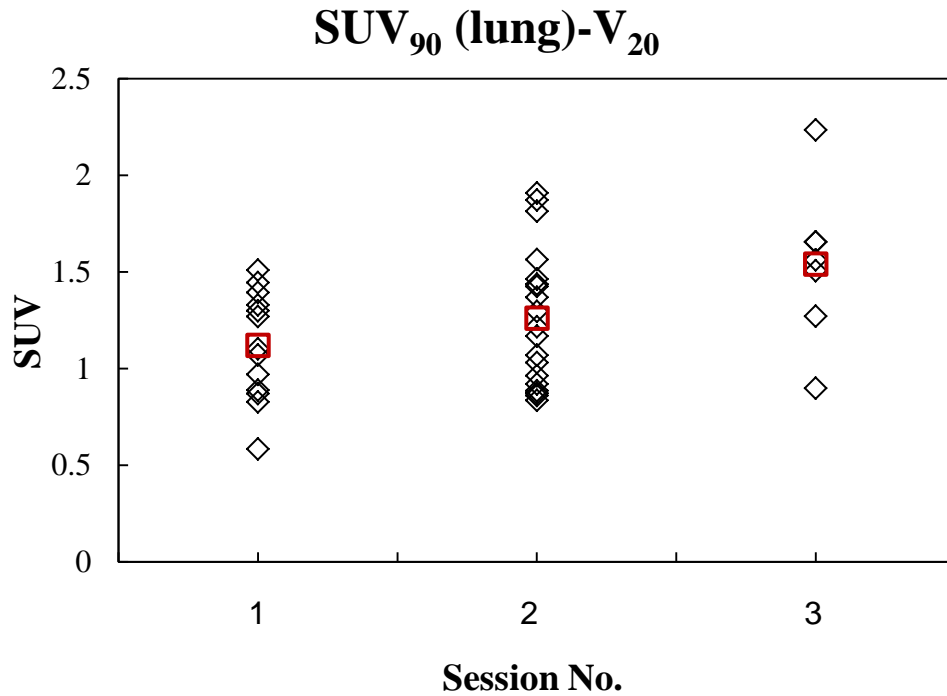
Figure 53: SUV_{90} in lung plotted versus time imaging session (before start of RT, mid therapy and 6 weeks after RT) for all individual patients with a ^{18}F-FDG PET-CT scans, using SUV data from voxels which received 20 Gy or higher .

Another possibility for the lack of response in the normal lung could be that the duration of six weeks after RT is not long enough to see significant changes in the lung metabolism. In other words, more time may be needed to observe radiation induced metabolic changes with PET in lung, as was indicated by Kong and colleagues (25) three to four months after RT. Moreover, based on the study by Ruysscher and colleagues (43), we can speculate that most of the patients did not develop RILT after completion of treatment. However, patients in this study were not evaluated for RILT, and this conclusion thus remains untestable.

5.4.2. FDG uptake response versus dose

In order to have a better understanding of any RT-induced lung injury the relation between the local dose and FDG uptake response may play an important role. Guerrero et al. (44) performed restaging ^{18}F-FDG PET-CT between 4 and 12 weeks after radiotherapy of 36 esophageal cancer

patients. The authors looked for a relationship between the local radiation dose and post-treatment FDG uptake in the lung. The average FDG uptake in the lung versus radiation dose was obtained for each patient and a linear relationship was found. McCurdy et al. (45) quantified the post radiotherapy FDG pulmonary uptake dose response in lung cancer patients. 24 lung cancer patients received restaging ^{18}F-FDG PET-CT approximately 6 weeks after completion of chemo-radiotherapy. In 22 patients, a positive linear relationship was found between the local radiation dose and the voxel-averaged post-treatment FDG uptake. Authors normalized the SUV in the irradiated lung to that in the un-irradiated lung and suggested that the slope of the regression is the pulmonary metabolic radiation response (PMRR). In our results a linear relationship was found between the local radiation dose and both mid-therapy and post-therapy FDG uptake in the lung. The slope of this relationship varied across the patients and could be reflecting the range of underlying biologic response to radiation. The individual slope (sensitivity) could be a measure of underlying intensity of lung injury (Figure 32). At mid-therapy, a positive linear relationship was found for 17 patients (patients 3 and 21 had negative slopes with values of –0.0008 and –0.005, respectively). At post-therapy, 6 patients have had a positive linear relationship (patient 21 had a negative slope with a value of –0.0025). This positive correlation between radiation dose and lung FDG uptake could result from radiation pneumonitis. Radiation pneumonitis is an inflammatory reaction which is characterized by rapidly resolving vascular changes. Radiation pneumonitis may happen within irradiated lung tissue in response to injury (46) and inflammatory cells have been reported to take up more FDG than normal cells (47).

Another possibility for the increased FDG uptake with dose could be the presence of lung fibrosis. RT dose induced fibrosis (48) and a fibrotic area increases the uptake of FDG (49). Fibrosis is defined by hardening or overgrowth of the lung tissue and is associated with abnormal interstitial accumulation of extracellular matrix proteins. It is usually the end result of chronic pneumonitis. On the other hand, it has recently been suggested that an increase in lung parenchymal vasculature (due to angiogenesis) in fibrotic areas results in an increased FDG uptake rather than up-regulation of the metabolic rate in fibrotic cells (50).

The slope of the linear dose FDG relationship mid-therapy and post-therapy are very similar (Figure 31). This implies that the increase in the FDG-uptake per dose post-therapy compared to mid-therapy for most of the patients is equal. However, there was a significant increase (15%) in the intercept of the linear relationship from mid-therapy to post-therapy. This implies that irradiation of healthy lung (by delivery of maximum 15 Gy) induced a general elevation in FDG activity in the lungs six weeks after the end of radiotherapy. This "additive effect", on average, was constant for all dose levels.

5.4.3. Influence of Tarceva

No articles were found reporting on the effect of Tarceva on lung FDG uptake. In our data no significant differences were found in the lung SUV_{median} between Tarceva and non-Tarceva groups of patients at each session. However, by looking at the FDG uptake response versus RT dose graphs for Tarceva and non-Tarceva groups, a linear relationship was found between the local radiation dose and mid-therapy FDG uptake in both groups. Both groups had the same slope, which implies that Tarceva does not affect the FDG uptake per radiation dose at this session. Nevertheless, there was a significant increase (16%) observed in the intercept for patients receiving Tarceva. This implies that Tarceva increase the general FDG uptake level in the healthy lung compared to radiation. Comparing the two groups in the post-therapy session, larger differences could be seen. The slope for the Tarceva group decreased by 70% compared to the non-Tarceva group, while the intercept increased by 120%. In other words, Tarceva administration results in lower sensitivity to dose; any dose levels will result in an identically high SUV. One way to interpret these trends is to consider that Tarceva acts in the same manner as radiation, but has an equal effect on all regions in the lung. Already after 5 days elevated SUV levels may be observed, but RT dose-response is also obtained. However, if Tarceva further administered, the glucose uptake in the lung is saturated and the radiation dose has no effect. In this case, any radiation dose level will result in an identical SUV level, as indeed was observed.

5.4.4. Time trend in HU

A dose-dependent increase lung density after RT has been reported after analyzing individual dose response curves of patients examined by either CT (51) (52) (53) (54) or routine chest x-

rays (55) post RT. Between 1978 and 1982, 329 breast cancer patients received post-mastectomy radiotherapy at the Department of Oncology, University Hospital of Aarhus, Denmark (55). Patients were irradiated with a minimum target dose of 36.6-40.92 Gy (12 fractions, 2 fractions per week and 22 fractions, 5 fractions per week, respectively). 207 of these patients had pre-treatment radiographs and at least three post-treatment radiographs. It was reported that the average lung density was significantly increased in the radiation field within a few weeks after radiotherapy (and up to 6 months after radiotherapy). From our data, no significant changes were found in HU_{median} between various sessions.

5.4.5. Density dose response

In this section, we studied the relationships between RT dose and the changes in regional lung CT number. Other than exploring FDG uptake response versus RT dose, changes in lung tissue density assessed with CT could also be important when assessing RT-induced lung injury. Levinson et al. (52), evaluated changes in lung tissue density in 13 patients with lung cancer. CT scans were performed prior to RT. Follow-up CT scans were performed at various intervals following RT (at 3, 6, and 12 months). The data suggest that the CT density increased markedly with dose by comparing post-treatment scans and pre-treatment scans. Jinli et al. (54) studied the temporal nature of regional lung density changes in 118 patients who received external beam RT. CT scans were performed before and after radiotherapy. Patients with different cancers received target doses up to a total dose of 73.6 Gy, with a fraction size between 1.25 Gy and 2 Gy. They observed that the lung density increased within 6 months after RT, and thereafter was stabilized. We measured lung density changes as a function of RT dose using voxel-by-voxel dose response analysis. Our result showed that there is a linear relationship between lung density and local RT dose during and after RT. It has been reported that lung density changes reflect both pneumonitis (56) and fibrosis (57) in the irradiated area of the lung, which indicates that these are pathological processes taking place in our patient cohort as well. Furthermore, a significant increase (135%) in the slope from mid-to post-therapy was observed. In other words, RT dose had a "multiplicative effect" on lung density. This may imply that lung tissue physical density changes correlated with pneumonitis and fibrosis incidence, and they increase with increasing RT dose level.

5.4.6. The effect of lung density on SUV

Another path to explore was to determine if lung's density changes with dose was responsible for the observed trends in lung SUV. From our results, increased dose gave increased lung density, and higher density could explain the increase in SUV. We tried to separate the effect of dose on density from the effect of dose on SUV by doing the following analysis. First, a graph was generated showing the relation between mean SUV and mean HU in given dose bins (Figure 54). The correlation between SUV and HU was 0.78 and 0.67 at mid and post-treatment, respectively. It is clear that a higher SUV is found in regions of the lung with higher HU.

In Figure 55, we made a correction for this slight increase in density by introducing another measure, $SUV_{CORR} = -SUV \times 1000 / HU$. Using this measure to compensate for the effect of increased density, we can still see that corrected SUV in post therapy had an increase in slope compared with the mid-therapy session. Furthermore, the SUV levels in post-therapy were elevated from the SUV levels in mid-therapy.

This may suggest that the change in FDG response versus dose was not entirely attributable to the changes in the lung's density. The trend from mid-therapy to post-therapy was observable even though we compensate for the effect of changes in density.
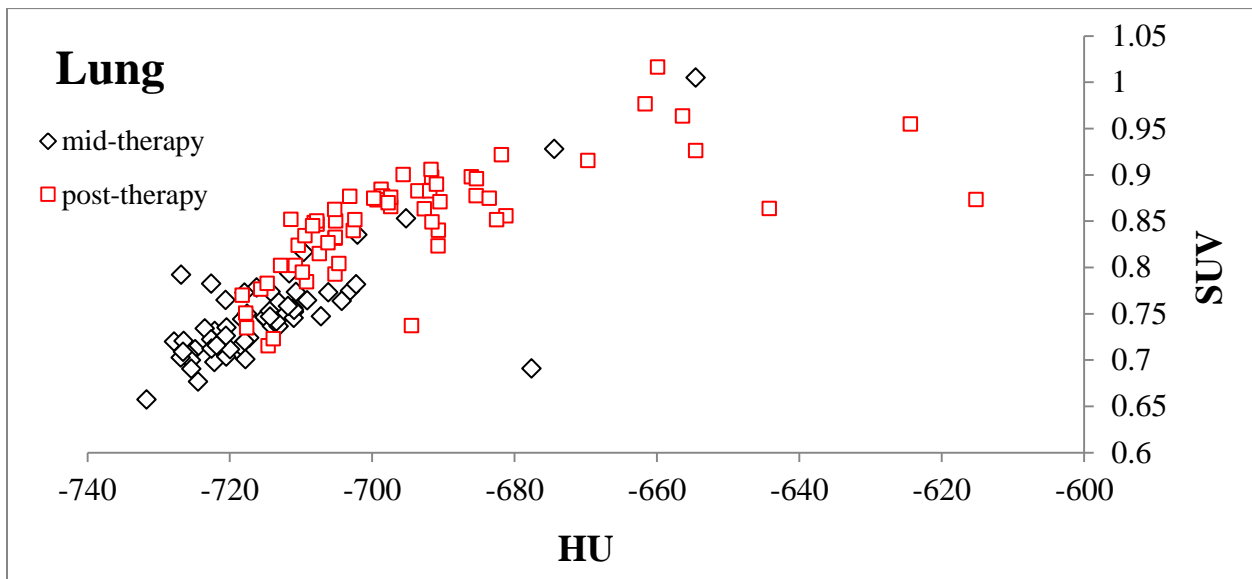
Figure 54: Correlation between lung HU and SUV.
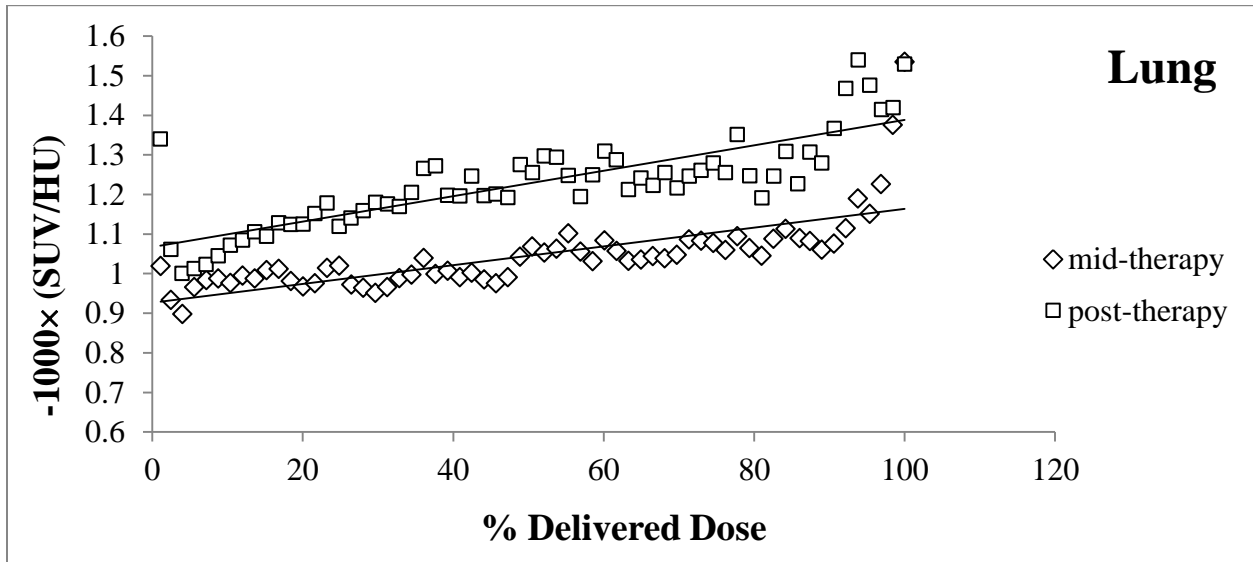
Figure 55: lung FDG uptake response (corrected for density) versus percentage delivered dose plotted for mid-therapy and post-therapy session.

5.5. Esophagus

The majority of reports about radiation induced esophagitis using ^{18}F-FDG PET-CT are from esophageal cancer patients. However, thoracic radiation therapy in patient with NSCLC can cause esophagitis. It is a common complication of such patients and a source of considerable morbidity.

5.5.1. Time trend in SUV

Bhargava et al. (58) performed post-therapy ^{18}F-FDG PET-CT scan on a patient with NSCLC. The PET images showed FDG uptake in the region of radiation-induced esophagitis. Yuan et al. (59) studied changes in esophageal FDG activity with time (from pre-RT to during-RT after delivery of 45 Gy) in fifty patients with NSCLC (stage I to III). All patients received more than

60 Gy RT dose. Authors found that esophageal NSUV[19] at the tumor level increased significantly during radiation therapy.

No significant differences in FGD uptake is found between sessions in esophagus. Similar to what we did for lung, we also extracted SUV_{90} from V_{10} and V_{20} for esophagus for all patients in three sessions. The results showed no significant difference between sessions.

5.5.2. FDG uptake response versus dose

Nijkamp et al. (60) investigated a correlation between RT dose and acute esophagitis using FDG PET scans acquired within 3 months after concurrent chemo-radiotherapy. Eighty-two NSCLC patients treated with 24×2.75 Gy included in the study. They reported that the dose levels higher than 55 Gy on the esophagus were indicative for increased FDG uptake.

In our study a linear relationship was found between the local radiation dose and both mid-therapy and post-therapy FDG uptakes in esophagus. This correlation between RT dose and FDG uptake could reflect acute esophagitis. Acute esophagitis is inflammation of esophagus and usually occurs in patients who have undergone thoracal radiotherapy within 90 days after initiation of radiation-therapy (61).

No significant changes were found in slope and intercept of this linear regression from mid-therapy to post-therapy sessions. This may reflect that esophagitis remained stable in time (from mid-therapy to post-therapy session).

5.6. Heart

Myocardium was known to be a relatively radiation resistant before the 1960'. Recently, however, many researchers reported that radiation induced myocardial damages in the late phase were happened to the patient receiving thoracic irradiation (62) (63).

---

[19] NSUV= SUV_{max} of ROI/ mean SUV of the aortic arch

5.6.1. Time trend in SUV

Jingu et al. (64) performed ^{18}F-FDG PET-CT scan on esophageal cancer patients treated with radiation therapy (median prescribed dose of 60 Gy, daily fraction dose of 2 Gy, 5 days a week). The examination was done at least 3 months after the completion of chemo-radiotherapy (median of 9.25 months). Authors reported that 13 of the 64 patients have shown high FDG uptake in the basal myocardium (comparing median of the myocardium SUV_{max} inside and outside of the irradiated fields). This finding might indicate radiation induced myocardial damage.

In contrast, Konski et al. (65) performed pre- and post-treatment ^{18}F-FDG PET-CT on 53 advanced esophageal cancer patients who received thoracic radiotherapy (median prescription dose of 50.4 Gy, raction size of 1.8 Gy). The post-treatment examination was performed 4-6 weeks after the end of the treatment and no correlation was found between changes myocardial SUV_{max} and cardiac toxicity.

We did not found any significant differences in the heart SUV_{median} (Figure 30) and SUV_{max} (data not shown) between sessions. As mentioned before, many articles report cardiac toxicity as a late effect of radiation. This suggests that the time window of six weeks after treatment is too small to see any changes in the heart's FDG uptake.

Moreover, researchers investigated the impact of heart co-irradiation on the radiation pneumonitis both in animals and humans. Experimental studies in animal models have shown heart exposure can influence the occurrence of RILT and thus it is important to prevent irradiating the heart when treating thoracic cancers (66). It has been reported that in patients with NSCLC, irradiation of the heart could enhance the risk of RILT (67). Thus avoiding cardiac irradiation could reduce the risk of RILT.

5.6.2. FDG uptake response versus dose

No articles were found to assess glycolytic activity dose response in irradiated heart for patients with thoracic cancer. Studying heart, a positive correlation is found between RT dose and FDG uptake in mid-therapy, while in post-therapy session the correlation between RD dose and FDG

is negative. This could imply that, for positive correlations in mid-therapy, a transient inflammation or cellular stress had occurred in the heart.

5.7. Bone marrow

Bone marrow is very sensitive to radiation because bone marrow cells are dividing rapidly. Damaging in bone marrow can lead to lower levels of platelets, white blood cells, and red blood cells. Accordingly, bone marrow in the spinal area is another organ to be considered for radiation toxicity when thoracic radiotherapy as a treatment for NSCLC is used.

5.7.1. Time trend in SUV

Kenser et al. (68) performed ^{18}F-FDG PET-CT scan in mice normal tissues during the 2 months of radiation. Four mice received 12 Gy in a single fraction to the left half of the body. Authors reported a decrease in femoral bone marrow FDG uptake (particularly between days 2 and 8) in the irradiated part of the body compared to the non-irradiated part.

The bone marrow resides in the trabecular spaces in the bone. Accordingly, the delineated area for bone marrow consists of both the marrow and bone. The calculated SUV for this area is in fact the SUV for such a mix.

In our study we did not find any significant changes in bone marrow FDG uptake in various sessions. Bone marrow SUV_{90} from V_{10} and V_{20} was extracted for all patients in three sessions. The results showed no significant difference between sessions.

5.7.2. FDG uptake response versus dose

No articles were found reporting the FDG uptake response in bone marrow against RT dose. In our study, a negative linear relationship was found between the local radiation dose and both mid-therapy and post-therapy FDG uptake in bone marrow. This negative correlation may imply that radiation sterilized some cells and inhibiting their ability to divide. Furthermore, a number of cells which received relatively high dose degenerated and died at the very first post-irradiation mitosis. After six weeks of radiation therapy this linear relationship decreased towards the lower

SUV levels. We speculated that at post-therapy, where twice as RT dose in mid-therapy was delivered, even though some of the cells repaired, more cells were sterilized. In addition, those cells that successfully repaired and underwent couple of divisions by delivery of 15Gy in mid-therapy, died after delivery of 30Gy. In other words, the number of sterilized or dead cells correlated with both high RT dose region in the bone marrow and the total amount of dose delivered.

5.8. Influence of Tarceva on orangs at risk

No significant differences were found in esophagus, heart, and bone marrow SUV_{median} between Tarceva receiving and non-Tarceva receiving groups of patients in each session. No useful results were achieved by separating patients to Tarceva and non-Tarceva groups and by analyzing esophagus and heart FDG uptake response versus dose at mid- and post-therapy (data not shown).

By comparing bone marrow FDG uptake response versus RT dose in post-therapy for patients who received Tarceva and for patients who didn't, the additive effect was observed in Tarceva receiving patients (Figure 47). This elevation in FDG uptake in Tarceva receiving patients could suggest that bone marrow stimulates Tarceva drug six weeks after completion of treatment.

6. Conclusion

The computer code developed for this work co-registers the planning CT, a series of PET-CT scans, and the RT dose. This program has been tested and debugged in a number of occasions and can be regarded as a reasonably well-working piece of software. It can also be used as a test and analysis platform by other researchers, and can be extended to be used in other similar studies.

The tumor's metabolic response and the FDG uptake before initiation of radiotherapy varied from patient to patient. Moreover, the FDG change from session to session was not identical for individual patients. However, this study has shown a significant reduction of tumor FDG activity (in SUV_{max}) in patients with NSCLC six weeks after fractionated radiotherapy.

Studying the SUV levels in healthy organs, it is concluded that the metabolic changes during radiotherapy does not have a significant relationship with the metabolic activity after treatment. Furthermore, the FDG uptake and radiotherapy dose at mid- and post-therapy in organs at risk revealed a significant linear dose-response relationship. A relationship between lung density and dose was also identified in both sessions from the CT images. After accounting for increased density in the lung, our conclusions about the relationship between dose and FDG uptake (a significant linear relationship) still remains valid.

This study also investigated the effect of Tarceva on FDG uptake of the tumor and healthy organs. The results show that this drug has minimal effect on the FDG uptake of tumor. However, the effect of Tarceva on the lungs was clearly observable.

7. Further Work

This work could benefit from extensions in a number of ways. For example, while in this work we used a single delineation from planning CT, it is also possible to further refine the analysis by having tumors delineated at all available sessions. This could provide us with a more accurate view of how FDG uptake changes in tumors during radiotherapy. Explicitly, we could see how the FDG uptake changes if patients indeed have tumor shrinkage or growth. Having such results from PET investigations, we could compare those with clinical outcome such as survival time. Moreover, with such a comparison we may be able to find the optimal timing for assessing local control using ^{18}F-FDG PET-CT scans.

Another extension of this work would be to separate various volumes in the lung, since different areas within the lung have different sensitivity to radiation. Such a refined delineation effort combined with study of the FDG uptake will help us understand the areas that are more sensitive to radiation. Later, we could arrange for a better treatment plan by reducing the exposure of these areas.

It has been reported in a preclinical study that heart irradiation results in increasing end-diastolic pressure and can promote pulmonary interstitial edema (69). Having patient's blood pressure measured before each session can help us to further investigate the correlation between blood pressure and heart FDG uptake. Furthermore, a preclinical study suggests that the breathing rate (BR) can be a surrogate measure of radiation pneumonitis (70). Accordingly, measuring BR before each session will also provide us with insight to understand RILT further. In addition if data about dyspnea grading for patients is gathered, it could help us further in understanding RILT.

Inflammation in the lung can be described as the accumulation of fluid, plasma proteins, and white blood cells. This phenomenon is generally marked by increased levels of cytokines (71). Cytokines are small proteins and are released by a broad range of cells, including immune cells. Accordingly, cytokine analysis can identify the presence of an activated immune response.

Analyzing blood samples for cytokines could help us identify the correlation between FDG uptake and inflammation as an outcome.

Epidermal growth factor receptor (EGFR) inhibitor treatment is associated with the development of dermatologic side effects (72). Skin toxicity such as skin rash is a common side effect in Tarceva-treated patients with advanced or metastatic non-small cell lung cancer (73). Such side effects can have an impact on a patient's quality of life. Thus skin toxicity grading could be valuable in order to search for correlation between degree of toxicity of skin and clinical outcome. Adapting Tarceva dose according to skin toxicity grade could improve a patient's quality of life.

8. Bibliography

1. *Early lung-cancer detection with spiral CT and positron emission tomography in heavy smokers: 2-year results.* **Pastorino U, Bellomi M, Landoni C, De Fiori E, Arnaldi P, Picchio M, Pelosi G, Boyle P, Fazio F.** 2003, Lancet., Vol. 362, pp. 593-7.

2. *Systemic treatment of advanced non-small cell lung cancer.* **Traynor AM, Schiller JH.** 2004, Drugs Today (Barc). , Vol. 40, pp. 697-710.

3. *Erlotinib versus standard chemotherapy as first-line treatment for European patients with advanced EGFR mutation-positive non-small-cell lung cancer (EURTAC): a multicentre, open-label, randomised phase 3 trial.* **Rosell R, Carcereny E, Gervais R, Vergnenegre A, Massuti B, Felip E, Palmero R, Garcia-Gomez R, Pallares C, Sanchez JM, Porta R, Cobo M, Garrido P, Longo F, Moran T, Insa A, De Marinis F, Corre R, Bover I, Illiano A, Dansin E, de Castro J, Milella M.** 2012, Lancet Oncol., Vol. 13, pp. 239-46.

4. *Erlotinib in previously treated non-small-cell lung cancer.* **Shepherd FA, Rodrigues Pereira J, Ciuleanu T, Tan EH, Hirsh V, Thongprasert S, Campos D, Maoleekoonpiroj S, Smylie M, Martins R, van Kooten M, Dediu M, Findlay B, Tu D, Johnston D, Bezjak A, Clark G, Santabárbara P, Seymour L.** 2005, N Engl J Med, Vol. 353, pp. 123-32.

5. *Erlotinib as maintenance treatment in advanced non-small-cell lung cancer: a multicentre, randomised, placebo-controlled phase 3 study.* **Cappuzzo F, Ciuleanu T, Stelmakh L, Cicenas S, Szczésna A, Juhász E, Esteban E, Molinier O, Brugger W, Melezínek I, Klingelschmitt G, Klughammer B, Giaccone G.** 2010, Lancet Oncol., Vol. 11, pp. 521-9.

6. *Physics in Nuclear Medicine.* **Simon R. Cherry, James A. Sorenson, Michael E. Phelps.** *Expert Consult.* s.l. : Elsevier, 2012.

7. *PET/CT: form and function.* **Blodgett TM1, Meltzer CC, Townsend DW.** 2007, Radiology., Vol. 242, pp. 360-85.

8. [Online] http://www.oncolex.org/en/Lung-cancer.aspx (25.09.2014).

9. *ODEC.* [Online] http://www.odec.ca/projects/2007/kimj7j2/index_files/Page1674.htm (25.09.2014).

10. *Clinical role of positron emission tomography in oncology.* **Bomanji JB, Costa DC, Ell PJ.** 2001, Lancet Oncol., Vol. 2, pp. 157-64.

11. *Wikipedia.* [Online] http://en.wikipedia.org/wiki/Positron_emission_tomography (25.09.2014).

12. *Siemens.* [Online]
http://www.siemens.com/press/en/pressrelease/?press=/en/pressrelease/2013/healthcare/imaging-therapy-systems/him201310002.htm&content[]=HIM (25.09.2014).

13. *Radiation effects in the lung.* **J E Coggle, B E Lambert, S R Moores.** 1986, Environ Health Perspect., Vol. 70, pp. 261-291.

14. *Erlotinib in previously treated non-small-cell lung cancer.* **Shepherd FA, Rodrigues Pereira J, Ciuleanu T, Tan EH, Hirsh V, Thongprasert S, Campos D, Maoleekoonpiroj S, Smylie M, Martins R, van Kooten M, Dediu M, Findlay B, Tu D, Johnston D, Bezjak A, Clark G, Santabárbara P, Seymour L.** 2005, N Engl J Med., Vol. 353, pp. 123-32.

15. Wikipedia. [Online] http://en.wikipedia.org/wiki/Erlotinib (25.09.2014)

16. *Molecular Biology of the Cell.* **B. Alberts, A. Johnson, J. Lewis, M. Raff, K. Roberts, P. Walter.** *Reference Edition.* fifth. s.l. : Garland Science, 2007.

17. *Radiation Oncology Physics: A Handbook for Teachers and Students.* **Podgorsak, E.B., [ed.].** 2005.

18. *Oncology for Palliative Medicine.* **Peter Hoskin, Wendy Makin.** Second edition. s.l. : Oxford, 2003.

19. *The Essential Physics of Medical Imaging.* **Bushberg, J.T; Seibert, J.A; Leidholdt Jr., E.M; Boone, J.M.** third edition. s.l. : Williams and Wilkins, 2011.

20. Coyote's Guide to IDL Programming. **Fanning, D.** [Online] http://www.idlcoyote.com.

21. *Coyote's Guide To: Traditional IDL Graphics.* s.l. **Fanning, David. W.** Coyote Book Publishing, 2011.

22. *In vivo assessment of lung inflammatory cell activity in patients with COPD.* **Jones HA, Marino PS, Shakur BH, Morrell NW.** 2003, Eur Respir J., Vol. 21, pp. 567-73.

23. *Effect of corrections for blood glucose and body size on [[sup 18] F]FDG PET standardised uptake values in lung cancer.* **Hallett, William A.; Marsden, Paul K.; Cronin, Bernadette F.; O'Doherty, Michael J.** 2001, European Journal of Nuclear Medicine, Vol. 28.

24. *Positron emission tomography in the pretreatment evaluation and follow-up of non-small cell lung cancer patients treated with radiotherapy: preliminary findings.* **Hebert ME, Lowe VJ, Hoffman JM, Patz EF, Anscher MS.** 1996, Am J Clin Oncol., Vol. 19, pp. 416-21.

25. *A Pilot Study of [18F]Fluorodeoxyglucose Positron Emission Tomography Scans During and After Radiation-Based Therapy in Patients With Non–Small-Cell Lung Cancer.* **Kong FM, Frey KA, Quint LE, Ten Haken RK, Hayman JA, Kessler M, Chetty IJ, Normolle D, Eisbruch A, Lawrence TS.** 2007, J Ciln Oncol, Vol. 25, pp. 3116-23.

26. *Time trends in the maximal uptake of FDG on PET scan during thoracic radiotherapy. A prospective study in locally advanced non-small cell lung cancer (NSCLC) patients.* **Van Baardwijk A, Bosmans G,**

Dekker A, van Kroonenburgh M, Boersma L, Wanders S, Ollers M, Houben R, Minken A, Lambin P, De Ruysscher D. 2007, Radiother Oncol., Vol. 82, pp. 145-52.

27. *Changes in glucose metabolism during and after radiotherapy in non-small cell lung cancer.* **Giovacchini G, Picchio M, Schipani S, Landoni C, Gianolli L, Bettinardi V, Di Muzio N, Gilardi MC, Fazio F, Messa C.** 2009, Tumori, Vol. 95, pp. 177-84.

28. *¹⁸F-FDG PET-CT during chemo-radiotherapy in patients with non-small cell lung cancer: the early metabolic response correlates with the delivered radiation dose.* **Massaccesi M, Calcagni ML, Spitilli MG, Cocciolillo F, Pelligrò F, Bonomo L, Valentini V, Giordano A.** 2012, Radiat Oncol.

29. *[18F]FDG uptake and PCNA, Glut-1, and Hexokinase-II expressions in cancers and inflammatory lesions of the lung.* **Mamede M, Higashi T, Kitaichi M, Ishizu K, Ishimori T, Nakamoto Y, Yanagihara K, Li M, Tanaka F, Wada H, Manabe T, Saga T.** 2005, Neoplasia., Vol. 7, pp. 369-79.

30. *Fluorodeoxyglucose uptake in human cancer cell lines is increased by hypoxia.* **Clavo AC, Brown RS, Wahl RL.** 1995, J Nucl Med., Vol. 36, pp. 1625-32.

31. *Lung cancer proliferation correlates with [F-18]fluorodeoxyglucose uptake by positron emission tomography.* **Vesselle H, Schmidt RA, Pugsley JM, Li M, Kohlmyer SG, Vallires E, Wood DE.** 2000, Clin Cancer Res., Vol. 6, pp. 3837-44.

32. *Lung tumor growth correlates with glucose metabolism measured by fluoride-18 fluorodeoxyglucose positron emission tomography.* **Duhaylongsod FG, Lowe VJ, Patz EF Jr, Vaughn AL, Coleman RE, Wolfe WG.** 1995, Ann Thorac Surg., Vol. 60, pp. 1348-52.

33. *From RECIST to PERCIST: Evolving Considerations for PET response criteria in solid tumors.* **Wahl RL, Jacene H, Kasamon Y, Lodge MA.** 2009, J Nucl Med., Vol. 50, pp. 122S-50S.

34. *18FDG-Positron emission tomography for the early prediction of response in advanced soft tissue sarcoma treated with imatinib mesylate (Glivec).* **Stroobants S, Goeminne J, Seegers M, Dimitrijevic S, Dupont P, Nuyts J, Martens M, van den Borne B, Cole P, Sciot R, Dumez H, Silberman S, Mortelmans L, van Oosterom A.** 2003, Eur J Cancer., Vol. 39, pp. 2012-20.

35. *Usefulness of 18FDG-positron emission tomography (FDG-PET) for early prediction of erlotinib (Eb) treatment outcome in non-small cell lung cancer (NSCLC) patients: Results of a pilot study.* **H. J. Soto Parra, M. Ippolito, M. Tiseo, S. Cosentino, A. Ardizzoni, F. Latteri, V. Pumo, S. Cordio, R. Bordonaro, P. Spadaro.** 2009, J Clin Oncol., Vol. 27.

36. *Predictive and prognostic value of early response assessment using 18FDG-PET in advanced non-small cell lung cancer patients treated with erlotinib.* **Tiseo M, Ippolito M, Scarlattei M, Spadaro P, Cosentino S, Latteri F, Ruffini L, Bartolotti M, Bortesi B, Fumarola C, Caffarra C, Cavazzoni A, Alfieri RR, Petronini PG, Bordonaro R, Bruzzi P, Ardizzoni A, Soto Parra HJ.** 2014, Cancer Chemother Pharmacol., Vol. 73, pp. 299-307.

37. *Early detection of erlotinib treatment response in NSCLC by 3'-deoxy-3'-[F]-fluoro-L-thymidine ([F]FLT) positron emission tomography (PET).* **Ullrich RT, Zander T, Neumaier B, Koker M, Shimamura T, Waerzeggers Y, Borgman CL, Tawadros S, Li H, Sos ML, Backes H, Shapiro GI, Wolf J, Jacobs AH, Thomas RK, Winkeler A.** 2008, PLoS One, Vol. 3.

38. *Is 18F-FDG PET/CT useful for the early prediction of histopathologic response to neoadjuvant erlotinib in patients with non-small cell lung cancer?* **Aukema TS1, Kappers I, Olmos RA, Codrington HE, van Tinteren H, van Pel R, Klomp HM.** 2010, J Nucl Med., Vol. 51, pp. 1344-8.

39. *[18F]FDG Positron Emission Tomography within Two Weeks of Starting Erlotinib Therapy Can Predict Response in Non-Small Cell Lung Cancer Patients.* **Mammar Hachemi, Couturier O, Vervueren L, Fosse P, Lacœuille F, Urban T, Hureaux J.** 2014, PLoS One, Vol. 9.

40. *Prognostic impact of number of resected and involved lymph nodes at complete resection on survival in non-small cell lung cancer.* **Saji H, Tsuboi M, Yoshida K, Kato Y, Nomura M, Matsubayashi J, Nagao T, Kakihana M, Usuda J, Kajiwara N, Ohira T, Ikeda N.** 2011, J Thorac Oncol., Vol. 6, pp. 1865-71.

41. *Effects of radiation on normal tissue: consequences and mechanisms.* **Stone HB, Coleman CN, Anscher MS, McBride WH.** 2003, Lancet Oncol. , Vol. 4, pp. 529-36.

42. *Early FDG-PET imaging after radical radiotherapy for non-small-cell lung cancer: inflammatory changes in normal tissues correlate with tumor response and do not confound therapeutic response evaluation.* **Hicks RJ, Mac Manus MP, Matthews JP, Hogg A, Binns D, Rischin D, Ball DL, Peters LJ.** 2004, Int J Radiat Oncol Biol Phys., Vol. 60, pp. 412-8.

43. *Increased (18)F-deoxyglucose uptake in the lung during the first weeks of radiotherapy is correlated with subsequent Radiation-Induced Lung Toxicity (RILT): a prospective pilot study.* **De Ruysscher D, Houben A, Aerts HJ, Dehing C, Wanders R, Ollers M, Dingemans AM, Hochstenbag M, Boersma L, Borger J, Dekker A, Lambin P.** 2009, Radiother Oncol., Vol. 91, pp. 415-20.

44. *Radiation pneumonitis: local dose versus [18F]-fluorodeoxyglucose uptake response in irradiated lung.* **Guerrero T, Johnson V, Hart J, Pan T, Khan M, Luo D, Liao Z, Ajani J, Stevens C, Komaki R.** 2007, Int J Radiat Oncol Biol Phys, Vol. 68, pp. 1030-5.

45. *[18F]-FDG uptake dose-response correlates with radiation pneumonitis in lung cancer patients.* **McCurdy MR, Castillo R, Martinez J, Al Hallack MN, Lichter J, Zouain N, Guerrero T.** 2012, Radiother Oncol, Vol. 104, pp. 52-7.

46. *Radiation pneumonitis: a possible lymphocyte-mediated hypersensitivity reaction.* **Roberts CM, Foulcher E, Zaunders JJ, Bryant DH, Freund J, Cairns D, Penny R, Morgan GW, Breit SN.** 1993, Ann Intern Med, Vol. 118, pp. 696-700.

47. *PET and PET-CT imaging in infection and inflammation: Its critical role in assessing complications related to therapeutic interventions in patients with cancer.* **Basu S,Kumar R,Alavi A.** 2010, Indian journal of cancer, Vol. 47, pp. 371-9.

48. *Cellular and molecular mechanisms of fibrosis.* **Wynn TA.** 2008, J Pathol, Vol. 214, pp. 199-210.

49. *Idiopathic pulmonary fibrosis and diffuse parenchymal lung disease: implications from initial experience with 18F-FDG PET/CT.* **Groves AM, Win T, Screaton NJ, Berovic M, Endozo R, Booth H, Kayani I, Menezes LJ, Dickson JC, Ell PJ.** 2009, J Nucl Med. , Vol. 50, pp. 538-45.

50. *Glucose transporter-1 distribution in fibrotic lung disease: association with [^{18}F]-2-fluoro-2-deoxyglucose-PET scan uptake, inflammation, and neovascularization.* **El-Chemaly S, Malide D, Yao J, Nathan SD, Rosas IO, Gahl WA, Moss J, Gochuico BR.** 2013, Chest., Vol. 143, pp. 1685-91.

51. *Dose-effect relations for local functional and structural changes of the lung after irradiation for malignant lymphoma.* **Boersma LJ, Damen EM, de Boer RW, Muller SH, Roos CM, Valdés Olmos RA, van Zandwijk N, Lebesque JV.** 1994, Radiother Oncol., Vol. 32, pp. 201-9.

52. *Regional dose response to pulmonary irradiation using a manual method.* **Levinson B, Marks LB, Munley MT, Poulson J, Hollis D, Jaszczak R, Coleman RE.** 1998, Radiother Oncol., Vol. 48, pp. 53-60.

53. *The risk of early and late lung sequelae after conformal radiotherapy in breast cancer patients.* **Kahán Z, Csenki M, Varga Z, Szil E, Cserháti A, Balogh A, Gyulai Z, Mándi Y, Boda K, Thurzó L.** 2007, Int J Radiat Oncol Biol Phys., Vol. 68, pp. 673-81.

54. *Regional lung density changes after radiation therapy for tumors in and around thorax.* **Ma J, Zhang J, Zhou S, Hubbs JL, Foltz RJ, Hollis DR, Light KL, Wong TZ, Kelsey CR, Marks LB.** 2010, Int J Radiat Oncol Biol Phys., Vol. 76, pp. 116-22.

55. *Time course of radiological lung density changes after postmastectomy radiotherapy.* **Skoczylas JZ, Bentzen SM, Overgaard M, Overgaard J.** 2000, Acta Oncol., Vol. 38, pp. 181-7.

56. *Early response of lung in breast cancer irradiation: radiologic density changes measured by CT and symptomatic radiation pneumonitis.* **Wennberg B, Gagliardi G, Sundbom L, Svane G, Lind P.** 2002, Int J Radiat Oncol Biol Phys., Vol. 52, pp. 1196-206.

57. *Correlation between lung fibrosis and radiation therapy dose after concurrent radiation therapy and chemotherapy for limited small cell lung cancer.* **Rosen II, Fischer TA, Antolak JA, Starkschall G, Travis EL, Tucker SL, Hogstrom KR, Cox JD, Komaki R.** 2001, Radiology., Vol. 221, pp. 614-22.

58. *Radiation-induced esophagitis on FDG PET imaging.* **Bhargava P, Reich P, Alavi A, Zhuang H.** 2003, Clin Nucl Med., Vol. 28, pp. 849-50.

59. *Timing and intensity of changes in FDG uptake with symptomatic esophagitis during radiotherapy or chemo-radiotherapy.* **Yuan ST, Brown RK, Zhao L, ten Haken RK, Gross M, Cease KB, Schipper M, Stanton P, Yu J, Kong FM.** 2014, Radiat Oncol., Vol. 9.

60. *Relating acute esophagitis to radiotherapy dose using FDG-PET in concurrent chemo-radiotherapy for locally advanced non-small cell lung cancer.* **Nijkamp J, Rossi M, Lebesque J, Belderbos J, van den Heuvel M, Kwint M, Uyterlinde W, Vogel W, Sonke JJ.** 2013, Radiother Oncol., Vol. 106, pp. 118-23.

61. *Radiation Dose-Volume Effects In the Esophagus.* **Maria Werner-Wasik, M.D., Ellen Yorke, Ph.D., Joseph Deasy, Ph.D., Jiho Nam, M.D., Lawrence B. Marks, M.D.** 2010, Int J Radiat Oncol Biol Phys., Vol. 76, pp. 86-93.

62. *Mortality from myocardial infarction following postlumpectomy radiotherapy for breast cancer: a population-based study in Ontario, Canada.* **Paszat LF, Mackillop WJ, Groome PA, Schulze K, Holowaty E.** 1999, Int J Radiat Oncol Biol Phys., Vol. 43, pp. 755-62.

63. *Morbidity of ischemic heart disease in early breast cancer 15-20 years after adjuvant radiotherapy.* **Gyenes G, Fornander T, Carlens P, Rutqvist LE.** 1994, Int J Radiat Oncol Biol Phys., Vol. 28, pp. 1235-41.

64. *The utility of 18F-fluorodeoxyglucose positron emission tomography for early diagnosis of radiation-induced myocardial damage.* **Jingu K, Kaneta T, Nemoto K, Ichinose A, Oikawa M, Takai Y, Ogawa Y, Nakata E, Sakayauchi T, Takai K, Sugawara T, Narazaki K, Fukuda H, Takahashi S, Yamada S.** 2006, Int J Radiat Oncol Biol Phys., Vol. 66.

65. *Symptomatic cardiac toxicity is predicted by dosimetric and patient factors rather than changes in 18F-FDG PET determination of myocardial activity after chemoradiotherapy for esophageal cancer.* **Konski A, Li T, Christensen M, Cheng JD, Yu JQ, Crawford K, Haluszka O, Tokar J, Scott W, Meropol NJ, Cohen SJ, Maurer A, Freedman GM.** 104, 2012, Radiother Oncol., pp. 72-7.

66. *Radiation damage to the heart enhances early radiation-induced lung function loss.* **van Luijk P, Novakova-Jiresova A, Faber H, Schippers JM, Kampinga HH, Meertens H, Coppes RP.** 2005, Cancer Res., Vol. 65, pp. 6509-11.

67. *Heart irradiation as a risk factor for radiation pneumonitis.* **Huang EX, Hope AJ, Lindsay PE, Trovo M, El Naqa I, Deasy JO, Bradley JD.** 2011, Acta Oncol, Vol. 50, pp. 51-60.

68. *Time-course of effects of external beam radiation on [18F]FDG uptake in healthy tissue and bone marrow.* **Kesner, Adam L; Lau, Victoria K; Speiser, Michael; Hsueh, Wei-Ann; Agazaryan, Nzhde; DeMarco, John J; Czernin, Johannes; Silverman, Daniel H S.** 2008, J Appl Clin Med Phys. , Vol. 9, p. 2747.

69. *Physiological interaction of heart and lung in thoracic irradiation.* **Ghobadi G, van der Veen S, Bartelds B, de Boer RA, Dickinson MG, de Jong JR, Faber H, Niemantsverdriet M, Brandenburg S, Berger RM, Langendijk JA, Coppes RP, van Luijk P.** 2012, Int J Radiat Oncol Biol Phys., Vol. 84, pp. 639-46.

70. *Renin-Angiotensin system suppression mitigates experimental radiation pneumonitis.* **Ghosh SN, Zhang R, Fish BL, Semenenko VA, Li XA, Moulder JE, Jacobs ER, Medhora M.** 2009, Int J Radiat Oncol Biol Phys., Vol. 75, pp. 1528-36.

71. *Neuro Science.* [Online] https://www.neurorelief.com/index.php?p=cms&cid=94&pid=87 (25.09.2014).

72. *Pharmacogenetic predictors for EGFR-inhibitor-associated skin toxicity.* **Parmar S, Schumann C, Rüdiger S, Boeck S, Heinemann V, Kächele V, Seeringer A, Paul T, Seufferlein T, Stingl JC.** 2013, Pharmacogenomics J., Vol. 13, pp. 181-8.

73. *Erlotinib-related skin toxicities: treatment strategies in patients with metastatic non-small cell lung cancer.* **Kiyohara Y, Yamazaki N, Kishi A.** 2013, J Am Acad Dermatol., Vol. 69, pp. 463-72.

9. Appendix A
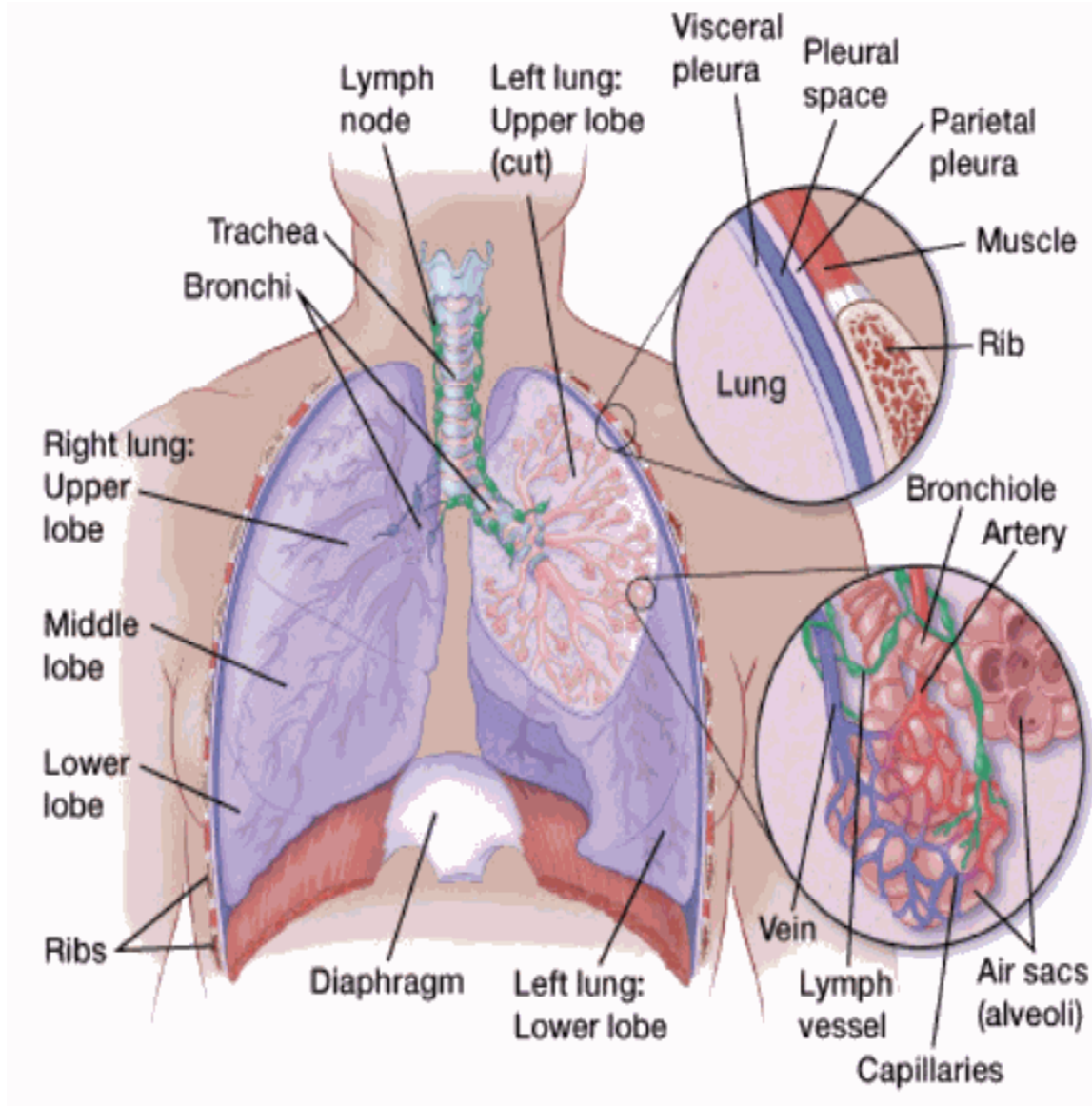
Figure 56: Anatomy of the lung

10. Appendix B

Table 6: Critical values of the Mann-Whitney U-test. n_1 and n_2 represent the number of elements in sample 1 and 2. U value required to reach the 5% of significance.

										Nondirectional α=.05 (Directional α=.025)										
										n_2										
n_1	1	2	3	4	5	6	7	8	9	10	11	12	13	14	15	16	17	18	19	20
1	-	-	-	-	-	-	-	-	-	-	-	-	-	-	-	-	-	-	-	-
2	-	-	-	-	-	-	-	0	0	0	0	1	1	1	1	1	2	2	2	2
3	-	-	-	-	0	1	1	2	2	3	3	4	4	5	5	6	6	7	7	8
4	-	-	-	0	1	2	3	4	4	5	6	7	8	9	10	11	11	12	13	13
5	-	-	0	1	2	3	5	6	7	8	9	11	12	13	14	15	17	18	19	20
6	-	-	1	2	3	5	6	8	10	11	13	14	16	17	19	21	22	24	25	27
7	-	-	1	3	5	6	8	10	12	14	16	18	20	22	24	26	28	30	32	34
8	-	0	2	4	6	8	10	13	15	17	19	22	24	26	29	31	34	36	38	41
9	-	0	2	4	7	10	12	15	17	21	23	26	28	31	34	37	39	42	45	48
10	-	0	3	5	8	11	14	17	20	23	26	29	33	36	39	42	45	48	52	55
11	-	0	3	6	9	13	16	19	23	26	30	33	37	40	44	47	51	55	58	62
12	-	1	4	7	11	14	18	22	26	29	33	37	41	45	49	53	57	61	65	69
13	-	1	4	8	12	16	20	24	28	33	37	41	45	50	54	59	63	67	72	76
14	-	1	5	9	13	17	22	26	31	36	40	45	50	55	59	64	67	74	78	83
15	-	1	5	10	14	19	24	29	34	39	44	49	54	59	64	70	75	80	85	90
16	-	1	6	11	15	21	26	31	37	42	47	53	59	64	70	75	81	86	92	98
17	-	2	6	11	17	22	28	34	39	45	51	57	63	67	75	81	87	93	99	105
18	-	2	7	12	18	24	30	36	42	48	55	61	67	74	80	86	93	99	106	112
19	-	2	7	13	19	25	32	38	45	52	58	65	72	78	85	92	99	106	113	119
20	-	2	8	14	20	27	34	41	48	55	62	69	76	83	90	98	105	112	119	127

Table 7: Statistical U-values for man-Whitney U-test comparing sessions ($N_1=14$, $N_2=19$, $N_3=7$)

Organ	U value (pre- therapy vs. mid-therapy)	U value (pre-therapy vs. post-therapy)	U value (mid-therapy vs. post-therapy)
GTV_{max}	119	21	115
GTV_{mean}	136	35	95
$Heart_{median}$	130	54	82
$Esophagus_{median}$	174	69	65
Bone marrow$_{median}$	192	73	89
Ipsilateral lung$_{median}$	156	66	65
Contralateral lung$_{median}$	126	55	52

Table 8: statistical U-values for Mann-Whitney U-test (p=0.05) comparing Tarceva and non-Tarceva group ($N_{tarceva}=10$, $N_{non-tarceva}=9$)

Organ	NSUV± SE (mid-therapy)		U value (Tarceva and non-Tarceva group)
	Non-Tarceva	Tarceva	
GTV$_{max}$	0.9±0.1	1.1±0.2	33
GTV$_{mean}$	0.8±0.1	1.0±0.1	32
Heart$_{median}$	0.9±0.1	1.1±0.1	24
Esophagus$_{median}$	1.1±0.1	1.3±0.1	29
Bone marrow$_{median}$	1.1±0.1	1.2±0.1	36
Ipsilateral lung$_{median}$	0.9±0.1	1.2±0.2	34
Contralateral lung$_{median}$	1.1±0.1	1.2±0.1	28
Lung$_{median}$	1.0±0.1	1.2±0.1	120

Table 9: List of patients' data

Patient ID	Sex	Age (year)	Histology	Available PET-CT			Interval time (days)		% weight change*		Tarceva Status	Stage	Follow Up	No. of delineated lymph nodes
				PET1	PET2	PET3	PET (2-1)	PET (3-2)	PET (2-1)	PET (3-2)				
1	M	65	Carcinoma			N/A	13		−8.1		A	IV		5
2	M	76	Adenocarcinoma			N/A	8		−3.4		B	IV		3
3	M	63	Adenocarcinoma	N/A				48		0.0	C	IV		2
4	F	67	Squamous cell				5	58	0.0	−3.6	A	IV		1
5			Was excluded from the study											
6	M	74	Squamous cell				65	45	0.0	0.0	C	IV	Alive	5
7	M	70	Carcinoma			N/A			0.0		A	IV		N/A
8	M	69	Squamous cell			N/A	34		−3.8		C	IV		N/A
9	M	60	Adenocarcinoma				10	38	7.0	0.0	B	IV		N/A
10	M	81	Adenocarcinoma			N/A	20		1.0		A	IV		11
11	M	80	*Carcinoma*	N/A		N/A					A	IV		2

Negative values represent a reduction in weight.

Patient ID	Sex	Age (year)	Histology	Available PET-CT			Interval time (days)		% weight change*		Tarceva Status	Stage	Follow Up	No. of delineated lymph nodes
				PET1	PET2	PET3	PET (2-1)	PET (3-2)	PET (2-1)	PET (3-2)				
12	M	63	Carcinoma				8	60	0.0	-2.1	A	III		N/A
13	F	70	Adenocarcinoma	N/A		N/A					A	IV		2
14	M	74	Squamous cell	N/A	N/A	N/A					A	IV		N/A
15	M	73	Squamous cell		N/A	N/A					B	IV		N/A
16	M	67	Adenocarcinoma			N/A	6		1.3		A	IV	Alive	1
17	Was excluded from the study													
18	F	73	Adenocarcinoma		N/A	N/A					B	IV		N/A
19	F	64	Squamous cell		N/A	N/A					B	IV	Alive	N/A
20	M	79	squamous cell	N/A				49		1.6	B	IV	Alive	5
21	M	63	Adenocarcinoma				7	32	0.0	-1.1	B	IV		1
22	Was excluded from the study													
23	F	-	N/A	N/A		N/A					B	-		N/A
24	F	-	N/A	N/A		N/A					B	-		1
25	M	-	N/A	N/A		N/A					C	-		3

11. Appendix C

Some of the main codes developed for this study are represented here.

```
;%%%%%%%%%%%%%%%%%%%%%Main routines%%%%%%%%%%%%%%%%%%%%%%%%%
ref_res=[3.0,3.0,3.0]
i = ''
READ, i, PROMPT='patient name: '

file = FILEPATH('PAT'+i, ROOT_DIR='C:', SUBDIRECTORY='THORAT')
        j=''
        READ, j, PROMPT='session: '
        path=file+('\PAT'+i+'PET'+j)

ct_cat=path+'\ACCT'
CT, ct_cat, ref_res, ct_image, ct_res, ct_pos

rct_cat=file+('\PAT'+i+'RT'+'\CT')
CT,  rct_cat, ref_res, rct_image, rct_res, rct_pos

ct_rct, ct_image, rct_image, ct_res,  rct_res, shif_xyz, ct_mod
d_cat=file+('\PAT'+i+'RT')
RT, d_cat,ref_res, rct_res, d_pos, d_image

        weight=''
        READ, weight, PROMPT='weight: '
im_ses=j
pt_cat=path+'\PET'
PET, pt_cat, ref_res, pt_res, pt_image, pt_pos,weight
slice=80
rct_d,slice, ref_res, rct_image, d_image, rct_pos, d_pos, d_mod
rct_pt,pt_pos,ct_pos,ref_res, slice, rct_image,pt_image, shif_xyz, pt_mod,ct_mod
file_mkdir, file+'\RESULTS'
cd, file+'\RESULTS'
;save, filename='D_recon.sav', d_mod
;save, filename='CT_recon'+im_ses+'.sav', ct_mod
;save, filename='RCT_recon.sav', rct_image
;save, filename='PET_recon'+im_ses+'.sav', pt_mod
;ANALYSIS, file, im_ses
End

;%%%%%%%%%%%%%%Reading and displaying planning CT and CT series%%%%%%%%%%%%%%

pro CT, ct_cat, ref_res, ct_image, ct_res, ct_pos

obj= OBJ_NEW('IDLffDICOM')
cd, ct_cat
files= FILE_SEARCH ('*', count= nct)
```

```
read=obj->Read(files(0))

dim_x=obj->getvalue('0028'x, '0011'x,/no_copy)
dim_x=*dim_x(0)
dim_y=obj->getvalue('0028'x, '0010'x,/no_copy)
dim_y=*dim_y(0)
dim_z=nct

ct_pos=obj->getvalue('0020'x, '0032'x,/no_copy)
ct_pos=*ct_pos(0)
ct_pos = float(STRSPLIT(ct_pos,'\', /EXTRACT ) )

ct_res = obj->getvalue('0028'x, '0030'x,/no_copy)
ct_res=*ct_res(0)
ct_res = float(STRSPLIT(ct_res,'\', /EXTRACT ) )


img=obj->getvalue('7FE0'x, '0010'x,/no_copy)
img=*img(0)

new=fltarr(nct)
for k=0, nct-1 do begin
        read=obj->Read(files(k))
        ct_pos=obj->getvalue('0020'x, '0032'x,/no_copy)
        ct_pos=*ct_pos(0)
        ct_pos = float(STRSPLIT(ct_pos,'\', /EXTRACT ) )

   new(k)=ct_pos(2)
endfor

ind_sort=sort(new)
sorted=new[sort(new)]

res_z=abs(sorted(2)-sorted(1))
ct_res=[ct_res(0), ct_res(1), res_z]

img_3d=fltarr(dim_x,dim_y,dim_z)
for i=dim_z-1, 0, -1 do begin
        ind=ind_sort(i)

        read=obj->Read(files(ind))
        img=obj->getvalue('7FE0'x, '0010'x,/no_copy)
        ct_pos=obj->getvalue('0020'x, '0032'x,/no_copy)
        ct_pos=*ct_pos(0)
        ct_pos = float(STRSPLIT(ct_pos,'\', /EXTRACT ) )
        img=*img(0)
        img_3d(*,*, i)=img

endfor

ct_image=img_3d

ct_image(where(ct_image le 0))=0
cf=ct_res*[dim_x, dim_y, dim_z]/ref_res
CT_image=congrid(CT_image, cf(0), cf(1), cf(2), /CENTER)
```

```
help,'dim=',img_3d
print, 'pos=',ct_pos
print,'res=',ct_res


; We only want to match bone

ct_congrid(where(ct_congrid lt 1200))=0
rct_mod(where(rct_mod lt 1200))=0

;match lungs
ct_congrid(where(ct_congrid gt 800))=0
rct_mod(where(rct_mod gt 800))=0

ct_congrid(where(ct_congrid lt 100))=0
rct_mod(where(rct_mod lt 100))=0

ct_congrid(where(ct_congrid))=1
rct_mod(where(rct_mod))=1
end
;%%%%%%%%%%%%%%%%Co-registragion of CT series and planning CT%%%%%%%%%
;resolution=[3,3,3] for both rct_image and ct_image.
;define ct_mod as an array with dim_x and dim_y equal to rct_image (crop edges).
;define rct_mod as an array with dim_z equal to ct_image.
;now ct_mod and rct_mod have the same dimentions, which is:[ dim_rct(0),dim_rct(1),dim_ct(2)].
;corr between rct_mod and ct_mod.
;use shif_xyz to shift the ct_mod on top of the rct_mod and cut unreqired regions..
;ct_mod now has the same dimentions as original rct_image.
;PATIENT NUMBER 11 SESSION 2: different position of the arms!.

pro ct_rct, ct_image, rct_image, ct_res,  rct_res, shif_xyz, ct_mod

dim_rct=(size(rct_image))[1:3]
dim_ct=(size(ct_image))[1:3]

ct_mod=intarr(dim_rct(0),dim_rct(1),dim_ct(2))

xs=( dim_ct(0)-dim_rct(0))/2
ys=( dim_ct(1)-dim_rct(1))/2

ct_mod=ct_image(xs:xs+dim_rct(0)-1,ys:ys+dim_rct(1)-1,*)

rct_mod=intarr(dim_rct(0),dim_rct(1),dim_ct(2))
rct_mod(*,*, 0:dim_rct(2)-1)=rct_image

correl=corr(rct_mod,ct_mod)
shif=where(correl eq max(correl))
shif_xyz=array_indices(correl, shif)


if abs(shif_xyz(0)) gt dim_rct(0)/2 then shif_xyz(0)=-(dim_rct(0)-shif_xyz(0))
if abs(shif_xyz(1)) gt dim_rct(1)/2 then shif_xyz(1)=-(dim_rct(1)-shif_xyz(1))
if abs(shif_xyz(2)) gt dim_ct(2)/2 then shif_xyz(2)=(dim_ct(2)-shif_xyz(2))
```

```
ct_mod=shift(ct_mod, shif_xyz(0) , shif_xyz(1), 0)
ct_mod=ct_mod(*,*,shif_xyz(2):shif_xyz(2)+dim_rct(2) -1)

rct_mod=rct_mod(*,*,0:dim_rct(2)-1)
rct_image=rct_mod & rct_mod=0
end
;%%%%%%%%%%%%%%%%% reading and displaying RT dose%%%%%%%%%%%%%%%%

PRO RT, d_cat,ref_res, rct_res, d_pos, d_image

obj= OBJ_NEW('IDLffDICOM')
cd, d_cat
files= FILE_SEARCH ('RD*', count= nd)

read=obj->Read(files(1))

dim_x=obj->getvalue('0028'x, '0011'x,/no_copy)
dim_x=*dim_x(0)
dim_y=obj->getvalue('0028'x, '0010'x,/no_copy)
dim_y=*dim_y(0)

d_pos=obj->getvalue('0020'x, '0032'x,/no_copy)
d_pos=*d_pos(0)

d_pos = float(STRSPLIT(d_pos,'\', /EXTRACT ) )

d_res = obj->getvalue('0028'x, '0030'x,/no_copy)
d_res=*d_res(0)


img=obj->getvalue('7FE0'x, '0010'x,/no_copy)
dim_z=(size(img))[1]


img_3d=fltarr(dim_x,dim_y,dim_z)

for k=0, nd-1 do begin
        read=obj->Read(files(K))
        img=obj->getvalue('7FE0'x, '0010'x,/no_copy)
        dgs=obj->getvalue('3004'x, '000E'x,/no_copy)
        dgs=*dgs(0)

        j=0
                for i=0, dim_z-1 do begin
                imag=float(*img(i))
                img_3d(*,*, j)=img_3d(*,*, i)+(imag*dgs)

                j=j+1
        endfor
endfor

d_res = [(float(STRSPLIT(d_res,'\', /EXTRACT )))[0], (float(STRSPLIT(d_res,'\', /EXTRACT )))[1],rct_res(2)]

d_image=img_3d
```

```
cf=d_res*[dim_x, dim_y, dim_z]/ref_res
d_image=congrid(d_image, cf(0), cf(1), cf(2), /CENTER)
end
;%%%%%%%%%%%%%%%%%%% Co-registration of RT dose and planning CT%%%%%%%%%%

;d_mod is d_image which is shifted along x and y directions
PRO rct_d, slice, ref_res, rct_image, d_image, rct_pos, d_pos, d_mod

dim_rct=(size(rct_image))[1:3]
dim_d=(size(d_image))[1:3]
;change dim_rct(0) to dim_d(0)
d_image=congrid(d_image, dim_d(0), dim_d(1), dim_rct(2),/center)

d_mod=rct_image*0.0
;add diff(0)
diff=[round((d_pos(0)-rct_pos(0))/ref_res(0)),round((d_pos(1)-rct_pos(1))/ref_res(1))]

; for some patients dim_d(1) is greater than dim_rct(0), ex. patient number 4.
for i=0, 2 do begin
        if dim_d(i) ge dim_rct(i) then begin
          dim_d(i)=dim_rct(i)
          endif
endfor
;replace * with (0:dim_d(0)-1)
d_mod(0:dim_d(0)-1, 0:dim_d(1)-1, *)=d_image(0:dim_d(0)-1, 0:dim_d(1)-1, *)
;replace 0 with diff(0)
d_mod=shift(d_mod, diff(0), diff(1), 0)


test=(d_mod/max(d_mod))+(rct_image/2048.)

window,0, xsize=500, ysize=500
tvscl, congrid(test(*, *, 75), 500, 500)



;%%%%%%%%%%%%%%%%%COLOR-BLENDING%%%%%%%%%%%%%%%%%%%%%%

d_min=1
d_max=30

LOADCT, 4
TVLCT, red, green, blue, /GET

image_d = BYTARR(3, dim_rct(0), dim_rct(1))
image_d(0,*,*) = red(bytscl(d_mod(*,*,slice), min=d_min, max=d_max))
image_d(1,*,*) = green(bytscl(d_mod(*,*,slice), min=d_min, max=d_max))
image_d(2,*,*) = blue(bytscl(d_mod(*,*,slice), min=d_min, max=d_max))

ct_min=700
ct_max=1300
LOADCT, 0
TVLCT, red, green, blue, /GET
image_CT =BYTARR(3, dim_rct(0), dim_rct(1))
image_CT(0,*,*) = red(bytscl(rct_image(*,*,slice), min=ct_min, max=ct_max))
```

```
image_CT(1,*,*) = green(bytscl(rct_image(*,*,slice), min=ct_min, max=ct_max))
image_CT(2,*,*) = blue(bytscl(rct_image(*,*,slice), min=ct_min, max=ct_max))

 blending av PET-CT skjer via alpha-faktor
alpha=0.6
image_fus = byte(alpha*float(image_CT)+(1.0-alpha)*float(image_d))
image_fus=congrid(image_fus,3,dim_rct(0)*3,dim_rct(1)*3,/center)
window, 4, xsize=dim_rct(0)*3, ysize=dim_rct(1)*3
tv, image_fus, true=1
End

;%%%%%%%%%%%%%%%%% Coregistration of planning CT and PET series%%%%%%%%%%%%%%

resolution=[3,3,3] for both rct_image and pt_image_mod.
define pt_mod as an array with dim_x and dim_y equal to rct_image. (crop edges)
use shif_xyz to shift the pt_mod on top of the rct_mod and cut unreqiured regions..
pt_mod now has the same dimentions as original rct_image.
PT_MOD_NEW IS MODIFED SHIFTE PT IMAGES. THE MOST TRUSTABLE!!!!

PRO rct_pt,pt_pos,ct_pos,ref_res, slice, rct_image,pt_image, shif_xyz,pt_mod,ct_mod
rct_image=ct_mod
working with pt_image_mod instead of pt_image.
dim_rct=(size(rct_image))[1:3]
dim_pt=(size(pt_image))[1:3]

pt_mod_new=intarr(dim_rct(0),dim_rct(1),dim_pt(2))

xs=( dim_pt(0)-dim_rct(0))/2
ys=( dim_pt(1)-dim_rct(1))/2

pt_mod_new=pt_image(xs:xs+dim_rct(0)-1,ys:ys+dim_rct(1)-1,*)

diff=round(-(pt_pos-ct_pos)/ref_res)
pt_mod_new=shift(pt_mod_new, diff(0), diff(1),diff(2))

pt_mod_new=shift(pt_mod_new, shif_xyz(0) , shif_xyz(1), 0)
pt_mod_new=pt_mod_new(*,*,shif_xyz(2):shif_xyz(2)+dim_rct(2) -1)
window, 2, xsize=dim_rct(0), ysize=dim_rct(1)
tvscl,(pt_mod_new(*,100,*)/max(pt_mod_new)+rct_image(*,100,*)/2048)
window,3, xsize=dim_rct(0), ysize=dim_rct(1)
tvscl,(pt_mod_new(100,*,*)/max(pt_mod_new)+rct_image(100,*,*)/2048)
%%%%%%%%%%%%%%%%%COLOR-BLENDING-CORONAL
SLICE%%%%%%%%%%%%%%%%%%%
PET_min=0.5
PET_max=2
LOADCT, 4
TVLCT, red, green, blue, /GET
slice=100

image_pt = BYTARR(3, dim_rct(1), dim_rct(2))
image_pt(0,*,*) = red(bytscl(pt_mod_new(*,slice,*), min=PET_min, max=PET_max))
image_pt(1,*,*) = green(bytscl(pt_mod_new(*,slice,*), min=PET_min, max=PET_max))
image_pt(2,*,*) = blue(bytscl(pt_mod_new(*,slice,*), min=PET_min, max=PET_max))

ct_min=700
```

114

```
ct_max=1300
LOADCT, 0
TVLCT, red, green, blue, /GET
image_CT =BYTARR(3, dim_rct(1), dim_rct(2))
image_CT(0,*,*) = red(bytscl(rct_image(*,slice,*), min=ct_min, max=ct_max))
image_CT(1,*,*) = green(bytscl(rct_image(*,slice,*), min=ct_min, max=ct_max))
image_CT(2,*,*) = blue(bytscl(rct_image(*,slice,*), min=ct_min, max=ct_max))

 blending av PET-CT skjer via alpha-faktor
alpha=0.6
image_fus = byte(alpha*float(image_CT)+(1.0-alpha)*float(image_pt))
image_fus=congrid(image_fus,3,dim_rct(0)*2,dim_rct(1)*2,/center)
window, 1, xsize=dim_rct(0)*3, ysize=dim_rct(2)*3
tv, image_fus, true=1
;%%%%%%%%%%%%%%%%COLOR-BLENDING-SAGGITAL SLICE%%%%%%%%%%%%%%%%%

PET_min=0.5
PET_max=2

LOADCT, 4
TVLCT, red, green, blue, /GET
slice=100
image_pt = BYTARR(3, dim_rct(1), dim_rct(2))
image_pt(0,*,*) = red(bytscl(pt_mod_new(slice,*,*), min=PET_min, max=PET_max))
image_pt(1,*,*) = green(bytscl(pt_mod_new(slice,*,*), min=PET_min, max=PET_max))
image_pt(2,*,*) = blue(bytscl(pt_mod_new(slice,*,*), min=PET_min, max=PET_max))

ct_min=700
ct_max=1300
LOADCT, 0
TVLCT, red, green, blue, /GET
image_CT =BYTARR(3, dim_rct(1), dim_rct(2))
image_CT(0,*,*) = red(bytscl(rct_image(slice,*,*), min=ct_min, max=ct_max))
image_CT(1,*,*) = green(bytscl(rct_image(slice,*,*), min=ct_min, max=ct_max))
image_CT(2,*,*) = blue(bytscl(rct_image(slice,*,*), min=ct_min, max=ct_max))

 blending av PET-CT skjer via alpha-faktor
alpha=0.6
image_fus = byte(alpha*float(image_CT)+(1.0-alpha)*float(image_pt))
image_fus=congrid(image_fus,3,dim_rct(0)*3,dim_rct(1)*3,/center)
window, 2, xsize=dim_rct(0)*3, ysize=dim_rct(2)*3
tv, image_fus, true=1
;%%%%%%%%%%%%%%%%COLOR-BLENDING-TRANSVERSAL SLICE%%%%%%%%%%%%%%

slice=70
PET_min=0.5
PET_max=2
LOADCT, 4
TVLCT, red, green, blue, /GET
image_pt = BYTARR(3, dim_rct(0), dim_rct(1))
image_pt(0,*,*) = red(bytscl(pt_mod_new(*,*,slice), min=PET_min, max=PET_max))
image_pt(1,*,*) = green(bytscl(pt_mod_new(*,*,slice), min=PET_min, max=PET_max))
image_pt(2,*,*) = blue(bytscl(pt_mod_new(*,*,slice), min=PET_min, max=PET_max))

ct_min=700
```

```
ct_max=1300
LOADCT, 0
TVLCT, red, green, blue, /GET
image_CT =BYTARR(3, dim_rct(0), dim_rct(1))
image_CT(0,*,*) = red(bytscl(rct_image(*,*,slice), min=ct_min, max=ct_max))
image_CT(1,*,*) = green(bytscl(rct_image(*,*,slice), min=ct_min, max=ct_max))
image_CT(2,*,*) = blue(bytscl(rct_image(*,*,slice), min=ct_min, max=ct_max))


blending av PET-CT skjer via alpha-faktor
alpha=0.6
image_fus = byte(alpha*float(image_CT)+(1.0-alpha)*float(image_pt))
image_fus=congrid(image_fus,3,dim_rct(0)*3,dim_rct(1)*3)

window,3, xsize=dim_rct(0)*3, ysize=dim_rct(1)*3
tv, image_fus , true=1
pt_mod=pt_mod_new
print,diff
end

;%%%%%%%%%%%%%%%%%%%%Analysis%%%%%%%%%%%%%%%%%%%%%%%

PRO ANALYSIS, file, im_ses

slice=70
ref_res=[3.0,3.0,3.0]

i = ''
READ, i, PROMPT='patient name: '

file = FILEPATH('PAT'+i, ROOT_DIR='C:', SUBDIRECTORY='THORAT')

%%%%white background%%%%
Device, Decomposed=0 ; Index color model.
LoadCT, 0 ; Normal black to white color table.
TVLCT, r, g, b, /Get
TVLCT, Reverse(r), Reverse(g), Reverse(b)
%%%%%%%

cd, file+'\RESULTS'

ct_files=file_search('CT*', count=nses)

ses=intarr(nses)

for i=0, nses-1 do ses(i)=fix(strmid(ct_files(i), 8, 1))

restore, ct_files(0)

si=size(ct_mod)
dim_x=si(1)
dim_y=si(2)
dim_z=si(3)
ct_images=fltarr(dim_x, dim_y, dim_z, nses)
```

```
ct_images(*,*,*, 0)=ct_mod

for i=1, nses-1 do begin
        restore, ct_files(i)
        ct_images(*,*,*, i)= ct_mod
endfor

for i=0, nses-1 do begin
        window, i, xsize=3*dim_x, ysize=3*dim_y
        tvscl, rebin(ct_images(*,*, slice, i),3*dim_x, 3*dim_y, /SAMPLE)
endfor

rct_file=file_search('RCT*')
restore,rct_file

d_file=file_search('D*')
restore,d_file


pt_files=file_search('PET*')
pt_images=fltarr(dim_x, dim_y, dim_z, nses)
for i=0, nses-1 do begin
        restore, pt_files(i)
        pt_images(*,*,*, i)=pt_mod

endfor

struk_file=file_search('struk*')
restore, struk_file

;%%%%%%%%%%%%%%%%%%%%%%%matchlungs%%%%%%%%%%%%%%%%%%%%%%%%%%%%
index=intarr(dim_x,dim_y,dim_z)
for i=0, nses-1 do begin
        ct_1=reform(ct_images(*,*,*,i))
        ct_1(where(ct_1 gt 800))=0
        ct_1(where(ct_1 lt 100))=0
        ct_1(where(ct_1))=1
        ;TVSCL,CT_1(*,*,80)
        index=index+ct_1
endfor

index(where(index ne nses))=0
; %%%%%%%%%%%%%%%%%%DOSE vs. SUV%%%%%%%%%%%%%%%%%%%%%%%%
g=      7
l=      12
r=      11
h=      5
e=      6
b=      13
N=9
for i=0, nses-1 do begin
print,i
pt=reform(pt_images(*,*,*, i))
;ctt=reform(ct_images(*,*,*,0))
```

117

```
GTV=reform(struk_new(g, *,*,*))
smooth_struc=intarr(5,5,5)+1
gtv_EXP = DILATE(GTV, smooth_struc)

HEART=reform(struk_new(h, *,*,*))

smooth_struc=intarr(3,3,3)+1
heart_EXP = DILATE(heart, smooth_struc)

eso=reform(struk_new(e, *,*,*))
ESO=congrid(ESO,dim_x,dim_y,dim_z)
smooth_struc=intarr(3,3,3)+1
esoph_EXP = DILATE(eso, smooth_struc)

bone=reform(struk_new(b, *,*,*))
BONE=congrid(BONE,dim_x,dim_y,dim_z)
smooth_struc=intarr(3,3,3)+1
bone_EXP = DILATE(bone, smooth_struc)

node=reform(struk_new(n, *,*,*))
NODE=congrid(NODE,dim_x,dim_y,dim_z)
smooth_struc=intarr(3,3,3)+1
node_EXP = DILATE(node, smooth_struc)

struc=reform(struk_new(b, *,*,*))
vec=where(struc gt 0  and d_mod gt 10  and gtv_exp ne 1 and heart_exp ne 1 $
          And esoph_exp ne 1 ); and bone_exp ne 1 and index gt 0); and node_exp ne 1)
me_suv=median(pt(vec))
m_suv=prank(pt(vec),90)
print, 'b_90_10=',m_suv
;print, 'r_med_10=', me_suv
struc=reform(struk_new(e, *,*,*))
vec=where(struc gt 0  and d_mod gt 10  and gtv_exp ne 1  and heart_exp ne 1 $
 and bone_exp ne 1); and node_exp ne 1)and index gt 0        And esoph_exp ne 1
me_suv=median(pt(vec))
m_suv=prank(pt(vec),90)
print,'e_90_10=', m_suv
;print,'l_med_10=', me_suv
struc=reform(struk_new(b, *,*,*))
vec=where(struc gt 0  and d_mod gt 20  and gtv_exp ne 1  and heart_exp ne 1 $
          And esoph_exp ne 1 ); and bone_exp ne 1  and index gt 0);and node_exp ne 1)
me_suv=median(pt(vec))
m_suv=prank(pt(vec),90)
print, 'b_90_20=',m_suv
;print, 'r_med_20=', me_suv
struc=reform(struk_new(e, *,*,*))
vec=where(struc gt 0  and d_mod gt 20  and gtv_exp ne 1 and heart_exp ne 1 $
 and bone_exp ne 1); and index gt 0 And esoph_exp ne 1); and node_exp ne 1)
me_suv=median(pt(vec))
m_suv=prank(pt(vec),90)
print, 'e_90_20=',m_suv
endfor
stop
print, 'l_med_10=', me_suv
struc=reform(struk_new(e, *,*,*))
```

```
vec=where(struc gt 0  and d_mod gt 20  and gtv_exp ne 1  and heart_exp ne 1 $
          and bone_exp ne 1 and node_exp ne 1and index gt 0And esoph_exp ne 1)
me_suv=median(pt(vec))
m_suv=mean(pt(vec))

print, 'e_mn_20=',m_suv
print, 'e_med_20=', me_suv

struc=reform(struk_new(L, *,*,*))
vec=where(struc gt 0  and d_mod gt 20  and gtv_exp ne 1 and index gt 0 and heart_exp ne 1 $
          And esoph_exp ne 1 and bone_exp ne 1 and node_exp ne 1)
me_suv=median(pt(vec))
m_suv=mean(pt(vec))
print,'l_mn_20=', m_suv
print,'l_med_20=', me_suv

do_ca=findgen(64)*0.5
m_d=do_ca*0.0
m_SUV=do_ca*0.0
m_ct=do_ca*0.0
print,'CT'
for i=1, 63 do begin

        vec=where(struc gt 0  and d_mod le do_ca(i) $
        and d_mod gt do_ca(i-1) and gtv_exp ne 1 and index gt 0 and heart_exp ne 1 $
        and esoph_exp ne 1 and bone_exp ne 1 and node_exp ne 1)

        if vec(0) ne -1 then begin
                m_ct(i)=mean(ctt(vec))

                m_ct(I)=m_ct(I)-1024
                PRINT,M_ct(I)

        endif else begin
                m_d(i)=-1
        endelse
endfor
print,'SUV'
for i=1, 63 do begin

        vec=where(struc gt 0  and d_mod le do_ca(i) $
        and d_mod gt do_ca(i-1) and gtv_exp ne 1 and index gt 0 and heart_exp ne 1 $
        And esoph_exp ne 1 and bone_exp ne 1 and node_exp ne 1)

        if vec(0) ne -1 then begin
                m_suv(i)=mean(pt(vec))


                PRINT,M_SUV(I)

        endif else begin
                m_d(i)=-1
        endelse
endfor
PRINT,'D'
```

```
for i=1, 63 do begin

        vec=where(struc gt 0  and d_mod le do_ca(i) $
        and d_mod gt do_ca(i-1) and gtv_exp ne 1 and index gt 0 and heart_exp ne 1 $
        and esoph_exp ne 1 and bone_exp ne 1 and node_exp ne 1)

        if vec(0) ne -1 then begin
                m_d(i)=mean(d_mod(vec))
                PRINT,M_D(I)

        endif else begin
                m_d(i)=-1
        endelse
endfor
print, roi_name(g),roi_name(l),ROI_NAME(R)
STOP
m_d=m_d(where(m_d ne -1))
m_suv=m_suv(where(m_d ne -1))

;%%%%%%%%%%%%%%%%%%%%%%%%%%PLOT%%%%%%%%%%%%%%%%%%%%%%%%%%%%%

window, xsize=1200, ysize=600
plot, m_d, m_SUV, xtitle='Dose (Gy)',ytitle= 'SUV!Dmean!N',$
yrange=[min(m_suv)-0.1,max(m_suv)+0.1],$
xtickinterval=2.0,thick=2,xthick=2,ythick=2,charsize=2.5,xstyle=8,ystyle=8.0+1,psym=4,ytickinterval=0.1
xyouts,1.5,0.4,'Esophagus',charsize=3
;%%%%%%%%%%%%%%%%%%%%%%%%% contours%%%%%%%%%%%%%%%%%%%%%%%%%%

DEVICE, DECOMPOSED = 0, RETAIN = 2
LOADCT, 0
pt=reform(pt_images(*,100,*,1))
;GTV=reform(struk_new(14, *,*,80))

image=reform(struk_new(15, *,100,*))

; Define the structuring element, apply the
; morphological operator and display the image.
radius = 1
strucElem = SHIFT(DIST(2*radius+1), $
  radius, radius) LE radius
morphImg = MORPH_GRADIENT(image, strucElem)
;morphImg1 = MORPH_GRADIENT(gtv, strucElem)
tvs=pt+morphImg
Tvscl,tvs
stop
;%%%%%%%%%%%%%%%%%%%%%%%%%% HISTOGRAM%%%%%%%%%%%%%%%%%%%%%%%%
pt=reform(pt_images(*,*,*, 1))
GTV=reform(struk_new(11, *,*,*))
vec_GTV=where(GTV)
;;%%%%%%
FDG_GTV=pt(vec_GTV)
xmin=min(pt(vec_GTV))
xmax=max(pt(vec_GTV))
nbin=100
xspan=xmin+(findgen(nbin)*(xmax-xmin)/(nbin-1))
```

```
hist_FDG_GTV=histogram(pt(vec_GTV), nbins=nbin, min=xmin, max=xmax)
plot,    xspan,    hist_FDG_GTV2/11334.0,xtitle='SUV',ytitle='Normalized    Count',    charsize=1.5,linestyle=1,
psym=10,thick=2
pt=reform(pt_images(*,*,*, 2))
GTV=reform(struk_new(11, *,*,*))
vec_GTV=where(GTV)
;;%%%%%%
FDG_GTV=pt(vec_GTV)
xmin=min(pt(vec_GTV))
xmax=max(pt(vec_GTV))
nbin=100
xspan=xmin+(findgen(nbin)*(xmax-xmin)/(nbin-1))
hist_FDG_GTV=histogram(pt(vec_GTV), nbins=nbin, min=xmin, max=xmax)
oplot, xspan, hist_FDG_GTV2/11334.0,linestyle=5, psym=10,thick=2
pt=reform(pt_images(*,*,*, 0))
GTV=reform(struk_new(11, *,*,*))
vec_GTV=where(GTV)
;;%%%%%%
FDG_GTV=pt(vec_GTV)
xmin=min(pt(vec_GTV))
xmax=max(pt(vec_GTV))
nbin=100
xspan=xmin+(findgen(nbin)*(xmax-xmin)/(nbin-1))
hist_FDG_GTV=histogram(pt(vec_GTV), nbins=nbin, min=xmin, max=xmax)
oplot, xspan, hist_FDG_GTV2/11334.0,linestyle=0, psym=10,thick=2
end

;%%%%%%%%%%%%%%%%%%%%%Extracting data%%%%%%%%%%%%%%%%%%%%%%%
print,roi_name
for k=0, nses-1 do begin

g=8
h=10
e=11
n=9
r=12
l=13
b=14


pt=reform(pt_images(*,*,*, k))
GTV=reform(struk_new(g, *,*,*))
vec_GTV=where(GTV)

print,k+1
print,roi_name(g)
print,'min_GTV=',min(pt(vec_GTV))
print,'median_GTV=',median(pt(vec_GTV))
print, 'mean_GTV=',mean(pt(vec_GTV))
print, 'max_GTV=',max(pt(vec_GTV))
print,'25_GTV=',prank(pt(vec_GTV),25)
print,'75_GTV=',prank(pt(vec_GTV),75)

heart=reform(struk_new(h, *,*,*))
vec_GTV=where(heart)
```

```
print,roi_name(h)
print,'min_heart=',min(pt(vec_GTV))
print,'median_heart=',median(pt(vec_GTV))
print, 'mean_heart=',mean(pt(vec_GTV))
print, 'max_heart=',max(pt(vec_GTV))
print,'25_heart=',prank(pt(vec_GTV),25)
print,'75_heart=',prank(pt(vec_GTV),75)

eso=reform(struk_new(e, *,*,*))
vec_GTV=where(eso)

print,roi_name(e)
print,'min_eso=',min(pt(vec_GTV))
print,'median_eso=',median(pt(vec_GTV))
print, 'mean_eso=',mean(pt(vec_GTV))
print, 'max_eso=',max(pt(vec_GTV))
print,'25_eso=',prank(pt(vec_GTV),25)
print,'75_eso=',prank(pt(vec_GTV),75)


node=reform(struk_new(n, *,*,*))
vec_GTV=where(node)

print,roi_name(n)
print,'min_node=',min(pt(vec_GTV))
print,'median_node=',median(pt(vec_GTV))
print, 'mean_node=',mean(pt(vec_GTV))
print, 'max_node=',max(pt(vec_GTV))
print,'25_node=',prank(pt(vec_GTV),25)
print,'75_node=',prank(pt(vec_GTV),75)

rl=reform(struk_new(r, *,*,*))
vec_GTV=where(rl)
;vec_gtv=where(in_ct+vec_gtv)
print,roi_name(r)
print,'min_rl=',min(pt(vec_GTV))
print,'median_rl=',median(pt(vec_GTV))
print, 'mean_rl=',mean(pt(vec_GTV))
print, 'max_rl=',max(pt(vec_GTV))
print,'25_rl=',prank(pt(vec_GTV),25)
print,'75_rl=',prank(pt(vec_GTV),75)

ll=reform(struk_new(l, *,*,*))
vec_GTV=where(ll)
;vec_gtv=where(in_ct+vec_gtv)

print,roi_name(l)
print,'min_ll=',min(pt(vec_GTV))
print,'median_ll=',median(pt(vec_GTV))
print, 'mean_ll=',mean(pt(vec_GTV))
print, 'max_ll=',max(pt(vec_GTV))
print,'25_ll=',prank(pt(vec_GTV),25)
print,'75_ll=',prank(pt(vec_GTV),75)
```

```
bone=reform(struk_new(b, *,*,*))
vec_GTV=where(bone)

print,roi_name(b)
print,'min_bode=',min(pt(vec_GTV))
print,'median_bone=',median(pt(vec_GTV))
print, 'mean_bone=',mean(pt(vec_GTV))
print, 'max_bone=',max(pt(vec_GTV))
print,'25_bone=',prank(pt(vec_GTV),25)
print,'75_bone=',prank(pt(vec_GTV),75)
endfor
print,'g=',g,'h=',h, 'e=',e,'n=',n,'r=',r,'l=',l,'b=',b

;; %%%%%%%%%%%%%%%%%%%%%%dose vs SUV %%%%%%%%%%%%%%%%%%%%%%%%%%

do_ca=findgen(30)*1
m_d=do_ca*0.0
m_SUV=do_ca*0.0
;sig_d=m_d
;sig_SUV=m_SUV

for i=1, 29 do begin
        index=where(rct_image ge 200 and rct_image lt 800 and d_mod le do_ca(i) and d_mod gt do_ca(i-1))
        m_d(i)=mean(d_mod(index))
        sig_d(i)=stdev(d_mod(index))
        m_SUV(i)=mean(pt_mod_new(index))
        sig_SUV(i)=stdev(pt_mod_new(index))
pt=reform(pt_images(*,*,*, 1))
GTV=reform(struk_new(13, *,*,*))
vec_GTV=where(GTV and d_mod le do_ca(i) and d_mod gt do_ca(i-1))
m_d(i)=mean(d_mod(vec_GTV))
m_suv(i)=mean(pt(vec_GTV))
endfor

;;match lungs

index=fltarr(dim_x,dim_y,dim_z)
for i=0, nses-1 do begin
        ct_1=reform(ct_images(*,*,*,i))
        ct_1(where(ct_1 gt 800))=0
        ct_1(where(ct_1 lt 100))=0
        ct_1(where(ct_1))=1
        TVSCL,CT_1(*,*,80)
        STOP
        index=index+ct_1

endfor


for k=0, nses-1 do begin
r=11
l=12
print,k+1
print,roi_name(R)
pt=reform(pt_images(*,*,*, k))
```

```
RL=reform(struk_new(R, *,*,*))
RL(where(RL))=1
window,0
tvscl,rl(*,*,80)
index_R=index+RL
RL(where(index_R eq nses+1))=1
RL(where(index_R lt nses+1))=0
window,1
tvscl,RL(*,*,80)
vec_GTV=where(RL)
print,roi_name(r)
print,'min_rl=',min(pt(vec_GTV))
print,'median_rl=',median(pt(vec_GTV))
print, 'mean_rl=',mean(pt(vec_GTV))
print, 'max_rl=',max(pt(vec_GTV))
print,'25_rl=',prank(pt(vec_GTV),25)
print,'75_rl=',prank(pt(vec_GTV),75)

ll=reform(struk_new(l, *,*,*))
LL(where(LL))=1
window,2
tvscl,ll(*,*,80)
index_L=index+LL
LL(where(index_L eq nses+1))=1
LL(where(index_L lt nses+1))=0
window,3
tvscl,LL(*,*,80)
vec_GTV=where(LL)

print,roi_name(l)
print,'min_ll=',min(pt(vec_GTV))
print,'median_ll=',median(pt(vec_GTV))
print, 'mean_ll=',mean(pt(vec_GTV))
print, 'max_ll=',max(pt(vec_GTV))
print,'25_ll=',prank(pt(vec_GTV),25)
print,'75_ll=',prank(pt(vec_GTV),75)
ENDFOR
STOP
;;; %%%%%%%%%%%%%%%%%%%%dose vs SUV %%%%%%%%%%%%%%%%%%%%%%%%
;%%%%white background%%%
Device, Decomposed=0 ; Index color model.
 LoadCT, 0 ; Normal black to white color table.
 TVLCT, r, g, b, /Get
TVLCT, Reverse(r), Reverse(g), Reverse(b)
;%%%%%%
do_ca=findgen(30)*1
m_d=do_ca*0.0
m_SUV=do_ca*0.0

for k=0, nses-1 do begin
        for i=1, 29 do begin

        pt=reform(pt_images(*,*,*, k))
        GTV=reform(struk_new(11, *,*,*))
        GTV(where(GTV))=1
```

```
            index_x=index+GTV
            GTV(where(index_x eq nses+1))=1
            GTV(where(index_x lt nses+1))=0

            vec_GTV=where(GTV and d_mod le do_ca(i) and d_mod gt do_ca(i-1))
            m_d(i)=mean(d_mod(vec_GTV))
            m_suv(i)=mean(pt(vec_GTV))
            endfor
!y.omargin=[3,3]
plot, m_d, m_SUV, xtitle='Dose (Gy)',ytitle= 'SUV!Imean!N in the left lung',$
subtitle='!CPatient ID: 04. Second treatment session',$
title='"SUV!Imean!N                          versus                          Radiation
Dose"!C',FONT=1,xtickinterval=2.0,thick=1.5,xcharsize=1.1,ycharsize=1.1,charsize=1.3,xstyle=8,ystyle=8.0,psym
=4

endfor

end


;; %%%%%%%%%%%%%%%%%%%%%%dose vs delta SUV %%%%%%%%%%%%%%%%%%%%%%%%
%%%white background%%%
Device, Decomposed=0 ; Index color model.
 LoadCT, 0 ; Normal black to white color table.
 TVLCT, r, g, b, /Get
TVLCT, Reverse(r), Reverse(g), Reverse(b)
;%%%%%%
do_ca=findgen(30)*1
m_d=do_ca*0.0
m_SUV=do_ca*0.0

for i=1, 29 do begin
        ;pt_1=reform(pt_images(*,*,*, 2))
        ;pt_2=reform(pt_images(*,*,*, 1))
        pt_delta=reform(pt_images(*,*,*, 1)-pt_images(*,*,*, 2))
        GTV=reform(struk_new(11, *,*,*))
        GTV(where(GTV))=1
        index_x=index+GTV
        GTV(where(index_x eq nses+1))=1
        GTV(where(index_x lt nses+1))=0

        vec_GTV=where(GTV and d_mod le do_ca(i) and d_mod gt do_ca(i-1))
        m_d(i)=mean(d_mod(vec_GTV))
        m_suv(i)=mean(pt_delta(vec_GTV))
endfor

end
;%%%%%%%%%%%%%%%%%%%plot data%%%%%%%%%%%%%%%%%%%%%%
;PRO ANALYSIS, file, im_ses

slice=70
ref_res=[3.0,3.0,3.0]

i = ''
READ, i, PROMPT='patient name: '
```

```
file = FILEPATH('PAT'+i, ROOT_DIR='C:', SUBDIRECTORY='THORAT')

cd, file+'\RESULTS'
ct_files=file_search('CT*', count=nses)
ses=intarr(nses)

for i=0, nses-1 do ses(i)=fix(strmid(ct_files(i), 8, 1))
restore, ct_files(0)
si=size(ct_mod)
dim_x=si(1)
dim_y=si(2)
dim_z=si(3)
ct_images=fltarr(dim_x, dim_y, dim_z, nses)

ct_images(*,*,*, 0)=ct_mod
endfor
for i=1, nses-1 do begin
        restore, ct_files(i)
        ct_images(*,*,*, i)= ct_mod
endfor

for i=0, nses-1 do begin
        window, i, xsize=3*dim_x, ysize=3*dim_y
        tvscl, rebin(ct_images(*,*, slice, i),3*dim_x, 3*dim_y, /SAMPLE)
endfor

rct_file=file_search('RCT*')
restore,rct_file

d_file=file_search('D*')
restore,d_file

pt_files=file_search('PET*')
pt_images=fltarr(dim_x, dim_y, dim_z, nses)
for i=0, nses-1 do begin
        restore, pt_files(i)
        pt_images(*,*,*, i)=pt_mod

endfor

struk_file=file_search('struk*')
restore, struk_file
;print,roi_name

;%%%%%%%%%%% Analysis%%%%%%%%
index=intarr(dim_x,dim_y,dim_z)
for i=0, nses-1 do begin
        ct_1=reform(ct_images(*,*,*,i))
        ct_1(where(ct_1 gt 800))=0
        ct_1(where(ct_1 lt 100))=0
        ct_1(where(ct_1))=1
        ;TVSCL,CT_1(*,*,80)
        index=index+ct_1
endfor
index(where(index ne nses))=0
```

```
for k=0, nses-1 do begin
pt=reform(pt_images(*,*,*, k))
ct_i=reform(ct_images(*,*,*, k))

n1=7

node1=reform(struk_new(n1, *,*,*))
smooth_struc=intarr(3,3,3)+1
n1_EXP = DILATE(node1, smooth_struc)


node2=reform(struk_new(n2, *,*,*))
smooth_struc=intarr(3,3,3)+1
n2_EXP = DILATE(node2, smooth_struc)


node3=reform(struk_new(n3, *,*,*))
smooth_struc=intarr(3,3,3)+1
n3_EXP = DILATE(node3, smooth_struc)


node4=reform(struk_new(n4, *,*,*))
smooth_struc=intarr(3,3,3)+1
n4_EXP = DILATE(node4, smooth_struc)


node5=reform(struk_new(n5, *,*,*))
smooth_struc=intarr(3,3,3)+1
n5_EXP = DILATE(node5, smooth_struc)


node6=reform(struk_new(n6, *,*,*))
smooth_struc=intarr(3,3,3)+1
n6_EXP = DILATE(node6, smooth_struc)
node7=reform(struk_new(n7, *,*,*))
smooth_struc=intarr(3,3,3)+1
n7_EXP = DILATE(node7, smooth_struc)
node8=reform(struk_new(n8, *,*,*))
smooth_struc=intarr(3,3,3)+1
n8_EXP = DILATE(node8, smooth_struc)
node9=reform(struk_new(n9, *,*,*))
smooth_struc=intarr(3,3,3)+1
n9_EXP = DILATE(node9, smooth_struc)
node10=reform(struk_new(n10, *,*,*))
smooth_struc=intarr(3,3,3)+1
n10_EXP = DILATE(node10, smooth_struc)
node11=reform(struk_new(n11, *,*,*))
smooth_struc=intarr(3,3,3)+1
n11_EXP = DILATE(node11, smooth_struc)


vec_struc=where(node1)
print,'minim_NODE1=                    ',min(pt(vec_struc))
print,'25thp_NODE1=                    ',prank(pt(vec_struc),25)
print,'media_NODE1=                    ',median(pt(vec_struc))
print,'mean_NODE1=                     ',mean(pt(vec_struc))
print,'75thp_NODE1=                    ',prank(pt(vec_struc),75)
print,'maxim_NODE1=                    ',max(pt(vec_struc))
```

```
endfor

g=        2
l=        10
r=        11
h=        5
e=        6
b=        12


GTV=reform(struk_new(g, *,*,*))
vec_struc=where(GTV)

print,'minim_GTVVV=                      ',min(pt(vec_struc))
print,'25thp_GTVVV=                      ',prank(pt(vec_struc),25)
print,'media_GTVVV=                      ',median(pt(vec_struc))
print,'mean_GTVVV=                       ',mean(pt(vec_struc))
print,'75thp_GTVVV=                      ',prank(pt(vec_struc),75)
print,'maxim_GTVVV=                      ',max(pt(vec_struc))
print,'cminim_GTVVV=                     ',min(ct_i(vec_struc))
print,'c25thp_GTVVV=                     ',prank(ct_i(vec_struc),25)
print,'cmedia_GTVVV=                     ',median(ct_i(vec_struc))
print,'cmean_GTVVV=                      ',mean(ct_i(vec_struc))
print,'c75thp_GTVVV=                     ',prank(ct_i(vec_struc),75)
print,'cmaxim_GTVVV=                     ',max(ct_i(vec_struc))

smooth_struc=intarr(5,5,5)+1
gtv_EXP = DILATE(GTV, smooth_struc)

heart=reform(struk_new(h, *,*,*))
vec_struc=where(heart gt 0 and gtv_exp ne 1)

print,'minim_HEART=                      ',min(pt(vec_struc))
print,'25thp_HEART=                      ',prank(pt(vec_struc),25)
print,'media_HEART=                      ',median(pt(vec_struc))
print,'mean_HEART=                       ',mean(pt(vec_struc))
print,'75thp_HEART=                      ',prank(pt(vec_struc),75)
print,'maxim_HEART=                      ',max(pt(vec_struc))

smooth_struc=intarr(3,3,3)+1
heart_EXP = DILATE(heart, smooth_struc)

eso=reform(struk_new(e, *,*,*))
vec_struc=where(eso gt 0 and gtv_exp ne 1)

print,'minim_ESOPH=                      ',min(pt(vec_struc))
print,'25thp_ESOPH=                      ',prank(pt(vec_struc),25)
print,'media_ESOPH=                      ',median(pt(vec_struc))
print,'mean_ESOPH=                       ',mean(pt(vec_struc))
print,'75thp_ESOPH=                      ',prank(pt(vec_struc),75)
print,'maxim_ESOPH=                      ',max(pt(vec_struc))

smooth_struc=intarr(3,3,3)+1
esoph_EXP = DILATE(eso, smooth_struc)
```

128

```
bone=reform(struk_new(b, *,*,*))
vec_struc=where(bone and gtv_exp ne 1)

print,'minim_BONEM=                        ',min(pt(vec_struc))
print,'25thp_BONEM=                        ',prank(pt(vec_struc),25)
print,'media_BONEM=                        ',median(pt(vec_struc))
print,'mean_BONEM=                         ',mean(pt(vec_struc))
print,'75thp_BONEM=                        ',prank(pt(vec_struc),75)
print,'maxim_BONEM=                        ',max(pt(vec_struc))

smooth_struc=intarr(3,3,3)+1
bone_EXP = DILATE(bone, smooth_struc)

ll=reform(struk_new(l, *,*,*))
vec_struc=where(ll gt 0 and index gt 0 and gtv_exp ne 1 and heart_exp ne 1 and esoph_exp ne 1 and bone_exp ne
1);$
;and n1_exp ne 1 and n2_exp ne 1 and n3_exp ne 1 and n4_exp ne 1  and n5_exp ne 1 and n6_exp ne 1 and n7_exp
ne 1 $
; and n8_exp ne 1 and n9_exp ne 1 and n10_exp ne 1 and n11_exp ne 1)

print,'minim_LLUNG=                        ',min(pt(vec_struc))
print,'25thp_LLUNG=                        ',prank(pt(vec_struc),25)
print,'media_LLUNG=                        ',median(pt(vec_struc))
print,'mean_LLUNG=                         ',mean(pt(vec_struc))
print,'75thp_LLUNG=                        ',prank(pt(vec_struc),75)
print,'maxim_LLUNG=                        ',max(pt(vec_struc))
print,'cminim_LLUNG=                       ',min(ct_i(vec_struc))
print,'c25thp_LLUNG=                       ',prank(ct_i(vec_struc),25)
print,'cmedia_LLUNG=                       ',median(ct_i(vec_struc))
print,'cmean_LLUNG=                        ',mean(ct_i(vec_struc))
print,'c75thp_LLUNG=                       ',prank(ct_i(vec_struc),75)
print,'cmaxim_LLUNG=                       ',max(ct_i(vec_struc))

rl=reform(struk_new(r, *,*,*))
vec_struc=where(rl gt 0 and index gt 0 and gtv_exp ne 1 and heart_exp ne 1 and esoph_exp ne 1 and bone_exp ne
1);$
;and n1_exp ne 1 and n2_exp ne 1 and n3_exp ne 1 and n4_exp ne 1  and n5_exp ne 1 and n6_exp ne 1 and n7_exp
ne 1 $
 ;and n8_exp ne 1 and n9_exp ne 1 and n10_exp ne 1 and n11_exp ne 1)
print,'minim_RLUNG=                        ',min(pt(vec_struc))
print,'25thp_RLUNG=                        ',prank(pt(vec_struc),25)
print,'media_RLUNG=                        ',median(pt(vec_struc))
print,'mean_RLUNG=                         ',mean(pt(vec_struc))
print,'75thp_RLUNG=                        ',prank(pt(vec_struc),75)
print,'maxim_RLUNG=                        ',max(pt(vec_struc))
print,'cminim_RLUNG=                       ',min(ct_i(vec_struc))
print,'c25thp_RLUNG=                       ',prank(ct_i(vec_struc),25)
print,'cmedia_RLUNG=                       ',median(ct_i(vec_struc))
print,'cmean_RLUNG=                        ',mean(ct_i(vec_struc))
print,'c75thp_RLUNG=                       ',prank(ct_i(vec_struc),75)
print,'cmaxim_RLUNG=                       ',max(ct_i(vec_struc))

endfor
```

```
print,'GTV=',roi_name(G)
print,'HEART=',roi_name(H)
print,'ESOPHAGUS=',roi_name(E)
print,'RLUNG=',roi_name(R)
print,'LLUNG=',roi_name(L)
print,'BONE=',roi_name(B)
;print,roi_name(n1),roi_name(n2),roi_name(n3),roi_name(n4),roi_name(n5)

end
```